Gersonde, R., Hodell, D.A., Blum, P., et al., 1999
Proceedings of the Ocean Drilling Program, Initial Reports Volume 177

1. Leg 177 Summary: Southern Ocean Paleoceanography[1]

Shipboard Scientific Party[2]

ABSTRACT

Sediments in the southeast Atlantic sector of the Southern Ocean were cored during Ocean Drilling Program Leg 177 to study the paleoceanographic history of the Antarctic region on short (millennial) to long (Cenozoic) time scales. Seven sites were drilled along a north-south transect across the Antarctic Circumpolar Current (ACC) from 41° to 53°S: three sites at ~41°S near the Agulhas Ridge (Sites 1088, 1089, and 1090), two sites at ~47°S near and at the Meteor Rise (Sites 1091 and 1092), and two sites at 50° and 53°S within the circum-Antarctic opal belt (Sites 1093 and 1094). The water depths of the sites range from 1974 to 4620 m, intersecting all of the major deep- and bottom-water masses in the Southern Ocean.

The general goals of Leg 177 were twofold: (1) to document the biostratigraphic, biogeographic, and paleoceanographic history of the Paleogene and early Neogene, a period marked by the establishment of the Antarctic cryosphere and the ACC; and (2) to target expanded sections of late Neogene sediments, which can be used to resolve the timing of Southern Hemisphere climatic events on orbital and suborbital time scales, and can be compared with similar sedimentary and climatic records from other ocean basins and with climatic signals documented in ice cores from Greenland and Antarctica.

More than 4000 m of sediment was recovered at an average recovery rate of 81%, ranging in age from the middle Eocene to the Holocene. Composite records were constructed at each site from cores in multiple holes by aligning features in the signals of core logging data (magnetic susceptibility, gamma-ray attenuation [GRA] bulk density, spectral color reflectance, and lithologic markers). Leg 177 cores, for which spliced

[1]Examples of how to reference the whole or part of this volume.
[2]Shipboard Scientific Party addresses.

Ms 177IR-101

composite sections were constructed, represent the most complete sections yet obtained from the Southern Ocean.

A continuous 330-m sequence of middle Eocene to lower Miocene sediments, recovered at Site 1090, includes cyclic variations in lithologic parameters and a superb geomagnetic polarity reversal record. The shallow burial depth of this Paleogene section will enable oxygen isotopic measurements of diagenetically unaltered foraminifers. Site 1090 will likely become a deep-sea type section for biomagnetostratigraphic correlations, and the potential exists for development of an astronomically tuned time scale. Site 1090 will be used to reconstruct the paleoceanographic history of the Southern Ocean for the middle Eocene through early Miocene. This time period marked a shift in Earth's climate from a warm- ("hothouse") to a cold-climate ("icehouse") mode, and included the buildup of ice on the Antarctic continent and major paleogeographic changes in the Southern Ocean. The study of Site 1090 will help to decipher processes linked to the thermal isolation of Antarctica from warm subtropical gyres, as well as Antarctic ice-sheet development and attendant changes in sea level. Similar studies can be conducted on late Miocene sequences that were recovered at two other locations (Sites 1088 and 1092).

During Leg 177, we succeeded in recovering complete and expanded sequences at 41° (Site 1089), 47° (Site 1091), 50° (Site 1093), and 53°S (Site 1094) that accumulated at average rates ranging from 130 to 250 m/m.y. These sequences are well-suited for paleoceanographic studies of the late Pliocene–Pleistocene (particularly the past 1.5 m.y.) at a temporal resolution of less than 1 k.y. These sites represent the Southern Hemisphere analogs to North Atlantic drift deposits drilled during Legs 162 and 172, and they will be useful for studying the response of the Southern Ocean environment to orbital forcing and the phase relationships to climate change in the North Atlantic. The location of the sediment cores on a north-south transect between subtropical waters and the Antarctic Zone is optimal for monitoring some key aspects of the climatic system, including the extent of the Antarctic sea-ice field, frontal boundary movements within the ACC, changes in biological paleoproductivity and opal export rates, and changes in the input of North Atlantic Deep Water to the Southern Ocean.

Shipboard examination of lithologic components and measurements of physical properties (diffuse spectral reflectance, GRA bulk density, magnetic susceptibility, and natural gamma radiation) show distinct evidence of cyclicity at Milankovitch time scales, but millennial and perhaps centennial scale changes should be resolvable at some sites. Correlation of climate oscillations on millennial time scales detected in marine sediments of the Southern Ocean and in ice cores from Greenland and Antarctica offers the opportunity to study the linkages between atmosphere (temperature and CO_2) and ocean dynamics (sea-surface temperature, productivity, and deep-water circulation) over the past four climatic cycles of the late Pleistocene.

The high-quality sedimentary sequences recovered during Leg 177 fill a critical gap in the distribution of drilled ocean sites and will anchor the southern end of the global array of sites needed to decipher the role of the Southern Ocean in the history of Earth's climatic system.

INTRODUCTION

The Antarctic ice sheets and the adjacent Southern Ocean act together to form the Antarctic ocean-cryosphere system. Over the last decade, paleoceanographers, climatologists, and geochemists have recognized that processes occurring in the Southern Ocean have played a vital role in defining Earth's climate, yet many questions remain about the region's paleoenvironmental evolution (e.g., Kennett and Barron, 1992). To study the paleoceanographic history of the Southern Ocean, Ocean Drilling Program (ODP) Leg 177 drilled seven sites along a north-south transect from 41° to 53°S (Fig. F1) and in water depths ranging from 1974 to 4620 m (Fig. F2). The Southern Ocean is an extraordinarily important region for several reasons:

1. The Antarctic cryosphere represents the largest accumulation of ice on Earth's surface and should it melt, sea level would rise by 50 to 60 m. The development and evolution of the Antarctic ice sheet and sea-ice field have had a profound influence on global sea-level history, Earth's heat budget, atmospheric circulation, surface- and deep-water circulation, and the evolution of Antarctic biota.
2. The Southern Ocean is one of the primary sites of intermediate-, deep-, and bottom-water formation. For example, almost two-thirds of the global ocean floor is bathed by Antarctic Bottom Water (AABW) that mainly originates in the Weddell Sea region. The Southern Ocean represents the "junction box" of deep-water circulation where mixing occurs among water masses from all ocean basins (Fig. F3). As such, the Southern Ocean is perhaps the only region where the relative mixing ratios of deep-water masses can be monitored (e.g., North Atlantic Deep Water [NADW]; Charles and Fairbanks, 1992). As one of the primary sites of deep- and intermediate-water mass formation, the geochemical and climatic fingerprint of Southern Ocean processes is transmitted throughout the world's deep oceans.
3. The Antarctic continent is thermally and biogeographically isolated from the subtropics by the Antarctic Circumpolar Current (ACC), a ring of cold water that contains complex frontal features and upwelling/downwelling cells (Fig. F4). The zonal temperature, sea-ice distribution, and nutrient structure within the ACC control biogenic sedimentary provinces that are characteristic of the Southern Ocean. Upwelling of nutrient-rich water results in primary biological productivity that constitutes nearly one-third of the oceanic total (Berger, 1989). About two-thirds of the silica supplied annually to the ocean is removed by siliceous microorganisms in the Southern Ocean. This leads to high accumulation rates of biogenic opal between the Polar Front Zone (PFZ) and the northern seasonal limit of sea ice (e.g., DeMaster, 1981; Lisitzin, 1985).
4. Surface waters in the circum-Antarctic are also important globally because upwelling of deep water and sea-ice formation link the thermal and gas compositions of the ocean's interior with the atmosphere through air-sea exchange. As a result, in most paleogeochemical models, atmospheric CO_2 is highly sensitive to changes in nutrient utilization and/or alkalinity of Antarctic surface waters (e.g., Sarmiento and Toggweiler, 1984; Siegentha-

F1. Locations of Leg 177 drill sites and previous ODP and DSDP sites in the South Atlantic, p. 35.

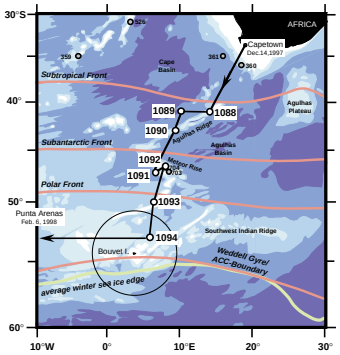

F2. Leg 177 sites relative to the vertical distribution of potential temperature in the southeast Atlantic Ocean, p. 36.

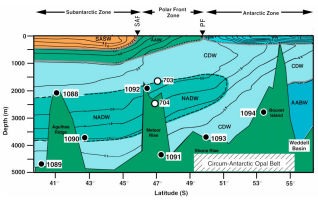

F3. Schematic representation of present ocean circulation and interocean exchange, p. 37.

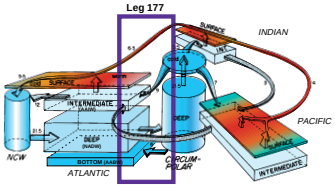

F4. ODP and DSDP sites in the Southern Ocean relative to oceanic frontal systems and sea-ice distribution, p. 38.

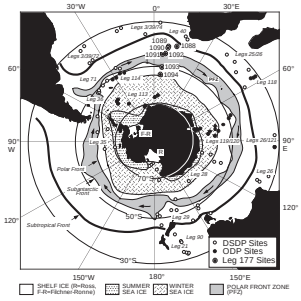

ler and Wenk, 1984; Knox and McElroy, 1984; Broecker and Peng, 1989).

5. The importance of Antarctica and the Southern Ocean is well known, yet many questions remain regarding the paleoceanographic and paleoclimatic history of this remote region of the world's oceans. The body of quantitative paleoceanographic data from the Southern Ocean is small relative to the climatic importance of the region.

To improve the present latitudinal and bathymetric coverage in the Southern Ocean, seven sites in the high latitudes of the southeast Atlantic Ocean were drilled during Leg 177 (Figs. **F1, F4;** Table **T1**). Leg 177 represented the return of the *JOIDES Resolution* to Antarctic waters for the first time in 10 years, since the last major Antarctic drilling campaign in 1987–1988 (Legs 113, 114, 119, and 120; Fig. **F4**). After departing Cape Town on 14 December 1997, a north-south transect of sites was drilled beginning at 41°S near the southern Subtropical Zone, extending across the PFZ from 47° to 50°S, and ending at 53°S in the northern Antarctic region, close to the present winter sea-ice edge (Fig. **F1**). The water depths of sites range from 1974 to 4620 m, intersecting most of the major deep- and bottom-water masses in the Southern Ocean (Fig. **F2**). Specific sites were targeted that contain expanded Quaternary, Neogene, and Paleogene sequences that had not been recovered adequately at these depths and latitudes by past drilling. As such, the sediments recovered during Leg 177 fill a critical gap in the distribution of ocean-drilled sites and constitute an invaluable archive of cores needed to extend our understanding of Southern Ocean paleoceanography. Leg 177, which recovered a total of 4046 m of sediment core, ended on 6 February 1998, in Punta Arenas (South Chile).

T1. Location, water depth, and coring summary of holes drilled during Leg 177, **p. 54.**

PREVIOUS DRILLING IN THE SOUTHERN OCEAN

Previous deep-sea drilling in the Southern Ocean (Fig. **F4**), especially sediment cores recovered with the Advanced Hydraulic Piston Corer (APC) and Extended Core Barrel (XCB) systems (Deep Sea Drilling Project [DSDP] Leg 71; ODP Legs 113, 114, 119, and 120), have provided a basic understanding of the paleoceanographic and paleoclimatic evolution of the southern high latitudes during the Cenozoic (see Kennett and Barron, 1992). Sections recovered by previous Antarctic drilling are often incomplete, however, because the APC and XCB systems miss intervals at core breaks even under ideal conditions and apparent 100% recovery in single holes (Ruddiman et al., 1986). In addition, cores are easily disturbed when recovered in the high seas often encountered in the Southern Ocean. Problems with incomplete core recovery, core disturbance, the presence of hiatuses, and diminished carbonate preservation at the high latitudes of the Southern Hemisphere have hampered efforts to obtain continuous paleoclimatic records in the Southern Ocean. One of the primary goals of Leg 177 was to recover complete sections by drilling multiple holes that are used to construct continuous composite sections in real time.

A major deficiency in the distribution of ocean-drilled cores is the lack of late Neogene sequences from the southern high latitudes that would permit the generation of continuous stratigraphic and paleoenvironmental signals. Compared to the superb records now available from the high-latitude North Atlantic Ocean (ODP Legs 94, 154, 162,

and 172), the Southern Ocean had relatively few sites suitable for high-resolution paleoclimatic studies. Expeditions by ODP to the South Atlantic and Indian sectors of the Southern Ocean during 1987–1988 (Legs 113, 114, 119, and 120) acquired good Paleogene sequences, but relatively few continuous late Neogene records were recovered. Of the 32 sites drilled during these four legs, only Site 704 (Leg 114) had sufficient stratigraphic continuity and carbonate content in the Pliocene–Pleistocene interval to be suitable for high-resolution paleoclimatic studies. Thus, the recovery of long, continuous sequences from the Southern Ocean was one of the major goals of Leg 177.

REGIONAL TECTONIC SETTING

Many of the sites drilled during Leg 177 are associated with the Agulhas Basin and are arranged along a north-south transect extending from the Agulhas Fracture Zone Ridge in the north, to Meteor Rise in the subantarctic, and to Shona Ridge and Bouvet Island in the south (Fig. F5). The Agulhas Basin lies on the African plate and is bounded by the Agulhas Fracture Zone to the north, the Southwest Indian Ridge to the south, the Meteor Rise to the west, and the Agulhas Plateau to the east. The topography of the Agulhas Basin bears testimony to its complex tectonic history (du Plessis, 1977; LaBrecque and Hayes, 1979; Cande et al., 1988; LaBrecque, 1986; Raymond and LaBrecque, 1988; Raymond et al., 1991; C. Ruppel, unpubl. data).

The three northern sites (1088, 1089, and 1090) are associated with the Agulhas Ridge (Fig. F5 and Fig. F6), which is an elongate topographic feature that parallels the Agulhas Fracture Zone. The Agulhas Ridge extends from the northern tip of the Meteor Rise and terminates abruptly at 40°S, 15°E, where it intersects the northern end of an abandoned spreading-ridge axis in the Agulhas Basin. At ~65 Ma, the spreading axis south of the Agulhas Fracture Zone jumped 825 km to the west, and motion along the transform fault was abandoned (du Plessis, 1977; LaBrecque and Hayes, 1979; Barker, 1979). Before the ridge jump, the very large offset Agulhas transform (1400 km displacement of the spreading axis or maximum age offset of ~45 Ma) was subjected to increasing compressional stress as a result of the changing relative motion of the South American and African Plates. This compression across the transform may have resulted in thrusting of the South American Plate over the African Plate, creating the Agulhas Fracture Zone Ridge (C. Raymond, pers. comm., 1996). Alternatively, the Agulhas Ridge may have formed from extension at the fracture zone resulting in serpentinite diapirism (Bonatti, 1978), or volcanic construction resulting from extension and/or a robust magma source, such as the Shona Hotspot (Menard and Atwater, 1969; Kastens, 1987; Hartnady and le Roex, 1985).

Site 1088 is located at the northeastern end of the Agulhas Ridge, near the intersection of the fossil ridge transform (Fig. F5 and Fig. F7), where it is a broad topographic feature with 2250 m of relief. Site 1089 is located north of the Agulhas Ridge in the southern Cape Basin where the oceanic crust is older than magnetic Anomaly 34 (Upper Cretaceous; Fig. F6). Site 1090 is located on the southwest portion of the Agulhas Ridge, where it narrows considerably and the topography steepens and becomes more intricate.

Sites 1091 and 1092 are associated with Meteor Rise, which is one of the dominant topographic features in the southeast Atlantic and

F5. Position of Leg 177 sites relative to the gravity field of the Agulhas Basin, p. 39.

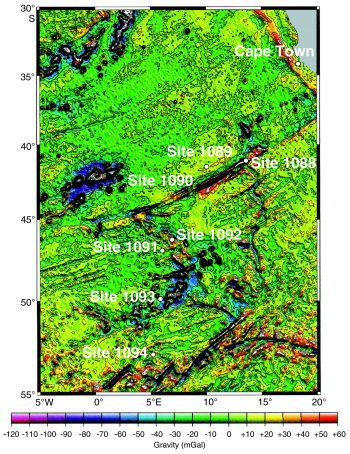

F6. Schematic tectonic map of the Agulhas Basin showing Leg 177 sites relative to seafloor magnetic anomalies, p. 40.

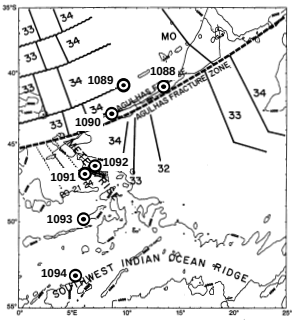

F7. Tectonic reconstruction of the South Atlantic during the late Paleocene and middle Eocene, p. 41.

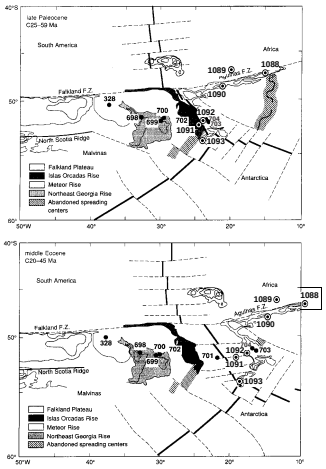

defines the westward limit of the Agulhas Basin (Fig. F5). This oval-shaped, aseismic plateau rises to water depths of 2000 m and consists of basement highs with intervening depositional basins. Meteor Rise is the conjugate feature of the Islas Orcadas Rise in the western South Atlantic and formed either by (1) effusive volcanism at the developing rift zone associated with the ridge jump from the Agulhas Basin to the west at ~62 Ma (Fig. F7; LaBrecque and Hayes, 1979; Mutter et al., 1988), or (2) passage of the Shona Hotspot across the Agulhas Fracture Zone and the subsequent ridge jump to the preweakened hotspot trace (Hartnady and le Roex, 1985). Site 1091 is located on the western flank of Meteor Rise on magnetic Anomalies 24–25 (early Eocene–late Paleocene), which represents the oldest oceanic crust between the Meteor Rise and the Mid-Atlantic Ridge (Fig. F6). Site 1092 is located on the north-central Meteor Rise (water depth 1974 m) and is probably underlain by volcanic basement of early Eocene age or older.

Site 1093 is associated with the Shona Ridge that was formed by the Shona Hotspot, which may presently reside between 50° and 52.5°S near an anomalously shallow segment of the Mid-Atlantic Ridge (Hartnady and le Roex, 1985; Douglass et al., 1995). Acoustic basement is anomalously smooth in the region of Site 1093, and is estimated to be located on late Miocene crust by extrapolating magnetic anomalies of Cande and Kent (1992). The southernmost Site 1094 is located in a small sedimentary basin north of Bouvet Island. This site is located close to the Bouvet Fracture Zone, where the basement age is not well defined from the available magnetic data.

HYDROGRAPHY

Leg 177 sites are situated along a north-south transect across the ACC (Fig. F1). The ACC consists of a cold, surface-water mass that surrounds Antarctica and contains complex fronts and upwelling/downwelling cells. In the South Atlantic, the ACC has a strongly banded velocity field and can be divided into three distinct zones separated by frontal boundaries (Peterson and Stramma, 1991). In the north, the ACC is bounded by the Subtropical Front (STF) that marks the northward limit of the Subantarctic Zone. Sites 1088, 1089, and 1090 are located in the northern Subantarctic Zone between the STF and the Subantarctic Front (SAF) to the south. Sites 1091 and 1092 are located in the PFZ that is bounded by the SAF to the north and the Polar Front (PF) to the south. The average width of the PFZ in the South Atlantic off Africa is 670 km, and it is centered at 45°S with a span of roughly ±2.5° latitude (Lutjeharms, 1985). The PFZ separates cold, nutrient-rich Antarctic surface water to the south from warmer, less nutrient-rich Subantarctic Surface Water to the north. The PFZ also represents a transition zone in sediment lithology from diatom ooze near the PF to a mixed siliceous-calcareous ooze near the SAF. South of the PF is the Antarctic Zone that is marked by cold, silica-rich Antarctic surface water. Site 1093 is located at ~50°S in the northern Antarctic Zone close to the present-day PF, and about 5° north of the average winter sea-ice edge. Site 1094 is located south of the PF in the ice-free Antarctic Zone, close to the average winter sea-ice edge.

The water depths of the sites range from 1974 to 4620 m (Fig. F2). The bathymetric distribution of sites intersects all major deep- and bottom-water masses in the Southern Ocean, including upper and lower Circumpolar Deep Water (CDW), NADW, and AABW. Two depth

transects were drilled on the Agulhas Ridge and Meteor Rise. Sites 1088, 1090, and 1089 form a depth transect at 2082, 3702, and 4620 m, respectively, from the crest of the Agulhas Ridge to the deep Cape Basin. On the Meteor Rise, Site 1092, Leg 114 Site 704, and Site 1091 form a depth transect at 1974, 2532, and 4363 m, respectively.

Sites 1088 (2082 m) and 1092 (1974 m) are the shallowest sites and are positioned near the interface of upper NADW and upper CDW. Site 1090 (3702 m) is near the interface of lower NADW and CDW. The remaining sites (1089, 1091, 1093, and 1094) are positioned within lower CDW, and fall along a linear trend marked by decreasing salinity and temperature toward the south, which may reflect the decreasing influence of NADW (Fig. F8).

F8. Temperature and salinity at water depths of Leg 177 sites, p. 42.

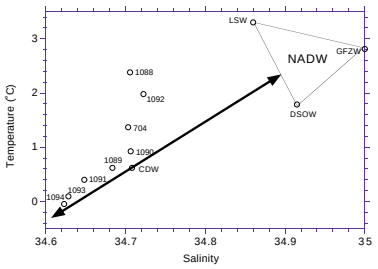

DRILLING STRATEGY

During the past several years, ODP has been drilling in the Atlantic Ocean to study past changes in Earth's climate. Leg 177 represents the southernmost anchor of sites needed to complete the Atlantic paleoceanographic transect. The strategy during Leg 177 was to drill a series of sites along a north-south transect that encompasses the past dynamic range of the Antarctic sea-ice field and frontal boundary movements within the ACC. Sites were also selected along a bathymetric gradient, ranging from 1974 to 4620 m, to study changes in deep-water circulation.

The drilling strategy included seven primary sites to recover expanded late Neogene sections across latitude and depth in the Subantarctic and Antarctic regions. We specifically targeted sites with high sedimentation rates on drift deposits and in the region of the circum-Antarctic opal belt (Fig. F9). Four of the sites (1089, 1091, 1093, and 1094) exhibit average sedimentation rates exceeding 100 m/m.y., offering the opportunity for paleoclimatic studies at millennial scale resolution or higher. The two southern sites (1093 and 1094) are the first to recover a complete composite section by triple-APC/XCB coring from the circum-Antarctic opal belt.

F9. Positions of Leg 177 sites relative to the depositional regimes in the basins of the southeast Atlantic Ocean, p. 43.

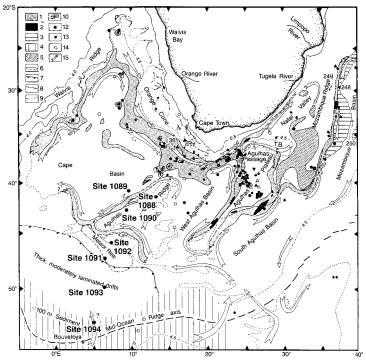

SCIENTIFIC OBJECTIVES

The broad scientific themes of Leg 177 were twofold:

1. Document the biostratigraphic, biogeographic, paleoceanographic, and paleoclimatic history of the Southern Ocean region during the Cenozoic, including the evolution and stability of the Antarctic cryosphere, and
2. Reconstruct paleoenvironmental records for the Quaternary and late Neogene with millennial or higher temporal resolution to better understand the role of the Southern Ocean in climate change on orbital and suborbital time scales.

Evolutionary History and Stability of the Antarctic Cryosphere

The Paleogene section at Site 1090 is well suited for paleoceanographic studies of the early Cenozoic because it is shallowly buried, continuously recovered, and well dated. Oxygen isotopic measure-

ments of foraminifers coupled with microfossil distribution and abundance patterns should provide insight into the growth and stability of the Antarctic ice sheet and the ACC during the Paleogene.

Development of the ACC and Its Associated Frontal Systems

Thermal isolation of the Antarctic continent was intimately linked to tectonic and paleoceanographic changes that led to the establishment of a zonal circulation system, the ACC (Kennett, 1977). Determining the timing and strength of thermal isolation is important for understanding polar heat transport and its effect on the development and stability of the Antarctic ice sheets. The establishment and expansion of the ACC has also influenced intermediate-, deep-, and bottom-water formation in the Southern Ocean. Together with sites previously drilled in the South Atlantic sector of the Southern Ocean (e.g., Sites 689, 690, 703, and 704), Sites 1088, 1090, and 1092 will permit us to study the development of the ACC during the Paleogene and early Neogene (Fig. F4). For the late Neogene, Leg 177 sites form a complete north-south transect from 41° to 53°S that is well suited for reconstructing the paleolatitudinal position of the PF, similar to studies conducted on piston cores from the late Quaternary (Prell et al., 1979; Morley, 1989; Howard and Prell, 1992).

History, Distribution, and Seasonal Variation of Sea Ice

Sea ice is presently characterized by rapid and large-scale seasonal variations, and it affects gas and heat exchange between ocean and atmosphere, ocean circulation and the formation of water masses by the rejection of salt, atmospheric circulation and wind speeds, surface albedo, and the biological production and distribution of organisms. Changes in sea-ice distribution undoubtedly influenced the Southern Hemisphere climate during the late Pleistocene. Analysis of sea-ice diagnostic taxa of siliceous microfossils in sediments from the southern sites (1091–1094) will be used to reconstruct the distribution and seasonality of sea ice in the Southern Ocean during the late Pliocene–Pleistocene.

History of Southern Ocean Primary Biological Productivity and Its Effect on Atmospheric pCO_2

During glacial periods, export production and accumulation rates of biogenic opal increased substantially within the PFZ and possibly were fueled by iron fertilization of surface water by enhanced eolian dust supply from periglacial Patagonian deserts (Kumar et al., 1995). Different opinions exist, however, regarding whether net productivity increased or remained the same in the Southern Ocean during the last glaciation (Kumar et al., 1995; Frank et al., 1996, in press; Francois et al., 1997). Leg 177 sediments will be important for testing various hypotheses related to glacial–interglacial changes in productivity and nutrient cycling in the Southern Ocean.

Evolution of the Circum-Antarctic Opal Belt and Its Effect on the Global Marine Silica Budget

Since at least ~36 Ma, the Southern Ocean has acted as a major sink for biogenic opal, reflecting increased surface-water bioproductivity as a result of polar cooling and upwelling in the circum-Antarctic (Baldauf et al., 1992). Expansion of the opal belt may have significantly influenced the distribution of nutrients in the ocean. During Leg 177, two sites (1093 and 1094) were drilled by APC in the circum-Antarctic opal belt, yielding continuous late Pliocene–Pleistocene sequences. Study of these thick sequences of diatom ooze, including laminated diatom mats, will permit estimation of opal accumulation rates, which will be important for assessing the role of these deposits in the dissolved silica budget of the world's oceans.

Changes in the Production and Mixing Ratios of Various Deep- and Bottom-Water Masses

The Southern Ocean is unique in that its deep water (mainly CDW) is a mixture of deep-water masses from all ocean basins (Fig. **F3**). As such, monitoring changes in the chemistry of Southern Ocean deep water provides a means to reconstruct changes in the mean water-mass composition of the deep ocean. The Southern Ocean is perhaps the only region where fluctuations in the production rate of NADW can be monitored unambiguously (Oppo and Fairbanks, 1987; Charles and Fairbanks, 1992). The Atlantic sector of the Southern Ocean represents the initial entry point of NADW into the ACC and, therefore, is highly sensitive to changes in the strength of the NADW conveyor. The bathymetric distribution of Leg 177 sites is ideal for reconstructing the long-term evolution of the dominant subsurface water masses in the Southern Ocean, and for assessing their role in global climate change (Fig. **F2**).

Timing and Response of Southern Ocean Surface and Deep Waters to Orbital Forcing

Relatively little is known about the interhemispheric phase response (lead, lag, or in-phase) between the high-latitude Northern and Southern Hemispheres to orbital forcing of climate. Imbrie et al. (1989, 1992) suggested an early response of surface and deep waters in the Southern Ocean relative to climate responses in other regions of the world ocean. This lead has also been confirmed by other studies (Labeyrie et al., 1986; Howard and Prell, 1992; Bender et al., 1994; Sowers and Bender, 1995; Charles et al., 1996), implying that the Antarctic region played a key role in the driving mechanism of glacial–interglacial climate change during the last climatic cycle. It is not known, however, if this early response of the Southern Ocean was characteristic of the entire mid- to late Pleistocene, which was dominated by 100-k.y. cyclicity, or whether this phase relationship also extends back into the early Pleistocene and Pliocene interval dominated by 41-k.y. cyclicity. Leg 177 sediments (especially Sites 1089, 1091, 1093, and 1094) will provide the material needed to study the response of the Southern Ocean to orbital forcing and its phase relationships with climatic changes in other regions.

Suborbital Climate Change by Comparison with Ice Cores and Other Marine Sediment Records

Highly expanded sections were recovered at four sites (1089, 1091, 1093, and 1094), which permit the study of climatic variations in the Southern Ocean region at suborbital (millennial) time scales. These sedimentary sequences represent the Southern Hemisphere analogs to the North Atlantic drift deposits recovered during ODP Legs 162 and 172. These cores will allow us to determine whether abrupt climate changes, similar to those documented in Greenland ice cores (Dansgaard et al., 1993) and marine records from the high-latitude North Atlantic (Bond et al., 1993; Bond and Lotti, 1995), have occurred in the southern high latitudes. Expanded sections along a north-south transect from 41° to 53°S will also permit study of the structure of glacial–interglacial transitions in the Southern Ocean, including the trajectories of deglacial meltwater from the Antarctic continent (Labeyrie et al., 1986). Lastly, correlation of climate proxies between Leg 177 sediment cores and ice cores from Greenland and Antarctica, which now span the last 400 k.y. at Vostok (Antarctica; Petit et al., 1997), will reveal the phase relationships between various variables in the atmosphere and ocean systems, and may contribute to identifying the mechanisms responsible for rapid climate change.

Southern High-Latitude Calcareous and Siliceous Biozonations

ODP Legs 113, 114, 119, and 120 provided an enormous improvement in southern high-latitude stratigraphy, but further refinement of these biozonations is desirable. Sediments drilled during Leg 177 provide the opportunity to improve dating of Neogene and Paleogene biostratigraphic markers by correlation with the geomagnetic polarity time scale and orbitally tuned paleoenvironmental signals. In addition, Leg 177 sequences permit study of evolutionary processes (patterns, modes, and timing of speciation and diversification), the development of Southern Hemisphere bioprovinces (e.g., endemism), and the response of the biota to long- and short-term environmental changes.

Early Low-Temperature Chert Diagenesis in Sediment from the Antarctic Opal Belt

Although chert is ubiquitous in the geologic record, few examples of recent porcellanites exist except those found in diatom deposits of the Southern Ocean (Bohrmann et al., 1990, 1994). The very early transformation of silica from opal-A to opal-CT (strongly cemented porcellanites) has been observed at shallow burial depth in a low-temperature environment in cores recovered near Site 1094 (Bohrmann et al., 1990, 1994). By sampling interstitial water and solid phases at Site 1094, it will be possible to study the nature and rates of silica diagenetic reactions in these young sediments. In addition, measurements of physical properties and heat flow at Site 1094 will better characterize the conditions under which these young porcellanites were formed.

Geomagnetic Paleointensity

U-channel sampling of Leg 177 cores will be used to construct continuous records of variations in the intensity of Earth's magnetic field. Comparison of these signals from the high-latitude Southern Hemisphere with similar results obtained from the North Atlantic will test whether these observed variations reflect changes in the intensity of Earth's dipole field. If so, then these dipolar paleointensity changes will provide a powerful stratigraphic tool that can be used to correlate cores globally. In addition, the high sedimentation rates of Leg 177 sites offer the opportunity to study transitional field behavior at polarity reversal boundaries and, perhaps, brief excursions and secular variation of the magnetic field in the high-latitude Southern Hemisphere.

PRINCIPAL RESULTS

Site 1088

Site 1088 (proposed site TSO-2B) is located on the Agulhas Ridge in the southeast Atlantic Ocean at a water depth of 2082 m (Figs. **F1, F5;** Table **T1**). This bathymetric setting places the site near the interface between NADW and CDW (Fig. **F2**). The primary objective of Site 1088 was to recover a long Cenozoic carbonate sequence that could be used to study paleoceanographic change near the Subtropical Front, which today is located north of the Agulhas Ridge.

Three holes were drilled representing a combined 223.4-m section (Table **T2,** also in ASCII format in the **TABLES** directory), consisting predominantly of carbonate microfossils representing sediment deposition from the Holocene to middle Miocene (~13–14 Ma). The sediments recovered are predominantly nannofossil ooze, foraminifer-bearing nannofossil ooze, foraminifer nannofossil ooze, and nannofossil foraminifer ooze. Carbonate percentages vary from 85 to 95 wt% and the abundance of foraminifers decreases progressively downhole.

Sedimentation rates average 10 m/m.y. in the Pleistocene, 7 m/m.y. in the Pliocene, 17–30 m/m.y. in the late Miocene, and 11 m/m.y. in the middle Miocene section (Fig. **F10**). Only two short depth intervals (0–5.5 and 122–129 m composite depth [mcd]) were cored in more than one hole and, as a result, the continuity of the sedimentary section could not be documented and a continuous spliced record was not constructed. Magnetic inclinations were low and less than expected for the site location (60°) and declinations were highly scattered, suggesting drill-string remagnetization of the core.

High-resolution samples (one per section) of interstitial waters were taken in Hole 1088B, between 1.5 and 51 meters below seafloor (mbsf), for major-ion and stable isotopic analysis. Many of the results from these samples must await shore-based analyses, but shipboard analyses show that, as expected, chlorinity increases downhole, with a slight local maximum at ~40 mbsf that probably resulted from diffusion of high-salinity water associated with the last glaciation.

Variations in diffuse spectral reflectance suggest the presence of marine isotopic Stages (MISs) 1 to 13 in Core 177-1088B-1H in the top 5.5 mbsf. Although the upper Pleistocene sequence was deposited with relatively low sedimentation rates (~10 m/m.y.), the record is similar to that from Site 704 to the south (47°S, 7.5°E, 2532 m), and comparison of the two holes will be useful for studying glacial–interglacial changes

T2. Coring summary for Site 1088, **p. 55.**

F10. Age-depth plots for Leg 177 Sites 1088, 1090, and 1092 for the middle Eocene–Pleistocene, **p. 44.**

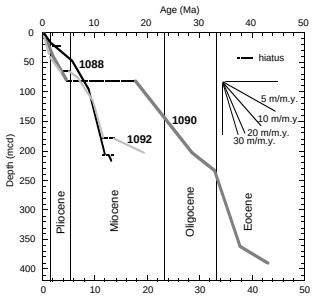

in NADW flux to the Southern Ocean. Sediments recovered at Site 1088 will also be useful for studying paleoceanographic changes during the Neogene at a temporal resolution of 10 to 100 k.y. The 140-m section of upper Miocene sediments recovered in Holes 1088B and 1088C is particularly promising in that variations in magnetic susceptibility show evidence of cyclicity in the Milankovitch frequency band. Although a complete composite section was not retrieved, the sediments should provide a detailed record of late Miocene changes in surface- and deep-water circulation.

Site 1089

Site 1089 (proposed site SubSAT-1B) is located in the southern Cape Basin in the southeast Atlantic Ocean, close to the northern flank of the Agulhas Ridge (Figs. **F1, F5;** Table **T1**). High sedimentation rates (84–180 m/m.y.) resulted in an expanded sedimentary sequence that is ideally suited for studying environmental changes in response to climate variability on orbital and suborbital time scales. Given these high sedimentation rates, Site 1089 is comparable to the North Atlantic drift deposits drilled during Legs 162 and 172, and it will be useful for determining the response of the Southern Ocean to orbital forcing and the phase relationships to climate change in the North Atlantic region. The high sedimentation rates at Site 1089 will also permit detailed correlation between marine sediment records and ice-core records, especially the Vostok ice-core signal.

A 264.9-m-thick sedimentary section, spanning the interval from the Holocene to late Pliocene (~2.4 Ma), was recovered at Site 1089 (Table **T3,** also in ASCII format in the **TABLES** directory). The sediments are predominantly composed of diatoms, nannofossils, and terrigenous mud in varying proportions. Calcium carbonate contents in Hole 1089A average 27.0 wt% and range from 0.6 to 69.3 wt%, whereas total organic carbon (TOC) varies between 0 and 0.82 wt% with an average value of 0.43 wt%. Although Site 1089 is deep (4620 m) and near the carbonate compensation depth (CCD), foraminifer abundance is fairly constant downhole to ~220 mbsf, below which it drops to zero. It should be possible, therefore, to produce a stable isotopic stratigraphy in the upper 220 mbsf. No major lithologic boundaries are present within Site 1089, and only one lithologic unit was identified.

T3. Coring summary for Site 1089, **p. 56.**

The upper 100 m of the section, representing approximately the Brunhes Chron (0.78 Ma to present), is nearly complete. Variations in spectral color reflectance, $CaCO_3$, bulk density, and magnetic susceptibility permit the prediction of glacial and interglacial MISs 1 to 19, constrained by diatom and calcareous nannofossil biostratigraphy (Fig. **F11**). With four holes drilled to more than 118 mbsf, a continuous spliced record was constructed to a depth of 94 mcd by aligning features in the records of closely spaced physical properties measurements. Core logging data obtained at 2- to 6-cm sampling intervals show cyclic variations at Milankovitch frequencies as well as variations at higher (sub-Milankovitch) frequencies. Postcruise analysis of these signals will be useful for delineating climatic variability on these time scales. Preservation of remanent magnetization is good in the upper 100 m and preliminary results are encouraging for constructing the first detailed Southern Hemisphere record of geomagnetic paleointensity during the Brunhes Chron.

F11. Correlation of red reflectance from Sites 1089, 1091, 1093, and 1094, **p. 45.**

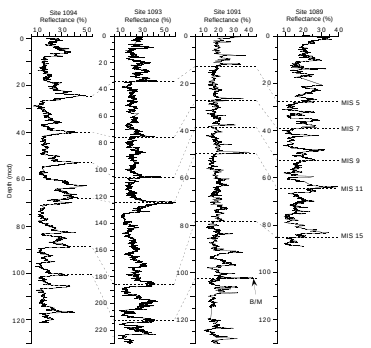

A series of 3- to 15-m-thick deformed sediment units, possibly slump or slide deposits, was cored between 95 and 156 mcd. Soft-sediment

deformation is manifested in the sediment by dipping and/or contorted beds, sharp color contacts, and microfaults. The Brunhes/Matuyama boundary is present in the interval from 105 to 114 mbsf in Hole 1089B; however, the transition is not well preserved because of soft-sediment deformation that affects the interval from the lowest Brunhes Chron to the top of the Jaramillo Subchron. Even within the deformed sediment interval, however, laminations and burrow structures are preserved and suggest that the stratigraphic section is relatively intact. Postcruise analysis may allow us to piece together a composite section that eliminates several of the deformed intervals.

Polarity transitions in cores from Hole 1089B define the lower boundary of the Jaramillo Subchron at 151.6–153.6 mbsf, and the upper and lower boundaries of the Olduvai Subchron at 213.8–215.8 and 225.5–227.6 mbsf, respectively. We place the Pliocene/Pleistocene boundary at ~229 mcd at Site 1089.

Biostratigraphic and magnetic datum levels provide an age-depth relationship that indicates continuous sedimentation at Site 1089 since the late Pliocene (~2.4 Ma). Sedimentation rates average ~128 m/m.y. in the upper 94 mcd (~0.7 Ma), ~180 m/m.y. between 94 and 156 mcd (~0.65–1 Ma), ~110 m/m.y. from 156 to 230 mcd (1–1.8 Ma), and ~84 m/m.y. from 230 to 280.6 mcd (1.7–2.4 Ma) (Fig. **F12**). The high–sedimentation-rate interval from 94 to 156 mcd corresponds to the disturbed section, but the superposition of biostratigraphic datums is as expected in this interval.

Interstitial water profiles from Site 1089 indicate reducing conditions such that sulfate reduction is complete by 50 mbsf and methane concentrations are high below this depth in the hole. The Ca^{2+} profile shows a dramatic decrease in the sulfate reduction zone, reaching a minimum at 50 mbsf. This Ca^{2+} decrease results in unusually high Mg/Ca values because Mg^{2+} concentrations remain near seawater values.

F12. Age-depth plots for Leg 177 Sites 1089, 1091, 1093, and 1094 for the Pliocene–Pleistocene, p. 46.

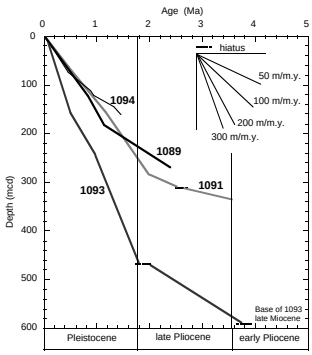

Site 1090

Site 1090 (proposed site TSO-3C) is located in the central part of the Subantarctic Zone on the southern flank of the Agulhas Ridge (Figs. **F1, F5;** Table **T1**). The water depth (3702 m) places it near the boundary between NADW and underlying lower CDW (Fig. **F2**), and above the CCD. Together with Sites 1088 (2082 m) and 1089 (4620 m) it forms a depth transect that intersects most of the major water masses of the South Atlantic. Five holes were drilled to 397.5 mbsf, spanning the Holocene to middle Eocene (~46 Ma), and including a ~14-m.y. hiatus at ~70 mcd that includes much of the lower Pliocene to lower Miocene record (Table **T4,** also in ASCII format in the **TABLES** directory). We constructed a continuous spliced record to 212 mcd (and perhaps 245 mcd), corresponding to the early Oligocene.

T4. Coring summary for Site 1090, p. 58.

Quaternary sediments, consisting of alternating foraminifer nannofossil ooze, diatom-bearing nannofossil ooze, and mud-bearing nannofossil ooze, extend to 44 mcd with sedimentation rates averaging 33 m/m.y. (Fig. **F10**). In Hole 1090C, the Brunhes/Matuyama boundary (0.78 Ma) lies between 18.0 and 19.2 mbsf. The top (0.99 Ma) and base (1.07 Ma) of the Jaramillo Subchron lie in the 24.6–25.4 and 27.7–28.4 mbsf intervals, respectively. Two hiatuses may be present between 0.42 and 0.64 Ma and from 1.3 to 1.8 Ma; shore-based analysis is needed for confirmation. Variations in color reflectance permit the identification of glacial and interglacial MISs 1 to 12 in the upper 18 mcd, supported by identification of biostratigraphic events. MIS 11 is particularly promi-

nent because of its exceptionally white color and high nannofossil carbonate content. Cyclic variations in the color reflectance (Fig. **F13**) and gamma-ray attenuation (GRA) bulk density signals may reflect the shift from the 41-k.y. world to the 100-k.y. world at ~30 mcd.

The upper Pliocene sequence was deposited at sedimentation rates of 11 to 13 m/m.y. In Hole 1090C, the top (1.77 Ma) and base (1.99 Ma) of the Olduvai Subchron were recognized in the 35.3–36.0 and 37.6–38.2 mbsf intervals, respectively. Diatom biostratigraphy indicates a hiatus at ~55 mcd that spans the Matuyama/Gauss boundary from 2.5 to 2.6 Ma.

A pronounced hiatus was encountered at ~70 mcd, marked by a lithologic change from white nannofossil ooze to reddish mud-rich nannofossil ooze. Below the hiatus, a tephra sequence composed of vitric ash and admixed with hemipelagic biogenic and terrigenous particles was recovered. Sedimentary structures and textural features suggest deposition of the tephra components by turbidity currents. Sediments above the hiatus are early Pliocene in age and contain manganese nodules. Below the hiatus, approximately 330 m of sediment was recovered consisting of mud-bearing diatom ooze and mud- and diatom-bearing nannofossil ooze and chalk ranging in age from early Miocene to middle Eocene. Sedimentation rates averaged 10 m/m.y. in the early Miocene to middle Eocene, and increased to 30 m/m.y. during deposition of upper Eocene opal-rich sediments that include intervals of well-laminated diatom ooze. Middle Eocene carbonate-rich sediments were deposited at lower sedimentation rates (~10 m/m.y.) (Fig. **F10**).

The potential for paleomagnetic reversal stratigraphy below the hiatus is excellent, even in the cores that were recovered by XCB. Site 1090 holds much promise for detailed correlations of biostratigraphic datums to the geomagnetic polarity time scale during the early Miocene to middle Eocene.

Interstitial waters of Site 1090 can be characterized as suboxic, with sulfate reduction occurring at very low rates. Interstitial water profiles indicate a sharp break at ~290 mbsf, corresponding to an impermeable layer (presumably a chert layer recovered as fragments in the top of Core 177-1090B-32X) that posed a barrier to diffusion of interstitial waters. Interstitial water regimes above and below the diffusion barrier evolved independently because of the isolation imposed by the impermeable chert.

In summary, the importance of Site 1090 is twofold: (1) the Pleistocene to upper Pliocene section deposited at sedimentation rates of 30 m/m.y. will be useful for the reconstruction of the high-latitude Southern Hemisphere paleoclimate at moderate temporal resolution, and (2) the middle Eocene–lower Miocene section below the hiatus will potentially be an important section for biomagnetostratigraphic correlations, astronomical tuning of time scales, and paleoceanographic studies of the late Paleogene and early Miocene. Cyclic variations in lithology may permit the development of an astronomically tuned time scale for the late Paleogene–early Neogene, similar to that developed during Leg 154 (Weedon et al., 1997). The Paleogene sequence is especially significant because it spans the time period associated with the onset of Antarctic glaciations, early production of cold Antarctic surface and bottom waters, and paleogeographic changes (e.g., the separation of Australia and Antarctica and opening of the Drake Passage) that led to the establishment of the ACC (Kennett, 1977).

F13. Percent blue and red reflectance at Site 1090, **p. 47.**

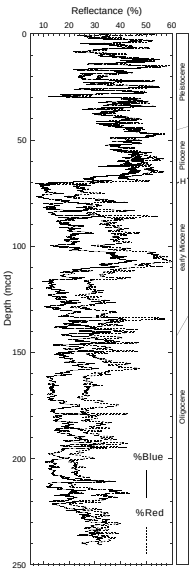

Site 1091

Site 1091 (proposed site TSO-5C) is located in the PFZ on the western flank of the Meteor Rise, ~2° north of the present-day PF (Fig. F1; Table T1). The water depth of 4363 m places the site within lower CDW (Fig. F2). The primary objective at Site 1091 was to recover a high-resolution Pliocene–Pleistocene sequence within the PFZ that could be used to study (1) the history of migration of the PF and Antarctic sea-ice field, (2) glacial–interglacial changes in biological export production, (3) millennial scale climate oscillations recorded in the Southern Ocean sediments and their relation to climate changes documented in North Atlantic sediments and polar ice cores, (4) the melting history of the Antarctic ice sheet and associated meltwater plumes during glacial–interglacial cycles of the late Pleistocene, and (5) changes in lower CDW properties in response to variable NADW flux to the Southern Ocean.

Five holes were drilled at Site 1091 to obtain a complete section that was deposited with high sedimentation rates. Hole 1091A was the deepest hole cored with the APC to a depth of 310.9 mbsf with a recovery rate of 90% (Table T5, also in ASCII format in the TABLES directory). Basal sediments are early Pliocene (~3.4 Ma) in age. The remaining four holes provided overlap to fill coring gaps in Hole 1091A and resulted in a continuous spliced section to 234 mcd (~1.7 Ma). One lithologic unit was defined consisting of diatom-rich ooze, with minor and varying amounts of nannofossils, foraminifers, and mud. Calcium carbonate contents in Hole 1091A are relatively low, ranging from 0.2 to 58.9 wt% with an average value of 5.7 wt%. Despite the low carbonate content, planktic and benthic foraminifers are sufficiently abundant in most samples for stable isotopic analysis. TOC contents vary between 0.17 and 0.91 wt% with an average value of 0.60 wt%.

T5. Coring summary for Site 1091, p. 60.

Because of the proximity of Site 1091 to the PF, the underlying sediments should document past movements of this front. Extensive laminated *Thalassiothrix* diatom-mat deposits, analogous to those recovered in sediments from the eastern equatorial Pacific Ocean (Kemp and Baldauf, 1993), are present at several horizons. Sedimentation rates were high, averaging 140 m/m.y. during the Pleistocene (Fig. F12). Carbonate-rich interglacial periods are easily recognized by their brightness in the signal of diffuse color reflectance (Fig. F11). For example, peaks in red reflectance (650–750 nm) at 26.5, 38, and 49 mcd correlate to MISs 7, 9, and 11, respectively, which is supported by biostratigraphic information. Downhole variations of physical properties (diffuse spectral reflectance, GRA bulk density, and magnetic susceptibility) show distinct evidence of cyclicity at Milankovitch and suborbital time scales.

A transition in sedimentation occurred at ~2.0 Ma. Sediments older than ~2.0 Ma were marked by relatively low opal content and sedimentation rates, whereas younger sediments were diatom rich and accumulated at high sedimentation rates. This event represents an important change in opal export production in the Southern Ocean during the latest Pliocene and was recognized previously at Site 704 (Froelich et al., 1991a; Hodell and Venz, 1992), which is located only ~60 km to the east of Site 1091 on the crest of Meteor Rise.

Natural remanent magnetization (NRM) at Site 1091 was affected by a drill-string overprint that was largely removed at peak demagnetization fields in excess of 10 mT; however, the resulting inclination values are highly scattered especially during the Matuyama Chron. The Brunhes/Matuyama boundary can be identified in the 95.5- to 102.4-mbsf

interval in Hole 1091A. The Matuyama/Gauss boundary is tentatively identified between 285.8 and 288.7 mbsf in Hole 1091A.

The redox conditions in Site 1091 sediments can be classified as reducing on the basis of dissolved H_2S (by scent), but sulfate concentrations decrease only modestly from near–bottom-water concentrations of ~28 mM at 4 mbsf to ~22 mM around 300 mbsf (Fig. **F14**).

In summary, Site 1091 represents the midpoint (at 47°S) of a Pliocene–Pleistocene north-south transect across the ACC (Fig. **F15**). The high sedimentation rates during the Pleistocene at Site 1091 (~145 m/m.y.) complement the records obtained at Sites 1089 (~128 m/m.y.), 1093 (~250 m/m.y.), and 1094 (~140 m/m.y.) at 41°, 50°, and 53°S, respectively. This north-south transect of sites with high sedimentation rates will be used to reconstruct the past movement of frontal boundaries and the Antarctic sea-ice field during the Pliocene–Pleistocene, and to study the impact of climate variability on processes in the Southern Ocean on orbital and suborbital (millennial) time scales.

Site 1092

Site 1092 (proposed site SubSAT-3B) is located on the northern Meteor Rise in the PFZ, ~3° north of the present-day position of the PF (Fig. **F1**; Table **T1**). The water depth (1974 m) places the site above the regional carbonate lysocline and CCD and within a mixing zone between upper NADW and CDW (Fig. **F2**). The impetus for drilling Site 1092 came from the record obtained at Site 704, located only 34 nmi southeast of Site 1092. The goal of Site 1092 was to improve upon Site 704 by recovering a continuous upper Miocene to Pleistocene section.

Three holes were drilled by the APC to depths of 188.5 mbsf (Hole 1092A), 168.9 mbsf (Hole 1092B), and 165.5 mbsf (Hole 1092C) with high recovery in all holes (97%, 86%, and 91%, respectively; Table **T6,** also in ASCII format in the **TABLES** directory). A continuous spliced section was constructed to 188.5 mcd. The sediments consist of pale brown green to pure white nannofossil ooze with varying mixtures of diatom and foraminifer ooze and mud. One lithologic unit was defined and divided into two subunits at ~54 mcd on the basis of a change from alternating calcareous and diatom ooze above to dominantly nannofossil ooze below. Calcium carbonate is present throughout the sediment column, varying from 16.7 to 94.6 wt% with an average content of 80.2 wt%. TOC contents vary between 0 and 0.70 wt% with an average value of 0.16 wt%.

The section at Site 1092 ranges in age from the Pleistocene to the early Miocene. Sedimentation rates varied from ~10 to ~29 m/m.y. during the Pliocene–Pleistocene and between ~4 and ~38 m/m.y. during the Miocene (Fig. **F10**). The pattern of sedimentation-rate change at Site 1092 is similar to Site 704, except that Site 1092 rates are considerably lower. For example, the Pleistocene section at Site 1092 appears to be condensed by ~50% relative to Site 704. The pattern of sedimentation rate is also similar to that at Site 1088, including the hiatus in the middle Miocene, with the exception that the lower Pleistocene section is more expanded at Site 1092. Winnowing of sediment is documented in the upper and mid-Pleistocene sections, as indicated by well-sorted foraminifer sands and reduced sedimentation rates averaging 10 m/m.y. Several hiatuses punctuate the sediment record at Site 1092: (1) a lower Pliocene hiatus at ~65 mcd spans the interval from ~3.8 to 4.6 Ma, (2) one or more hiatuses are present across the Miocene/Pliocene boundary

F14. Interstitial water profiles from Sites 1091, 1093, and 1094, **p. 48.**

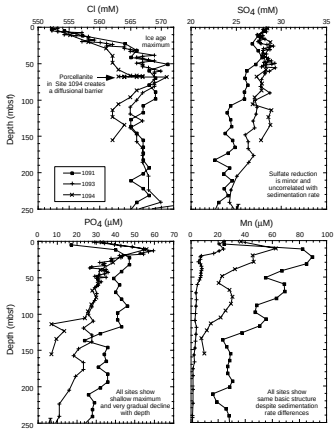

F15. Lithologic and paleomagnetic summary of Sites 1089, 1091, 1093, and 1094, **p. 49.**

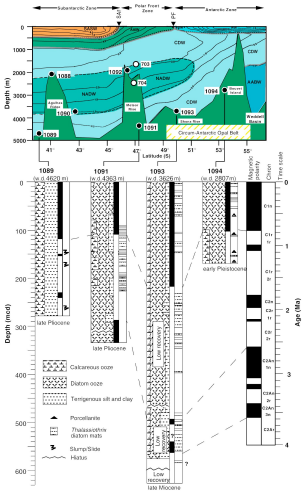

T6. Coring summary for Site 1092, **p. 62.**

that was tentatively placed between 70 and 75 mcd, and (3) a hiatus at ~178 mcd spans the earliest late Miocene to the middle middle Miocene from ~11 to 13 Ma (Fig. F10).

The paleomagnetic inclination records are highly discontinuous in the upper 60 mbsf because of drilling disturbance in poorly consolidated nannofossil ooze. Below 60 mbsf, the polarity reversal stratigraphy is well resolved for the early Pliocene sequence and a particularly good upper Miocene sequence. Correlation of the polarity sequence at Site 1092 awaits detailed shore-based biostratigraphy.

The redox characteristics of Site 1092 can be characterized as generally oxic or suboxic throughout the section. The major cations (Ca, Mg, and Sr) in interstitial waters vary similarly to those from Site 704 (Froelich et al., 1991b).

Measurements of physical properties show evidence of distinct cyclicity throughout the record. In the upper 35 mcd, large-amplitude variations in color reflectance mirror alternations between Pleistocene siliceous and carbonate sediments, whereas the signal is dampened below in sediments dominated by nannofossil ooze. Lithologic cyclicity in the upper Miocene section of Site 1092 may offer the opportunity to test the new late Miocene time scale derived by Shackleton and Crowhurst (1997) from the Site 926 (Leg 154) sedimentary record.

Site 1093

Site 1093 (proposed site TSO-6A) is located north of Shona Ridge, near the present PF and north of the average winter sea-ice edge (Fig. F1; Table T1). The site is characterized by moderately laminated pelagic sediments deposited at high sedimentation rates (~250 m/m.y.) within the circum-Antarctic opal belt (Figs. F12, F15). The high temporal resolution of biosiliceous sediment offers an excellent opportunity for paleoceanographic studies on millennial–centennial time scales over the last 1 m.y. At Site 1093, sediment cores were recovered for the first time from the circum-Antarctic opal belt in multiple APC holes, permitting the construction of a complete composite section. At 3626-m water depth, the site is located within lower CDW (Fig. F2).

Six holes were drilled with a maximum penetration of 597.7 mbsf (Table T7, also in ASCII format in the TABLES directory). A continuous spliced section was constructed to a depth of 252 mcd, representing the early Pleistocene (~1.0 Ma) to Holocene. For Holes 1093A and 1093B, the Brunhes/Matuyama boundary (0.78 Ma) was found in the interval between 205 and 210 mcd, yielding an average sedimentation rate of ~250 m/m.y. (Figs. F12, F15). Shipboard multisensor track (MST) data (natural gamma radiation [NGR], GRA bulk density, and magnetic susceptibility) and diffuse color reflectance document lithologic variations on orbital and suborbital time scales, which can be used to interpret climatic changes during the past 1.0 m.y. (Fig. F11). Preliminary age models derived from shipboard MST results indicate that in some interglacial intervals sedimentation rates were as high as 300 to 700 m/m.y., permitting a temporal sampling resolution of 100 yr or less!

The lithology at Site 1093 consists almost exclusively of diatom ooze, including distinctive intervals of laminated diatom mats up to several meters thick (Fig. F16). Calcium carbonate contents are generally low (<15 wt%) with occasional peaks of as high as 56.9 wt%. Despite the low carbonate content, core-catcher samples indicate that a nearly continuous planktic foraminifer isotopic stratigraphy (*Neogloboquadrina*

T7. Coring summary for Site 1093, p. 64.

F16. Laminated diatom mat (interval 177-1093A-23H-4, 78–120 cm), p. 50.

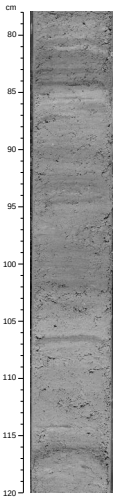

pachyderma sinistral) and a more-or-less continuous benthic stable isotopic record should be possible over the last 1 m.y.

Relatively carbonate-rich interglacial intervals are recognized by their brightness in the diffuse color reflectance signal (Fig. F11). On this basis, we were able to predict MISs 1 through 11 (~400 k.y.). MIS 11, at ~124 mcd, stands out as the brightest, most carbonate-rich interglacial interval of the Pleistocene section. The transition from glacial MIS 12 to interglacial MIS 11 (Termination V) occurs over an 8-m interval (from ~133 to 125 mcd) and is marked by a thick laminated interval of *Thalassiothrix* diatom mats. This expanded interval provides an unprecedented opportunity to study abrupt climate changes associated with Termination V.

The recovery of the deeper section below ~255 mcd, averaging only 26%, was disappointingly low in Hole 1093D. This is thought to be the result of thick intervals of laminated diatom mats that were difficult to recover using the APC and particularly the XCB coring systems. Apparently, a brief hiatus (spanning 0.2 m.y.) marks the Pliocene/Pleistocene boundary, and sedimentation rates were lower (57 m/m.y.) below this level. A hiatus spanning ~2.5 m.y. also marks the latest early Pliocene to latest late Miocene. The oldest sediment recovered at 595 mcd was latest Miocene (6.3–6.9 Ma) in age and contained a *Neobrunia mirabilis* diatom ooze with similar composition to that recovered at ODP Site 701 (Fig. F12).

Closely spaced (one per section) interstitial water samples were taken from cores from Hole 1093A between 0 and 63 mbsf for major-ion and stable isotopic analysis. One to three samples per core were taken at Holes 1093A and 1093D to a maximum depth of 498 mbsf. Shipboard analyses show a chlorinity increase downhole, with a well-defined Cl^- maximum in the interval from 50 to 60 mbsf, probably resulting from diffusion of higher salinity water associated with the last glaciation. The chloride profile is identical (within analytical uncertainty) to its lower resolution counterpart from Site 1091 (Fig. F14). Both sites are characterized by high sedimentation rates, and the presence of diatom mats may be responsible for creating such a distinct chloride maximum. Additional shore-based isotopic analyses and modeling of interstitial water profiles may permit the estimation of the oxygen isotopic composition and salinity of bottom waters at Site 1093 during the last Ice Age.

Hole 1093D was wireline-logged between 70 and 560 mbsf using the triple combination tool and the geological high-sensitivity magnetic tool. Good quality resistivity, NGR, and magnetic susceptibility data were obtained that should permit core-log integration using the MST core-logging data. The magnetic susceptibility record obtained from the Pliocene section of Site 1093 shows close similarities to the Pliocene record obtained at Site 1092, deposited at lower sedimentation rates.

In summary, the purpose of Site 1093 was to obtain an expanded record of biosiliceous sediments near the present-day position of the PF to study past changes in Antarctic surface-water properties and sea-ice extent. We succeeded in obtaining Pleistocene sediments that were deposited at the highest sedimentation rates yet recovered in any pelagic deep-sea section, affording the opportunity to study paleoceanographic processes in response to climate variability on millennial and even centennial time scales. In particular, the high temporal resolution of the sedimentary record will permit detailed correlation of the paleoceanographic history at Site 1093 with climate signals from the Greenland and Antarctic ice cores.

Site 1094

Site 1094 (proposed site TSO-7C) is located in a small sedimentary basin north of Bouvet Island (Fig. F1; Table T1). It was the highest latitude site drilled during Leg 177 and represents the southernmost anchor of sites drilled along a north-south transect across the ACC. The site is located in the southern part of the ice-free Antarctic Zone, but it was covered by sea ice during the last glaciation and preceding glacial intervals. The water depth of 2807 m places the site within the core of CDW (Fig. F2).

Four APC holes were drilled to depths of 159.6 mbsf (Hole 1094A), 38.0 mbsf (Hole 1094B), 73.1 mbsf (Hole 1094C), and 171.1 mbsf (Hole 1094D; Table T8, also in ASCII format in the TABLES directory). The oldest sediments recovered are Pleistocene in age (~1.4 to 1.5 Ma) and the section consists predominantly of olive gray to gray diatom ooze, with minor and varying amounts of foraminifers, nannofossils, and siliciclastic mud. A continuous spliced section was constructed to ~121 mcd, representing the last 1 m.y., with one gap at the bottom of Core 177-1094A-7H.

T8. Coring summary for Site 1094, p. 67.

Lithologic variations (as expressed by lithologic compositional signals of magnetic susceptibility, GRA bulk density, color reflectance, NGR, and geochemistry) reflect in great detail the glacial and interglacial cycles of the late Pleistocene (Fig. F17). MISs 1–12 are readily identifiable in the upper 80 mcd. Glacial intervals are marked by relatively high magnetic susceptibility, high NGR, low GRA bulk density, and low color reflectance (450–550 nm). Glacial terminations are marked by abrupt decreases of magnetic susceptibility and NGR and by increases in GRA bulk density and color reflectance. Sedimentation rates averaged ~140 m/m.y. during deposition of the diatom-dominated middle to upper Pleistocene sequence above ~80 mcd (Fig. F12). Below MIS 12, sedimentation rates decreased to ~91 m/m.y. during the early mid- and early Pleistocene. The transition between the Brunhes and Matuyama Chrons is identified between 98.20 and 101.58 mcd in Hole 1094A (Fig. F15).

F17. Site 1094 blue reflectance, magnetic susceptibility, bulk density, and natural gamma radiation, p. 51.

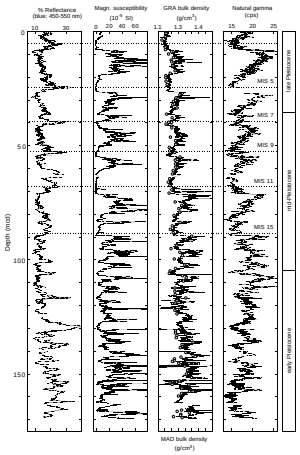

Fragments of porcellanite layers (opal-CT) were recovered at 68 mbsf (Holes 1094A and 1094D), 104 mbsf (Hole 1094A), and 164 mbsf (Hole 1094D), and an individual loaf-shaped porcellanite concretion was found at 141 mbsf (Hole 1094A). These porcellanite layers were also detected in Parasound sediment echosounding lines by high-amplitude reflectors. The upper porcellanite horizon occurs in the lower portion of MIS 11 and is the same as that previously described in piston cores from this area (Bohrmann et al., 1994). An anomalously low temperature gradient (~8°/km) was measured at Site 1094, indicating that the porcellanites formed under low (near bottom-water) temperatures. The upper porcellanite (at 68 mbsf) coincides with a sharp discontinuity in interstitial chloride concentrations, suggesting that the porcellanite layer may have acted as a diffusion barrier (Fig. F14). Shore-based geochemical analyses of interstitial water and solid-phase samples taken from near these porcellanite beds will be important for studying early silica diagenesis in Site 1094.

In summary, the purpose of Site 1094 was to obtain a record of biosiliceous sediments at high temporal resolution south of the present-day position of the PF. Together with Sites 1089 (41°S), 1091 (47°S), and 1093 (50°S), Site 1094 (53°S) represents the southernmost end member of the north-south transect of sites across the ACC needed to reconstruct past changes in frontal boundaries and sea-ice distribution during

glacial–interglacial cycles of the Pleistocene (Fig. F15). The expanded upper and mid-Pleistocene sedimentary succession at Site 1094 will permit study of rapid climate change on suborbital time scales, including comparison with paleoclimatic signals from Antarctic and Greenland ice cores.

SUMMARY

Core Summary

A total of 4046 m of sediment ranging in age from middle Eocene to Holocene was recovered during Leg 177. To the extent possible, composite records were constructed at each site from cores in multiple holes by aligning features in the signals of core-logging data (Table T1). We were successful in achieving the following drilling objectives.

1. A north-south transect of Pleistocene sections across the ACC (41°–53°S), including Sites 1089 (41°S), 1091 (47°S), 1093 (50°S), and 1094 (53°S) (Fig. F15). Average sedimentation rates vary between 130 and 250 m/m.y., permitting studies at millennial scale resolution (Fig. F12). Close to the base of three of these sites (1089, 1091, and 1093) upper Pliocene sequences were recovered. with sedimentation rates between 30 and 84 m/m.y.
2. Several Pliocene–Pleistocene sections were obtained with lower sedimentation rates ranging between 7 and 33 m/m.y., at Sites 1088 (41°S), 1090 (43°S), and 1092 (47°S).
3. Two relatively complete upper Miocene sequences were drilled at Sites 1088 (41°S) and 1092 (47°S), where sedimentation rates varied between 7–17 and 30–38 m/m.y. in the late to middle late Miocene and in the early late Miocene, respectively (Fig. F10). In conjunction with Leg 113 Sites 689 and 690, these sites represent a north-south transect of upper Miocene sequences across the ACC.
4. A middle Eocene to lower Miocene sequence (~46–18 Ma) was obtained at Site 1090 (43°S). The section was recovered in multiple holes to ensure completeness and possesses a clear polarity reversal stratigraphy.
5. Two partial depth transects of cores were drilled on (1) the Agulhas Ridge, including Sites 1088 (2082 m), 1090 (3702 m), and 1089 (4620 m); and (2) the Meteor Rise, including Site 1092 (1974 m), Leg 114 Site 704 (2532 m), and Site 1091 (4363 m) (Fig. F2).

Lithostratigraphy

Leg 177 sediments are dominated by calcareous and siliceous biogenic components comprising foraminifers, nannofossils, diatoms and subordinate radiolarians, silicoflagellates, and sponge spicules (Fig. F18). Almost pure calcareous sediments were recovered at Sites 1088 and 1092, which were situated well above the regional CCD in intermediate water depths on the Agulhas Ridge (2082 m) and the Meteor Rise (1974 m). South of the Subantarctic Front, diatom-rich sediments predominate at Sites 1091 (4363 m), 1093 (3626 m), and 1094 (2807 m), within the circum-Antarctic opal belt. At all sites, the terrigenous sediment fraction mainly consists of siliciclastic silt and clay. At the south-

F18. Summary of lithologies for Leg 177 Sites 1088 through 1094, p. 52.

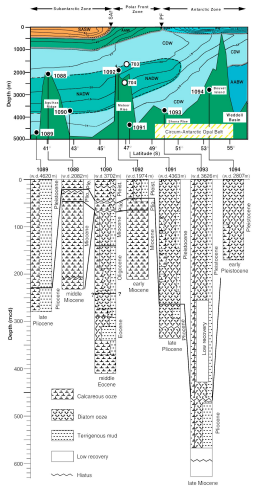

ern sites (1091–1094), sand- to gravel-sized ice-rafted debris (IRD) represents a minor but ubiquitous constituent of the sediments.

Pelagic calcareous sediments at Site 1088 (Agulhas Ridge) consist of Quaternary foraminifer nannofossil ooze that grades into nannofossil ooze in Pliocene to middle Miocene sediments. Biogenic opal and siliciclastics represent minor components. Downhole lithologic changes were associated with an increase in clay-sized particles in the terrigenous fraction.

Site 1089 (4620 m) is located on a drift deposit in the southern Cape Basin close to the northern flank of the Agulhas Ridge. Quaternary to Pliocene calcareous sediments contain the highest concentrations (as much as 50 wt%) of terrigenous silt and clay encountered at Leg 177 sites, which will permit the study of relative current strengths of paleobottom water from grain-size parameters of the terrigenous silt fraction (Diekmann and Kuhn, 1997). Lithologic alternations between mud- and carbonate-rich sediments probably reflect sedimentary cycles attributed to glacial–interglacial periods that triggered oscillations in carbonate production and/or terrigenous sediment supply.

At Site 1090 (3702 m) on the southern flank of the Agulhas Ridge, we recovered a 400-m-thick sedimentary succession that yields a long-term record of lithologic and paleoenvironmental change from the Quaternary to the middle Eocene, interrupted by several hiatuses. A hiatus at 70 mcd, marked by a color change to redder sediments below, separates a Pleistocene to lower Pliocene calcareous ooze from lower Miocene sediments that are more opal and mud rich. The hiatus is underlain by a redeposited tephra layer. The older sediments contain high opal concentrations (as much as 50 wt%) in the late Eocene. The lower part of the section is composed of zeolite-bearing calcareous ooze of middle Eocene age.

In addition to Site 1088, Site 1092 on Meteor Rise provides a low–sedimentation-rate record of pelagic calcareous deposits, spanning the Pleistocene to middle Miocene. The Quaternary part of the section reveals distinct variations in opal and siliciclastics, probably associated with glacial–interglacial cycles.

Sites 1091 and 1093 yielded diatom ooze deposited with high sedimentation rates from the Holocene to the Pliocene. They represent typical pelagic deposits of the southern abyssal portion of the southeast Atlantic (Fig. **F9**). Distinct carbonate-rich intervals indicate peak interglacial periods, which were frequent in the late Pleistocene to Pliocene. At Site 1093, the Pliocene part of the section accumulated at lower sedimentation rates and is marked by an increase in terrigenous silt and clay. Several millimeter-thick marker beds, consisting of sand-sized foraminifer ooze, are intercalated in the section of Site 1091 and probably represent turbidites.

Rapidly deposited diatom ooze of Pleistocene age was also obtained at Site 1094, which was drilled in 2807-m water depth in a small sedimentary basin north of Bouvet Island. In contrast to Sites 1091 and 1093, only a few carbonate-bearing intervals were found. Downhole lithologic variations are marked by pronounced changes in the abundance of siliciclastics, as illustrated by fluctuations in magnetic susceptibility that show peak values in glacial intervals.

Four porcellanite horizons were penetrated at Site 1094 (Fig. **F15**) that form discrete layers as documented in Parasound seismograms. Porcellanite mainly is present as brownish amorphous fragments derived from the crushing of concrete porcellanite layers during coring. It also occurs as individual loaf-shaped concretions that are as much as

6 cm in diameter and exhibit internal bedding structures that indicate an early diagenetic growth within the host sediment. Fragments of porcellanite washed downhole during drilling were also found in Site 1093 cores. Shipboard X-ray diffraction measurements indicate an opal-CT composition of the porcellanites. Joint investigations among Leg 177 scientists on the geochemical and mineralogical properties of porcellanite, interstitial water, and host-sediment composition in the context of regional heat flow and spatial distribution patterns of porcellanite layers will provide information about the conditions under which these young porcellanites were formed.

Sediments from Sites 1091, 1093, and 1094 contain scattered IRD throughout and should provide a high-temporal resolution record of past ice-rafting activity in response to Antarctic ice-sheet dynamics. IRD mainly consists of volcaniclastic particles along with minor quartz and crystalline rock fragments.

A significant proportion of the sediment at southern Sites 1091, 1093, and 1094, consists of mats of the needle-shaped diatom *Thalassiothrix*, which proved difficult to recover with the APC or XCB coring systems (Fig. **F15**). The mats occur as intervals of laminated sediment as much as 20 m thick (Fig. **F16**), as intermittently laminated sediment, or as bioturbated mat fragments or burrow-fills of mat material. This mat sediment is common in the transitions to and from interglacial, carbonate-rich sediment resulting in expanded sections of glacial terminations (e.g., the 8-m-thick MIS 12/11 boundary at Site 1093; see **Frontispiece 2,** p.3). At the two southernmost sites (1093 and 1094), diatom mats were recovered in upper and mid-Pleistocene sediment. At Site 1091, located in the PFZ, the youngest diatom mats were noted at the lower/mid-Pleistocene boundary (Fig. **F15**). At both Sites 1091 and 1093, the most significant diatom-mat sediment was deposited in the late early and mid-Pleistocene. Diatom mats also occur in the mid-Pliocene section. The Leg 177 *Thalassiothrix* diatom-mat deposits are remarkably similar to the vast Neogene laminated diatom-mat deposits of the eastern equatorial Pacific Ocean (Kemp and Baldauf, 1993). Such deposits are thought to form beneath intense frontal zones (Kemp et al., 1995) and, in the Leg 177 sites, the *Thalassiothrix* mat intervals may track the paleoposition of the Southern Ocean frontal systems. These laminated sequences also represent a paleosediment trap that preserves individual flux events and provides the potential to generate pelagic records of climate/ocean change at key time intervals at a resolution that rivals that of ice cores.

Biostratigraphy

Primary age control points were provided by calcareous nannofossil, diatom, and radiolarian biostratigraphy, integrated in some sites with magnetostratigraphy. The calcareous nannofossil assemblages show a clear difference between the northern and southern sites, with an important decrease in diversity to the south. Datums previously calibrated in middle- and low-latitude areas were used for the Pleistocene time interval. A more accurate age model will provide the possibility to recalibrate these events and estimate their synchronism or diachronism. The Pliocene–Eocene time interval offers the opportunity to generate a new biostratigraphic scheme for the Southern Ocean, as well as to correlate these events with low-latitude zonations. Furthermore, calcareous nannofossil assemblages are marked by cyclic abundance variations at

all sites and ages, offering a potential tool for paleoceanographic investigations.

Paleoceanographic reconstructions using foraminifer-based stable isotopic results will be possible for most sites. Although the absolute abundance of both planktic and benthic foraminifers is low in many cases, particularly at the southernmost deep-water sites, the high sedimentation rates in these areas have clearly increased the preservation of foraminifers. Radiolarian assemblages sharply change along the north-south transect, which makes it possible to elucidate temporal and spatial distributions of radiolarian assemblages from mid- to high-latitude regions. In addition, abundant radiolarians from high-resolution sites may allow us to obtain detailed paleoceanographic information such as biogenic opal productivity and sea-surface temperature (SST) changes. A detailed late Pliocene to Pleistocene biostratigraphic diatom zonation developed for subantarctic waters was successfully applied throughout most of the north-south transect (Gersonde and Bárcena, 1998). Diatom analyses of Leg 177 sediment provide a great potential to improve the diatom biostratigraphic zonation for the Southern Ocean. In particular, the diatom record of the Miocene–Eocene time interval, when correlated to a nearly continuous paleomagnetic record, will provide a detailed biostratigraphic zonation for the Paleogene. Recovered material from the two southernmost sites located within the circum-Antarctic opal belt will allow reconstructions of paleoenvironmental parameters such as SST (by means of diatom transfer functions) and sea-ice occurrence (by means of diagnostic diatom taxa).

Paleomagnetism

All Leg 177 sites, with the exception of Site 1088, yielded magnetic polarity reversal stratigraphies to augment other chronostratigraphic information. Of the sites with high sedimentation rates, the primary magnetization was most clearly recorded at Sites 1089 and 1094. At the two other sites (1091 and 1093) with expanded sections, the magnetization is affected by secondary components that were not entirely removed by shipboard demagnetization treatments. Nonetheless, all four high-resolution sites along the north-south transect have high potential for detailed (U-channel) studies of directional and bulk magnetic properties (Fig. **F15**). The objectives of these studies will be to: (1) generate the first geomagnetic paleointensity records from the Southern Ocean for long-distance stratigraphic correlation; (2) generate proxies for magnetic grain size and mineralogy that can be used for paleoenvironmental interpretation, and monitor detrital fluxes; and (3) obtain detailed polarity transition records from the high-latitude Southern Hemisphere.

Sites 1090 and 1092, which are marked by lower sedimentation rates, both yielded well-defined magnetic stratigraphies, although the upper part of the section at both sites was severely compromised by drilling-related core deformation. Below ~60 mcd at both sites, the shipboard magnetic polarity stratigraphies are well defined; however, correlation of polarity zones to the geomagnetic polarity time scale is ambiguous in the absence of detailed biostratigraphic analyses. Even in the XCB section of Site 1090, magnetic stratigraphies were well defined mainly because of the exceptional quality (lack of drilling deformation) of these cores. The middle Miocene to early Pliocene magnetostratigraphic record at Site 1092 and the exceptional Eocene to early Miocene record

at Site 1090 will provide important new biomagnetostratigraphic correlations, and may allow orbital tuning of this part of the time scale.

Whole-Core, Split-Core, and Downhole Logging Data

Closely spaced measurements of sedimentary physical properties were obtained from all cores recovered during Leg 177, using the standard ODP whole-round MST. The Oregon State University Split Core Analysis Track (OSU-SCAT) was deployed for diffuse color reflectance and resistivity measurements. Downhole logging data were obtained from Hole 1093D.

Measuring the cored sediments every 2 to 4 cm with the MST provided us with the highest temporal resolution data set collected during Leg 177. Physical properties are a function of sediment composition, structure, and porosity. Moreover, they are a tool for hole-to-hole correlations and comparisons among sites. Glacial–interglacial fluctuations in sediment composition were observed in GRA bulk density. High bulk-density values are consistent in sediments at the northern sites with overall high carbonate contents, particularly in interglacial intervals. High percentages of biogenic opal (high porosity) result in a decrease of sediment bulk density in interglacial sediments at southern Sites 1093 and 1094. The opposite is observed in sediments deposited during glacial stages that are marked by higher percentages of terrigenous material. At Site 1094, magnetic susceptibility and NGR show high signal amplitudes, but with different character. The shape of the magnetic susceptibility signal is rectangular, whereas NGR displays an asymmetric, sawtooth pattern with highest intensities toward the end of glacial periods (Fig. **F17**). This indicates that both signals contain different information regarding terrigenous sediment components. The signals are strongly cyclic in the Pleistocene sequences at Sites 1089, 1091, 1093, and 1094, and also in the continuous early Miocene to late Eocene sequence at Site 1090. These cyclic variations in lithologic parameters may permit the development of orbitally tuned age models in conjunction with biomagneto- and stable-isotopic stratigraphies.

Diffuse spectral reflectance measurements obtained with the OSU-SCAT and the Minolta CM-2002 spectrophotometers contributed greatly to the overall success of the leg, providing a high-resolution proxy for lithostratigraphic records in real time. These data provided important stratigraphic constraints for hole-to-hole correlation during the generation of shipboard spliced composite sections. At Sites 1088, 1089, and 1092, interglacial carbonate-bearing sediments were easily discernible from darker, diatom-rich glacial sediments. The spectral reflectance signals were especially important for correlation of the biosiliceous oozes at Sites 1091, 1093, and 1094, where magnetic susceptibility signals dropped below measurable values in interglacial sediments. Records of reflectance also proved extremely useful as geochronologic tools during Leg 177. In conjunction with biostratigraphic and magnetostratigraphic datums, preliminary estimates of MISs were inferred on the basis of sediment brightness (Fig. **F11**).

Some of the oldest sediments thus far measured for diffuse spectral reflectance were recovered in the Miocene to Eocene sequences from Sites 1088, 1090, and 1092. The continuous lower Miocene to upper Eocene sequence at Site 1090 is noteworthy for the high-amplitude OSU-SCAT signal in the APC cores that span from early Miocene to Oligocene time, as well as in the deeper XCB sequence from which the cores were measured with the CM-2002 spectrophotometer (Fig. **F13**).

Leg 177 spectral reflectance records hold great potential for development of high-resolution age models and proxy estimation of sediment mineralogy.

Interstitial Water Geochemistry

The interstitial water chemistry of Leg 177 sites can be divided into two broad categories: (1) sites with a high biogenic carbonate content, low biosiliceous content, and low sedimentation rates (10–30 m/m.y.) that are located to the north of the PFZ (Sites 1088, 1090, and 1092); and (2) sites with low carbonate content, high opal content, and high sedimentation rates (140–250 m/m.y.) that are located within or to the south of the PFZ (Sites 1091, 1093, and 1094). The interstitial water geochemistry of the carbonate-rich sites is, in general, quite similar to that of many other carbonate-rich sites drilled on previous ODP and DSDP legs; that is, oxic to suboxic sediments with ample evidence for carbonate diagenesis occurring at depth. The closely spaced interstitial water sampling employed during Leg 177 will permit more detailed analyses of some interesting features observed from these carbonate-rich sites. However, the highlight of the interstitial water geochemistry obtained during Leg 177 derives from the unique (and still somewhat enigmatic) results observed at sites with sequences dominated by diatom ooze deposited at high sedimentation rates within or south of the PFZ, and also from the early diagenetic porcellanites (opal-CT) observed at Site 1094. The collection of a series of closely spaced interstitial water samples across several of the porcellanite intervals should provide important insights into the formation of these early porcellanites.

A synthesis of several interstitial water profiles from Sites 1091, 1093, and 1094 is shown in Figure **F14.** The chloride profiles show evidence for the downward diffusion of higher salinity glacial-age seawater (McDuff, 1985). The uppermost porcellanite layer at ~68 mbsf at Site 1094 has apparently interrupted this downward diffusion and presents the intriguing suggestion that the porcellanite may have formed in the past 10 to 20 k.y. These diatom oozes were suboxic to mildly reducing. H_2S was detected by scent at Sites 1091 and 1093 throughout most of these profiles, but H_2S was not detected at Site 1094 except very faintly in one whole-round near the top of the section. In addition, sulfate depletion is much less than would be expected based on sedimentation rate, and it appears to be inversely correlated with our preliminary estimates of TOC (see site chapters for data not shown here). Phosphate profiles show little correlation with alkalinity and ammonium except at Site 1094, and dissolved manganese is observed to varying degrees throughout the profiles. We offer the following preliminary interpretation of these observations. The highest sedimentation-rate site is Site 1093 (~250 m/m.y.), which is located very near the contemporaneous PF at ~50°S. Sedimentation rates at Site 1093 were least likely to be affected by glacial–interglacial migrations of the PF compared to Sites 1091 and 1094 located about 3° to the north and south, respectively. Thus, the mildly reducing conditions at Site 1093 have likely persisted through glacial–interglacial cycles as evidenced by the low downhole dissolved-Mn profile. Sites 1091 and 1094 have undergone much more drastic perturbations in average sedimentation rates (both ~140 m/m.y.) and are out of phase with each other over the glacial–interglacial climate cycles. This resulted in a periodicity in the redox state of the sediments that has permitted reactive Mn to persist at depth. The low sulfate reduction rates observed (despite the high sedimentation rates)

may result from the fact that a significant, if not major, fraction of the organic carbon in these diatom-rich oozes is highly refractory opal-intrinsic organic carbon that is unavailable for degradation until the opal has dissolved. Opal-intrinsic organic carbon may have relatively low phosphate content, thus offering some explanation for the nature of the phosphate profiles observed in these diatom-rich oozes.

In summary, this preliminary and general interpretation of these first deep interstitial water profiles from the circum-Antarctic opal belt will need to be verified and enhanced with additional shore-based analyses. Additionally, shore-based analyses of closely spaced interstitial water samples across some of the porcellanite intervals observed in the sediments at Site 1094 may offer important insight into the mechanisms involved in the transformation of diatom opal to opal-CT.

Postcruise Research

Sediments recovered during Leg 177 will be used to study the paleoceanographic history of the southeast Atlantic sector of the Southern Ocean on a variety of time scales, including suborbital (10^2 to 10^3 yr, centennial to millennial), orbital (10^4 to 10^5 yr, Milankovitch), and supraorbital (10^5 to 10^6 yr, Cenozoic). Future research will focus on generating signals of faunal, isotopic, and sedimentologic paleotracers that will be used to study the role played by the Southern Ocean in the global climate system.

Undoubtedly, one of the most exciting results of Leg 177 was the successful recovery of expanded sequences arrayed across the ACC from 41° to 53°S (Fig. F15). Average sedimentation rates during the Pleistocene varied from ~132 m/m.y. at Site 1089, to ~140 m/m.y. at Site 1094, ~145 m/m.y. at Site 1091, and ~250 m/m.y. at Site 1093 (Fig. F12). Detailed sampling and measurements of proxy variables in these cores will permit us to reconstruct paleoenvironmental changes on time scales of hundreds to thousands of years. We intend to use isotopic and micropaleontological methods to reconstruct changes in the position of the oceanic frontal systems of the ACC, and diatom sea-ice indicators to assess changes in sea-ice distribution during glacial–interglacial cycles of the Pliocene–Pleistocene interval. Foraminifer, diatom, and radiolarian transfer functions, as well as $U^{k'}_{37}$ temperature estimations, will be used to reconstruct variations in past SST. Accumulation rates of carbonate, opal, and organic matter, as well as stable isotopic studies, radiotracer studies, and microfossil distribution patterns will be used to study variation in biological export productivity of the Southern Ocean. Micropaleontological, isotopic, and trace-element studies of benthic-foraminifer and clay-mineral distribution will be used to study changes in deep-water masses, including the variable input of NADW into the Southern Ocean during glacial–interglacial cycles. Variations in coarse-grained IRD, magnetic properties, sediment particle size and geochemistry, and clay mineralogy will be used to study variations in the accumulation rate, source, and transport modes (eolian, ice rafted, or bottom water) of terrigenous material. These studies will produce multiproxy data sets for the reconstruction of the interglacial and glacial modes of Southern Ocean surface and deep circulation. They will also provide insight into the impact of Southern Ocean paleoceanographic variability on global ocean biogeochemical cycles and atmospheric gas concentrations (CO_2), as well as on past current velocities, wind fields, and the stability of the Antarctic ice sheets.

The high temporal resolution of Leg 177 sediments will permit detailed correlation of paleotracer signals with those from other rapidly deposited sediments from the North Atlantic (Legs 162 and 172) and with ice-core records from Greenland, Antarctica, and low-latitude glaciers. Leg 177 sediments will be used to study the origin of millennial scale climate variability that was first recognized in ice cores on Greenland (Daansgard et al., 1993) but now appears to be manifested globally in marine and terrestrial sediments (Broecker, 1997). MIS 11 (423–363 ka) is a particularly interesting time period, and sediment of this age was recovered during Leg 177 in several sites. Sediments of MIS 11 are characterized at all sites by white, nannofossil-rich oozes that display the highest values of color reflectance (Fig. **F11**). MIS 11 may have been one of the warmest periods of the late Pleistocene, and the PF possibly was located farther south than during succeeding interglacials (Howard, 1997). The transition from MIS 12 to 11 (Termination V) is linked to the largest shift in oxygen isotopic values during the late Pleistocene, although insolation forcing at 65°N was very weak during this termination ("Stage 11 problem" of Imbrie et al., 1993). What role did the Southern Ocean play during Termination V? We will take a multiproxy approach to addressing this question by generating detailed stable isotopic, geochemical, micropaleontological, and sedimentological paleotracers along the north-south transect of high–sedimentation-rate sites across the ACC.

Another time period of considerable interest is MIS 5, which is represented in several Leg 177 cores with a maximum thickness of as much as ~15 m. In several cores, there is as much as 3 m of sediment representing Substage 5.5 (Eemian). Sediments of this substage show significant variations in sedimentary physical properties that are tentatively interpreted to reflect short-term environmental changes during peak interglacial periods. Detailed studies can elucidate the stability of climate conditions during the penultimate climatic optimum, which remains a controversial issue considering the results of the Greenland Ice-core Project (GRIP, 1993). Natural climate variability in the Holocene is also of great interest in light of anticipated future global warming.

Studying the response of the Southern Ocean to orbital forcing and determining the phase relationships to climatic changes in other regions is important for assessing the role that the Antarctic region played in glacial–interglacial cycles of the late Pleistocene. Only the combination of marine, terrestrial, and atmospheric paleoclimatic records from key areas on our globe will elucidate the mechanisms driving global climate. As such, the expanded sequences recovered during Leg 177 provide much needed deep-sea records from the southern high latitudes for such global comparisons.

Important questions that now can be addressed with the Pleistocene sequences recovered during Leg 177 include the following. Is there evidence for millennial scale variability in SST and sea ice in the Southern Ocean? If so, how does it relate to short-term climatic events recorded in Antarctic and Greenland ice cores? What role does Antarctic sea ice play in internal feedback mechanisms driving rapid climate change? Sea ice represents a fast-changing environmental parameter with multiple impacts on Earth's heat budget, oceanic and atmospheric circulation, and biological productivity. Did pulse-like surges occur in the Antarctic ice sheet during the late Pleistocene, and is there a record of these events preserved in the Southern Ocean sediments, similar to the Heinrich events preserved in the North Atlantic? What was the nature

and structure of terminations in the Southern Hemisphere during the late Pleistocene? What role did thermohaline circulation (NADW flux to the Southern Ocean) play in coupled ice-sheet and ocean oscillations on millennial and longer time scales? To what extent do processes in the Southern Ocean control atmospheric CO_2 variations? What is the phase relationship between millennial scale climate change in the high-latitude Southern and Northern Hemispheres, and what is the mechanism linking climate in the polar regions? Could the paleoclimatic record of the southern high latitudes represent a potential forecast for millennial–centennial climate change in the future (Howard and Prell, 1992; Labeyrie et al., 1996)?

At about 900 ka, a shift occurred in the dominant power of climatic variability from 41 to 100 k.y., the so-called Mid-Pleistocene Revolution (MPR; Berger and Jansen, 1994). The MPR has not been well studied from the Southern Ocean because sediments are disturbed in the only existing record of this event at Site 704 (Hodell and Venz, 1992). Interestingly, between 0.7 and 1.6 Ma the area of the present PFZ was characterized by accumulation of laminated diatom mats deposited at high sedimentation rates, as documented in Sites 1091 and 1093 (Fig. **F15**). What was the role of the Southern Ocean during the shift from 41-k.y. to 100-k.y. climatic variability? Was the phase relationship between the polar oceans different during the 41-k.y. world of the early Pleistocene compared to the 100-k.y. world of the late Pleistocene? How is the rapid deposition of biosiliceous sediments in the Southern Ocean during the late early Pleistocene linked with the MPR? To address these questions, groups of Leg 177 scientists will focus on the 100-k.y. world, 41-k.y. world, and MPR in Leg 177 sediments using multiproxy approaches.

Although early and early late Pliocene sequences were recovered partially at only a few sites (1088, 1090, 1092, and 1093) during Leg 177, combined isotopic and microfossil distribution studies of these sediments may contribute to the debate on the extent and volume of the Antarctic ice sheet during the early–late Pliocene. There are those who assume an essentially stable, combined East and West Antarctic ice sheet since the early Pliocene (Kennett and Barker, 1990; Clapperton and Sugden, 1990), and those who envision a highly dynamic Antarctic ice sheet during the early and early late Pliocene (Webb and Harwood, 1991; Hambrey and Barrett, 1993). Shipboard diatom studies on Leg 177 sequences indicate changes in surface-water parameters (e.g., temperature) during the early/late Pliocene transition. Although sequences assigned to the upper Gauss Chron contain assemblages reflecting rather glacial-type conditions, the lower Gauss Chron sequences are characterized by warm-water diatoms, such as the *Hemidiscus* ooze found at Site 1091. This preliminary result may suggest that the mid-Pliocene was punctuated by a time period of significant warming, as suggested by Dowsett et al. (1996). Pliocene sediments will also be examined for traces of the Eltanin asteroid impact that occurred at ~2.15 Ma in the Southern Ocean (Bellingshausen Sea) to constrain the maximum size of the bolide, which is now estimated to have been at least 1 km in diameter, by mapping the flux of impact-related ejecta (Gersonde et al., 1997).

Two upper Miocene sequences were recovered at Sites 1088 and 1090, forming a north-south transect across the Southern Ocean in conjunction with Leg 113 Sites 689 and 690 (Maud Rise). At both sites, the late and middle late Miocene (~5.3–9 Ma) is marked by low sedimentation rates (~15–17 m/m.y.) and the early late Miocene by higher rates (almost double). Similar upper Miocene sequences were recovered

during Legs 113, 114, and 119 (Gersonde et al., 1990; Ciesielski, Kristoffersen, et al., 1988; Barron et al., 1991b). Combined isotopic and microfossil analyses will focus on late Miocene climate evolution along this north-south transect, and may elucidate the waxing and waning of the Antarctic ice sheets during this interval. Evidence of cyclicity in the Milankovitch frequency band at Site 1092 may permit the development of an astronomically tuned time scale (Shackleton and Crowhurst, 1997) that will provide a detailed chronology of upper Miocene changes in surface- and deep-water circulation.

The Cenozoic objectives of Leg 177 will be addressed mainly at Site 1090. This site contains a lower Miocene to middle Eocene sequence that is remarkable for several reasons: (1) a verifiably complete spliced section was constructed using three holes ranging in age from the early Oligocene to early Miocene; (2) the co-occurrence of well-preserved calcareous and siliceous microfossils throughout most of the section will allow intercalibration of foraminifer, calcareous nannofossil, diatom, silicoflagellate, and radiolarian biostratigraphies; (3) the paleomagnetic inclination records indicate clearly defined polarity zones throughout the sequence, offering the potential of excellent chronological control after correlation of the reversal pattern to the geomagnetic polarity time scale with the aid of detailed shore-based biostratigraphy; (4) the development of geomagnetic paleointensity and/or reversal records may provide long-distance stratigraphic correlation; (5) cyclic variations in lithologic parameters may permit the development of an astronomically tuned time scale for the Oligocene to early Miocene; and (6) the shallow burial depth (<370 mbsf) of the section offers an opportunity to produce uncompromised stable isotopic stratigraphies.

Approximately 330 m of sediment was recovered below the hiatus at 70 mcd at Site 1090, ranging in age from the early Miocene to middle Eocene. Sedimentation rates averaged 10 m/m.y. in the early Miocene and middle Eocene, and increased to 30 m/m.y. during the deposition of opal-rich sediments in the late Eocene that include intervals of well-laminated diatom ooze. The spliced Oligocene–early Miocene section at Site 1090 complements the records obtained during Leg 154 (Sites 925, 926, 928, and 929), and comparisons among these records can be used to test orbitally tuned time scales (Weedon et al., 1997), study Milankovitch-scale cyclicity of paleotracers during the late Paleogene–early Neogene (Zachos et al., 1997), and calibrate biostratigraphic datums to the geomagnetic polarity time scale. Combined with the results from Paleogene sections recovered on Maud Rise during Leg 113 (Kennett and Barker, 1990), Site 1090 provides an opportunity to study major paleoceanographic changes in the Southern Ocean from the middle Eocene to early Miocene (Fig. **F19**). This time period includes the development and intensification of the ACC and the growth of the East Antarctic Ice Sheet (Barron et al., 1991a, 1991b; Zachos et al., 1992) in conjuction with the changing paleogeography of the high-latitude Southern Hemisphere (Lawver et al., 1992).

F19. Variation in sea level and oxygen isotopes of benthic foraminifers from the Atlantic Ocean, **p. 53.**

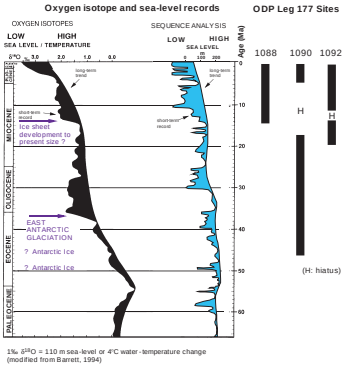

REFERENCES

Baldauf, J.G., Barron, J.A., Ehrmann, W.U., Hempel, P., and Murray, D., 1992. Biosiliceous sedimentation patterns for the Indian ocean during the last 45 million years. *Geophys Monogr.*, 70:335–349.

Barker, P.F., 1979. The history of ridge-crest offset at the Agulhas Fracture zone from a small-circle geophysical profile. *Geophys. J. R. Astron. Soc.,* 59:131–145.

Barrett, P.J., 1994. Progress towards a Cenozoic Antarctic glacial history. *Terra Antarct.*, 1:247–248.

Barron, J., Larsen, B., and Baldauf, J.G., 1991a. Evidence for late Eocene to early Oligocene Antarctic glaciation and observations on late Neogene glacial history of Antarctica: results from Leg 119. *In* Barron, J., Larsen, B., et al., *Proc. ODP, Sci. Results,* 119: College Station, TX (Ocean Drilling Program), 869–891.

Barron, J.A., Baldauf, J.G., Barrera, E., Caulet, J.-P., Huber, B.T., Keating, B.H., Lazarus, D., Sakai, H., Thierstein, H.R., and Wei, W., 1991b. Biochronologic and magnetochronologic synthesis of Leg 119 sediments from the Kerguelen Plateau and Prydz Bay, Antarctica. *In* Barron, J., Larsen, B., et al., *Proc. ODP, Sci. Results,* 119: College Station, TX (Ocean Drilling Program), 813–847.

Bender, M., Sowers, T., Dickson, M., Orchardo, J., Grootes, P., Mayewski, P., and Messe, D., 1994. Climate teleconnections between Greenland and Antarctica throughout the last 100,000 years. *Nature,* 372:663–666.

Berger, W.H., 1989. Global maps of ocean productivity. *In* Berger, W.H., Smetacek, V.S., and Wefer, G. (Eds.), *Productivity of the Oceans: Present and Past:* New York (Wiley), 429–455.

Berger, W.H., and Jansen, E., 1994. Mid-Pleistocene climate shift: the Nansen connection. *In* Johannessen, O.M., Muensch, R.D., and Overland, J.E. (Eds.), *The Role of the Polar Oceans in Shaping the Global Environment*. Geophys. Monogr., Am. Geophys. Union, 85:295–311.

Bohrmann, G., Abelmann, A., Gersonde, R., Hubberten, H., and Kuhn, G., 1994. Pure siliceous ooze, a diagenetic environment for early chert formation. *Geology,* 22:207–210.

Bohrmann, G., Kuhn, G., Abelmann, A., Gersonde, R., and Fütterer, D., 1990. A young porcellanite occurence from the Southwest Indian Ridge. *Mar. Geol.,* 92:155–163.

Bonatti, E., 1978. Vertical tectonism in oceanic fracture zones. *Earth Planet. Sci. Lett.,* 37:369–379.

Bond, G., Broecker, W., Johnsen, S., McManus, J., Labeyrie, L., Jouzel, J., and Bonani, G., 1993. Correlations between climate records from the North Atlantic sediments and Greenland ice. *Nature,* 365:143–147.

Bond, G.C., and Lotti, R., 1995. Iceberg discharges into the North Atlantic on millennial time scales during the last glaciation. *Science,* 276:1005–1010.

Broecker, W.S., 1997. Will our ride into the Greenhouse future be a smooth one? *GSA Today,* 7:1–6.

Broecker, W.S., and Peng, T.-H., 1989. The cause of the glacial to interglacial atmospheric CO_2 change: a polar alkalinity hypothesis. *Global Biogeochem. Cycles,* 3:215–239.

Cande, S.C., and Kent, D.V., 1992. A new geomagnetic polarity time scale for the Late Cretaceous and Cenozoic. *J. Geophys. Res.,* 97:13917–13951.

Cande, S.C., LaBrecque, J.L., and Haxby, W.F., 1988. Plate kinematics of the South Atlantic: Chron C34 to present. *J. Geophys. Res.,* 93:13479–13492.

Charles, C.D., and Fairbanks, R.G., 1992. Evidence from Southern Ocean sediments for the effect of North Atlantic deep-water flux on climate. *Nature,* 355:416–419.

Charles, C.D., Lynch-Stieglitz, J., Ninnemann, U.S., and Fairbanks, R.G., 1996. Climate connections between the hemispheres revealed by deep sea sediment core/ice core correlations. *Earth Planet. Sci. Lett.*, 142:19–27.

Ciesielski, P.F., Kristoffersen, Y., et al., 1988. *Proc. ODP, Init. Repts.,* 114: College Station, TX (Ocean Drilling Program).

Clapperton, C.M., and Sugden, D.E., 1990. Late Cenozoic glacial history of the Ross Embayment, Antarctica. *Quat. Sci. Rev.,* 9:253–272.

Dansgaard, W., Johnsen, S.J., Clausen, H.B., Dahl-Jensen, D., Gundestrup, N.S., Hammer, C.U., Hvidberg, C.S., Steffensen, J.P., Sveinbjörnsdottir, A.E., Jouzel, J., and Bond, G., 1993. Evidence for general instability of past climate from a 250-kyr ice-core record. *Nature,* 364:218–220.

DeMaster, D.J., 1981. The supply and accumulation of silica in the marine environment. *Geochim. Cosmochim. Acta,* 45:1715–1732.

Diekmann, B., and Kuhn, G., 1997. Terrigene Partikeltransporte als Abbild spätquartärer Tiefen- und Bodenwasserzirkulation im Südpolarmeer. *Z. Deutsch. Geol. Ges.,* 148:405–429.

Douglass, J., Schilling, J.-G., Kingsley, R.H., and Small, C., 1995. Influence of the Discovery and Shona mantle plumes on the southern Mid-Atlantic Ridge: Rare earth evidence. *J. Geophys. Res.*, 21:2893–2396.

Dowsett, H., Barron, J., and Poore, R., 1996. Middle Pliocene sea surface temperatures: a global reconstruction. *Mar. Micropaleontol.*, 27:13–25.

duPlessis, A., 1977. Seafloor spreading south of the Agulhas Fracture Zone. *Nature,* 270:719–721.

Francois, R., Altabet, M.A., Ein-Fen, Y., Sigman, D.M., Bacon, M.P., Frank, M., Bohrmann, G., Bareille, G., and Labeyrie, L.D., 1997. Contribution of Southern Ocean surface-water stratification to low atmospheric CO_2 concentrations during the last glacial period. *Nature*, 389:929–935.

Frank, M., Gersonde, R., and Mangini, A., in press. Quantification of lateral sediment redistribution applying 230Thex: implications for the reconstruction of particle flux and export paleoproductivity from marine sediments. *In* Wefer, G. and Fischer, G. (Eds.), *Proxies in Paleoceanography.*

Frank, M., Gersonde, R., Rutgers van der Loeff, M., Kuhn, G., and Mangini, A., 1996. Late Quaternary sediment dating and quantification of lateral sediment redistribution applying 230Thex: a study from the eastern Atlantic sector of the Southern Ocean. *Geol. Rundsch.,* 85:554–566.

Froelich, P.N., Malone, P.N., Hodell, D.A., Ciesielski, P.F., Warnke, D.A., Westall, F., Hailwood, E.A., Nobes, D.C., Fenner, J., Mienert, J., Mwenifumbo, C.J., and Müller, D.W., 1991a. Biogenic opal and carbonate accumulation rates in the subantarctic South Atlantic: the late Neogene of Meteor Rise Site 704. *In* Ciesielski, P.F., Kristoffersen, Y., et al., *Proc. ODP, Sci. Results,* 114: College Station, TX (Ocean Drilling Program), 515–550.

Froelich, P.N., Mortlock, R.A., Mefferd, M., and Powers, J., 1991b. Interstitial-water chemistry: abyssal South Atlantic and East Georgia Basins, Islas Orcadas and Meteor Rises. *In* Ciesielski, P.F., Kristoffersen, Y., et al., *Proc. ODP, Sci. Results,* 114: College Station, TX (Ocean Drilling Program), 719–731.

Gersonde, R., Abelmann, A., Burckle, L.H., Hamilton, N., Lazarus, D., McCartney, K., O'Brien, P., Spieß, V., and Wise, S.W., Jr., 1990. Biostratigraphic synthesis of Neogene siliceous microfossils from the Antarctic Ocean, ODP Leg 113 (Weddell Sea). *In* Barker, P.F., Kennett, J.P., et al., *Proc. ODP, Sci. Results,* 113: College Station, TX (Ocean Drilling Program), 915–936.

Gersonde, R., and Bárcena, M.A., 1998. Revision of the late Pliocene–Pleistocene diatom biostratigraphy for the northern belt of the Southern Ocean. *Micropaleontology*, 44:1–15.

Gersonde, R., Kyte, F.T., Bleil, U., Diekmann, B., Flores, J.A., Gohl, K., Grahl, G., Hagen, R., Kuhn, G., Sierro, F.J., Voelker, D., Abelmann, A., and Bostwick, J. A., 1997. Geological record and reconstruction of the late Pliocene impact of the Eltanin asteroid in the Southern Ocean. *Nature*, 390:357–363.

GRIP (Greenland Ice-core Project) Members, 1993. Climate instability during the last interglacial period recorded in the GRIP ice core. *Nature,* 364:203–207.

Hambrey, M.J., and Barrett, P.J., 1993. Cenozoic sedimentary and climatic record, Ross Sea Region, Antarctica. *In* Kennett, J.P., and Warnke, D.A., (Eds.), *The Antarctic Paleoenvironment: A Perspective on Global Change, 2*. Antarct. Res. Ser., 60:91–124.

Hartnady, C.J.H., and le Roex, A.P., 1985. Southern ocean hotspot tracks and the Cenozoic absolute motion of the African, Antarctic, and South American plates. *Earth Planet. Sci. Lett.*, 75:245–257.

Hodell, D.A., and Venz, K., 1992. Toward a high-resolution stable isotopic record of the Southern Ocean during the Pliocene-Pleistocene (4.8 to 0.8 Ma). *In* Kennett, J.P., Warnke, D.A. (Eds.), *The Antarctic Paleoenvironment: A Perspective on Global Change* (Pt. 1). Am. Geophys. Union, Antarct. Res. Ser., 56:265–310.

Howard W., 1997. A warm future in the past. *Nature*, 388:418–419.

Howard, W.R., and Prell, W.L., 1992. Late Quaternary surface circulation of the southern Indian Ocean and its relationship to orbital variations. *Paleoceanography,* 7:79–117.

Imbrie, J., Berger, A., Boyle, E., Clemens, S., Duffy, A., Howard, W., Kukla, G., Kutzbach, J., Martinson, D., McIntyre, A., Mix, A., Molfino, B., Morley, J., Peterson, L., Pisias, N., Prell, W., Raymo, M., Shackleton, N., and Toggweiler, J., 1993. On the structure and origin of major glaciation cycles, 2. The 100,000-year cycle. *Paleoceanography,* 8:699–735.

Imbrie, J., Boyle, E.A., Clemens, S.C., Duffy, A., Howard, W.R., Kukla, G., Kutzbach, J., Martinson, D.G., McIntyre, A., Mix, A.C., Molfino, B., Morley, J.J., Peterson, L.C., Pisias, N.G., Prell, W.L., Raymo, M.E., Shackleton, N.J., and Toggweiler, J.R., 1992. On the structure and origin of major glaciation cycles, 1. Linear responses to Milankovitch forcing. *Paleoceanography,* 7:701–738.

Imbrie, J., McIntyre, A., and Mix, A., 1989. Oceanic response to orbital forcing in the late Quaternary: observational and experimental strategies. *In* Berger, A., Schneider, S., and Duplessy, J.C. (Eds.), *Climate and Geo-Sciences:* Dordrecht (Kluwer Academic), 121–164.

Kastens, K.A., 1987. A compendium of causes and effects of processes at transform faults and fracture zones. *Rev. Geophys.*, 25:1554–1562.

Keir, R.S., 1988. On the late Pleistocene ocean geochemistry and circulation. *Paleoceanography,* 3:413–445.

Kemp, A.E.S., and Baldauf, J.G., 1993. Vast Neogene laminated diatom mat deposits from the eastern equatorial Pacific Ocean. *Nature,* 362:141–144.

Kemp., A.E.S., Baldauf, J.G., and Pearce, R.B., 1995. Origins and paleoceanographic significance of laminated diatom ooze from the eastern equatorial Pacific Ocean. *In* Pisias, N.G., Mayer, L.A., Janecek, T.R., Palmer-Julson, A., and van Andel, T.H. (Eds.), *Proc. ODP, Sci. Results,* 138: College Station, TX (Ocean Drilling Program), 641–645.

Kennett, J.P., 1977. Cenozoic evolution of Antarctic glaciation, the circum-Antarctic Ocean, and their impact on global paleoceanography. *J. Geophys. Res.,* 82:3843–3860.

Kennett, J.P., and Barker, P.F., 1990. Latest Cretaceous to Cenozoic climate and oceanographic developments in the Weddell Sea, Antarctica: an ocean-drilling perspective. *In* Barker, P.F., Kennett, J.P., et al., *Proc. ODP, Sci. Results,* 113: College Station, TX (Ocean Drilling Program), 937–960.

Kennett, J.P., and Barron, J.A., 1992. Introduction. *In* Kennett, J.P., and Warnke, D.A. (Eds.), *The Antarctic Paleoenvironment: A Perspective on Global Change*. Am. Geophys. Union, 56:1–6.

Knox, F.E., and McElroy, M.B., 1984. Changes in atmospheric CO_2: influence of the marine biota at high latitudes. *J. Geophys. Res.*, 89:4629–4637.

Kumar, K., Anderson, R.F., Mortlock, R.A., Froelich, P.N., Kubik, P., Dittrich-Hannen, B., and Suter, M., 1995. Increased biological productivity and export production in the glacial Southern Ocean. *Nature*, 378:675–680.

Labeyrie, L., Labracherie, M., Gorfti, N., Pichon, J.J., Vautravers, M., Arnold, M., Duplessy, J.-C., Paterne, M., Michel, E., Duprat, J., Caralp, M., and Turon, J.L., 1996.

Hydrographic changes of the Southern Ocean (southeast Indian sector) over the last 230 kyr. *Paleoceanography,* 11:57–76.

Labeyrie, L., Pichon, J.-J., Labracherie, M., Ippolito, P., Duprat, J., and Duplessy, J.-C., 1986. Melting history of Antarctica during the past 60,000 years. *Nature,* 322:701–706.

LaBrecque, J.L. (Ed.), 1986. *South Atlantic Ocean and Adjacent Continental Margin, Atlas 13:* Ocean Margin Drilling Program Reg. Atlas Ser., 13.

LaBrecque, J.L., and Hayes, D.E., 1979. Seafloor spreading history of the Agulhas basin. *Earth Planet. Sci. Lett.,* 45:411–428.

Lawver, L.A., Gahagan, L.M., and Coffin, M.F., 1992. The development of paleoseaways around Antarctica. *In* Kennett, J.P., and Warnke, D.A. (Eds.), *The Antarctic Paleoenvironment: a Perspective on Global Change.* Am. Geophys. Union, Antarct. Res. Ser., 56:7–30.

Lisitzin, A.P., 1985. The silica cycle during the last ice age. *Palaeogeogr., Palaeoclimatol., Palaeoecol.,* 50:241–270.

Lutjeharms, J.R.E., 1985. Location of frontal systems between Africa and Antarctica: some preliminary results. *Deep-Sea Res. Part A,* 32:1499–1509.

McDuff, R.E., 1985. The chemistry of interstitial waters, Deep Sea Drilling Project Leg 86. *In* Heath, G.R., Burckle, L.H., et al., *Init. Repts. DSDP,* 86: Washington (U.S. Govt. Printing Office), 675–687.

Menard, H.W., and Atwater, T., 1969. Origin of fracture zone topography. *Nature,* 222:1037–1040.

Morley, J.J., 1989. Variations in high-latitude oceanographic fronts in the southern Indian Ocean: an estimation based on faunal changes. *Paleoceanography,* 4:547–554.

Mutter, J.C., Buck, W.R., and Zehnder, C.M., 1988. Convective partial melting, 1. A model for the formation of thick basaltic sequences during the initiation of spreading. *J. Geophys. Res.,* 93:1031–1048.

Oppo, D.W., and Fairbanks, R.G., 1987. Variability in the deep and intermediate water circulation of the Atlantic Ocean during the past 25,000 years: Northern Hemisphere modulation of the Southern Ocean. *Earth Planet. Sci. Lett.,* 86:1–15.

Peterson, R.G., and Stramma, L., 1991. Upper-level circulation in the South Atlantic Ocean. *Progr. Oceanogr.,* 26:1–73.

Petit, J.R., Basile, I., Leruyuet, A., Raynaud, D., Lorius, C., Jouzel, J., Stievenard, M., Lipenkov, V.Y., Barkov, N.I., Kudryashov, B.-B., Davis, M., Saltzman, E., and Kotlyakov, V., 1997. Four climatic cycles in Vostok ice core. *Nature*, 387:121–164.

Prell, W.L., Huston, W.H., and Williams, D.F., 1979. The Subtropical Convergence and late Quaternary circulation in the southern Indian Ocean. *Mar. Micropaleontol.*, 4:225–234.

Raymond, C.A., and LaBrecque, J.L., 1988. Geophysical signatures of the Agulhas Fracture Zone Ridge and Meteor Rise, Indo-Atlantic Basin. *In* Ciesielski, P.F., Kristoffersen, Y., et al., *Proc. ODP, Init. Repts.,* 114: College Station, TX (Ocean Drilling Program), 27–34.

Raymond, C.A., LaBrecque, J.L., and Kristoffersen, Y., 1991. Islas Orcadas Rise and Meteor Rise: the tectonic and depositional history of two aseismic plateaus from Sites 702, 703, and 704. *In* Ciesielski, P.F., Kristoffersen, Y., et al., *Proc. ODP, Sci. Results,* 114: College Station, TX (Ocean Drilling Program), 5–22.

Ruddiman, W.F., Raymo, M.E., Martinson, D.G., Clement, B.M., and Backman, J., 1986. Pleistocene evolution of Northern Hemisphere climate. *Paleoceanography,* 4:353–412.

Sarmiento, J.L., and Toggweiler, J.R., 1984. A new model for the role of the oceans in determining atmospheric carbon dioxide pCO_2 levels. *Nature,* 308:621–624.

Shackleton, N.J., and Crowhurst, S., 1997. Sediment fluxes based on an orbitally tuned time scale 5 Ma to 14 Ma, Site 926. *In* Shackleton, N.J., Curry, W.B., Richter, C., and Bralower, T.J. (Eds.), *Proc. ODP, Sci. Results*, 154: College Station, TX (Ocean Drilling Program), 69–82.

Siegenthaler, U., and Wenk, T.H., 1984. Rapid atmospheric CO_2 variations and ocean circulation. *Nature,* 308:624–626.

Sowers, T., and Bender, M., 1995. Climate records covering the last deglaciation. *Science*, 269:210–214.

Tucholke, B.E., and Embley, R.W., 1984. Cenozoic regional erosion of the abyssal seafloor off South Africa. *In* Schlee, J.S. (Ed.), *Interregional Unconformities and Hydrocarbon Accumulation*. AAPG Mem., 36:145–164.

Webb, P.-N., and Harwood, D.M., 1991. Late Cenozoic glacial history of the Ross Embayment, Antarctica. *In* Cronin, T.M., and Dowsett, H.J. (Eds.), *Pliocene Climates*. Quat. Sci. Rev., 10:215–223.

Weedon, G.P., Shackleton, N.J., and Pearson, P.N., 1997. The Oligocene time scale and cyclostratigraphy on the Ceara Rise, western equatorial Atlantic. *In* Shackleton, N.J., Curry, W.B., Richter, C., and Bralower, T.J. (Eds.), *Proc. ODP, Sci. Results*, 154: College Station, TX (Ocean Drilling Program), 101–114.

Zachos, J.C., Flower, B., and Paul, H., 1997. Orbitally paced climate oscillations across the Oligocene/Miocene boundary. *Nature*, 388:567–570.

Zachos, J.C., Rea, D.K., Seto, K., Nomura, R., and Niitsuma, N., 1992. Paleogene and early Neogene deep water history of the Indian Ocean: inferences from stable isotopic records. *In* Duncan, R.A., Rea, D.K., Kidd, R.B., von Rad, U. and Weissel, J.K. (Eds.), *The Indian Ocean: A Synthesis of Results from the Ocean Drilling Program*. Am. Geophys. Union, Geophys. Monogr., 70:351–386.

Figure F1. Locations of Leg 177 drill sites and previous ODP and DSDP sites in the South Atlantic relative to major frontal boundaries.

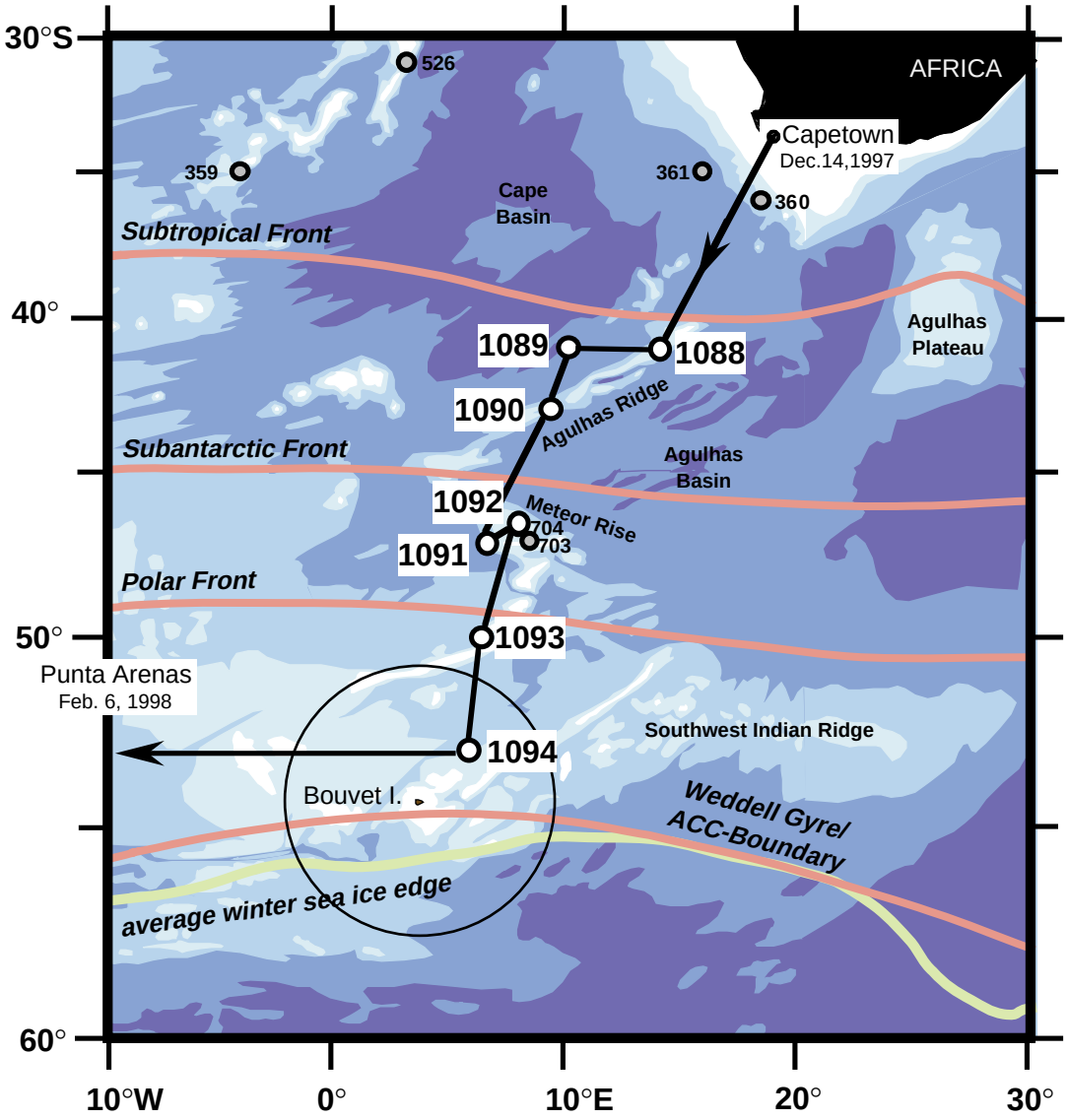

Figure F2. Leg 177 sites relative to the vertical distribution of potential temperature on a north-south transect from the Agulhas Ridge to Bouvet Island in the southeast Atlantic Ocean. NADW = North Atlantic Deep Water; CDW = Circumpolar Deep Water; AABW = Antarctic Bottom Water; AAIW = Antarctic Intermediate Water; SASW = Subantarctic Surface Water; SAF = Subantarctic Front; and PF = Polar Front.

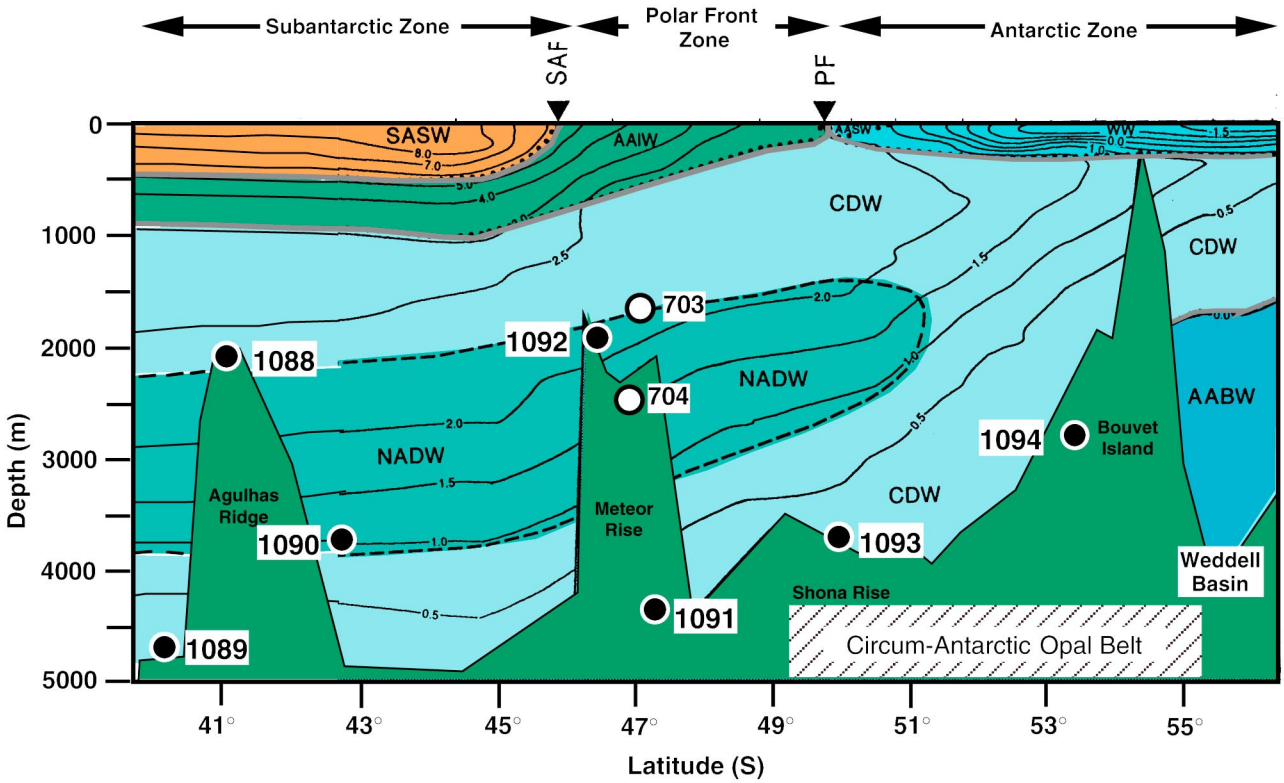

Figure F3. Schematic representation of present ocean circulation and interocean exchange showing the central role of the circumpolar region in global circulation (numbers are water fluxes in Sverdrups, 1 sv = 10^6 m^3/s). Not shown are the deep Indian and Pacific reservoirs (after Keir, 1988).

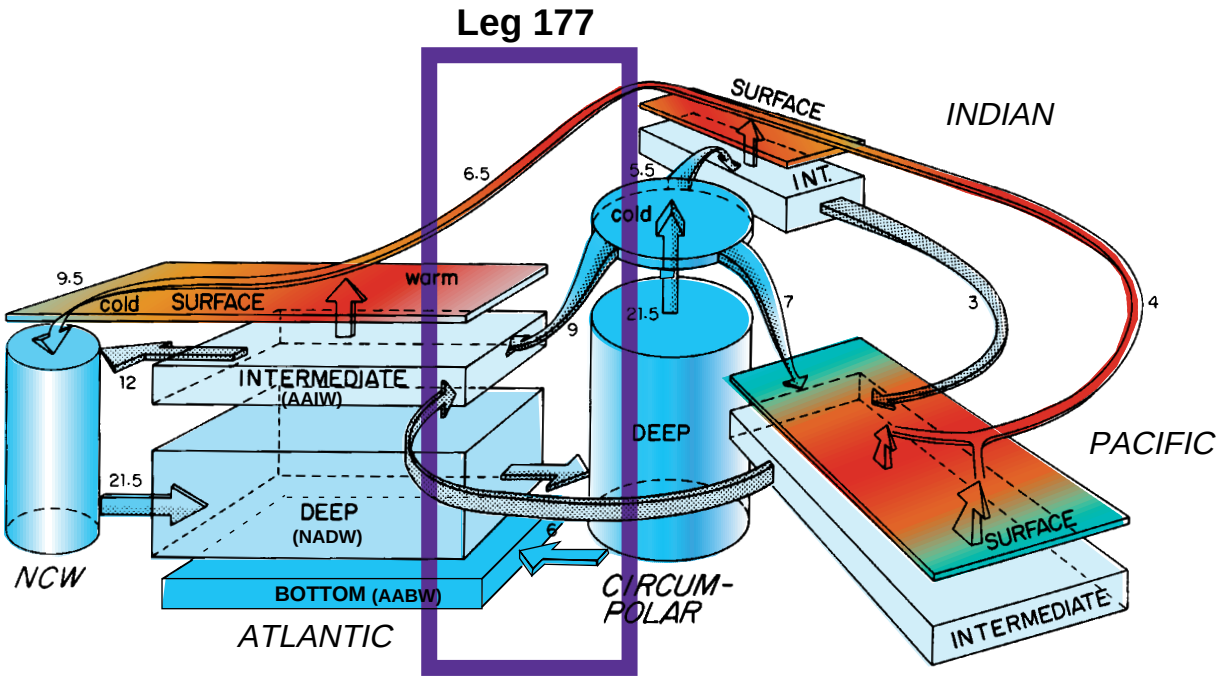

Figure F4. Location of ODP and DSDP sites drilled in the Southern Ocean relative to ocean frontal systems and sea-ice distribution.

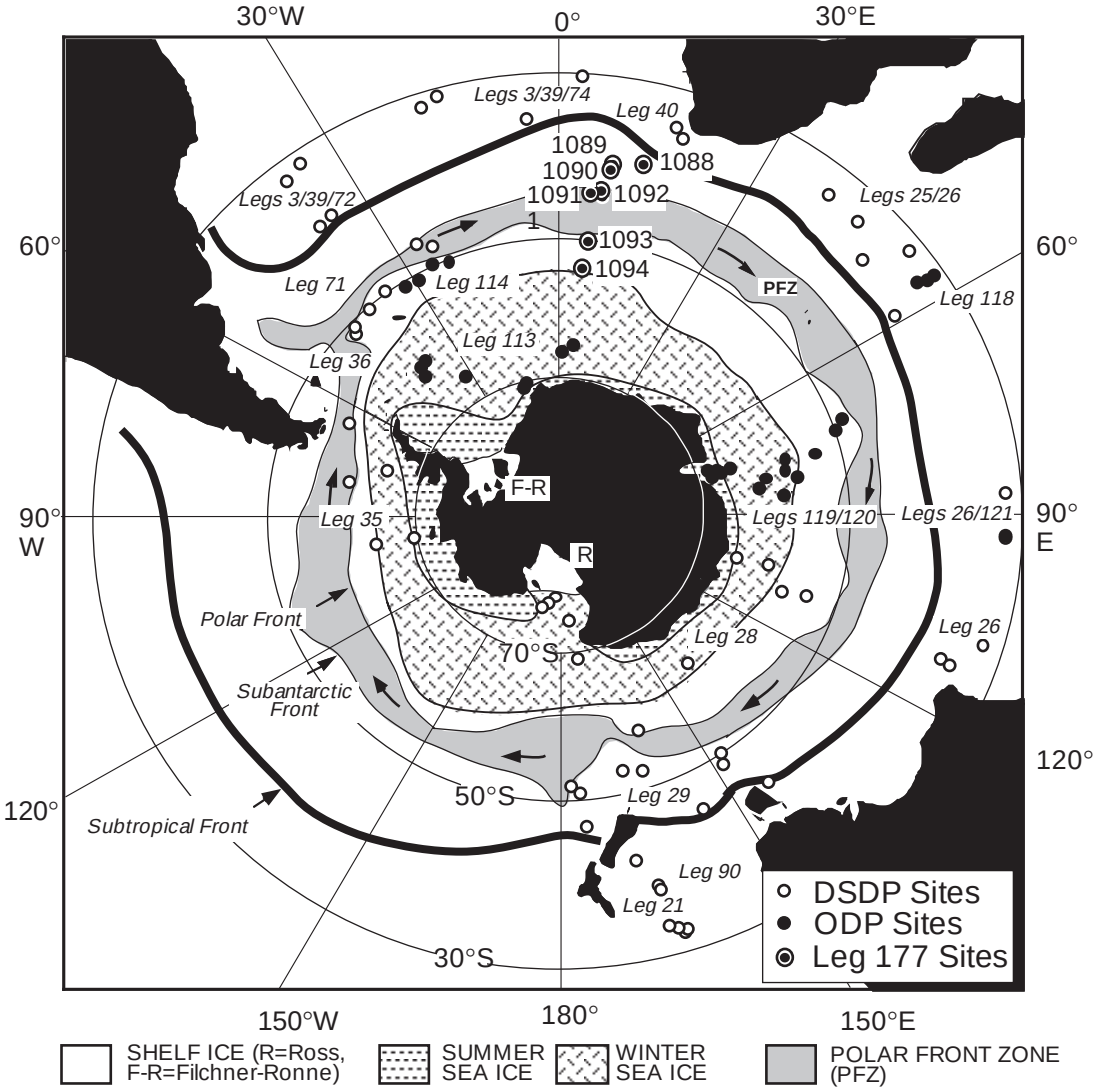

Figure F5. Position of Leg 177 sites relative to the gravity field of the southeast Atlantic Ocean derived from Geosat Exact Repeat Mission (ERM) and Geodetic Mission (GM) data.

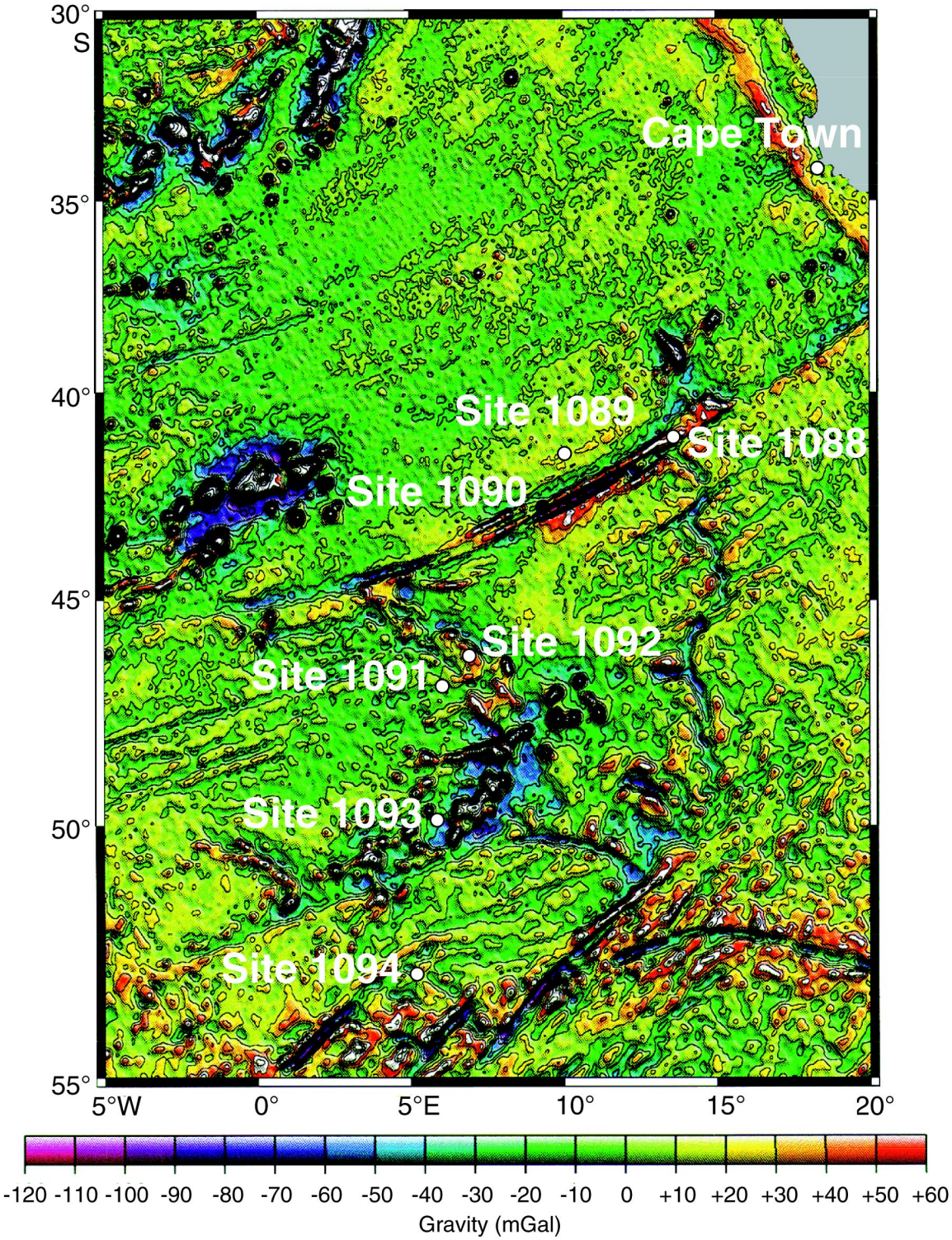

Figure F6. Schematic tectonic map of the Agulhas Basin showing Leg 177 sites relative to seafloor magnetic anomalies (after Raymond and LaBrecque, 1988). Contours are in meters.

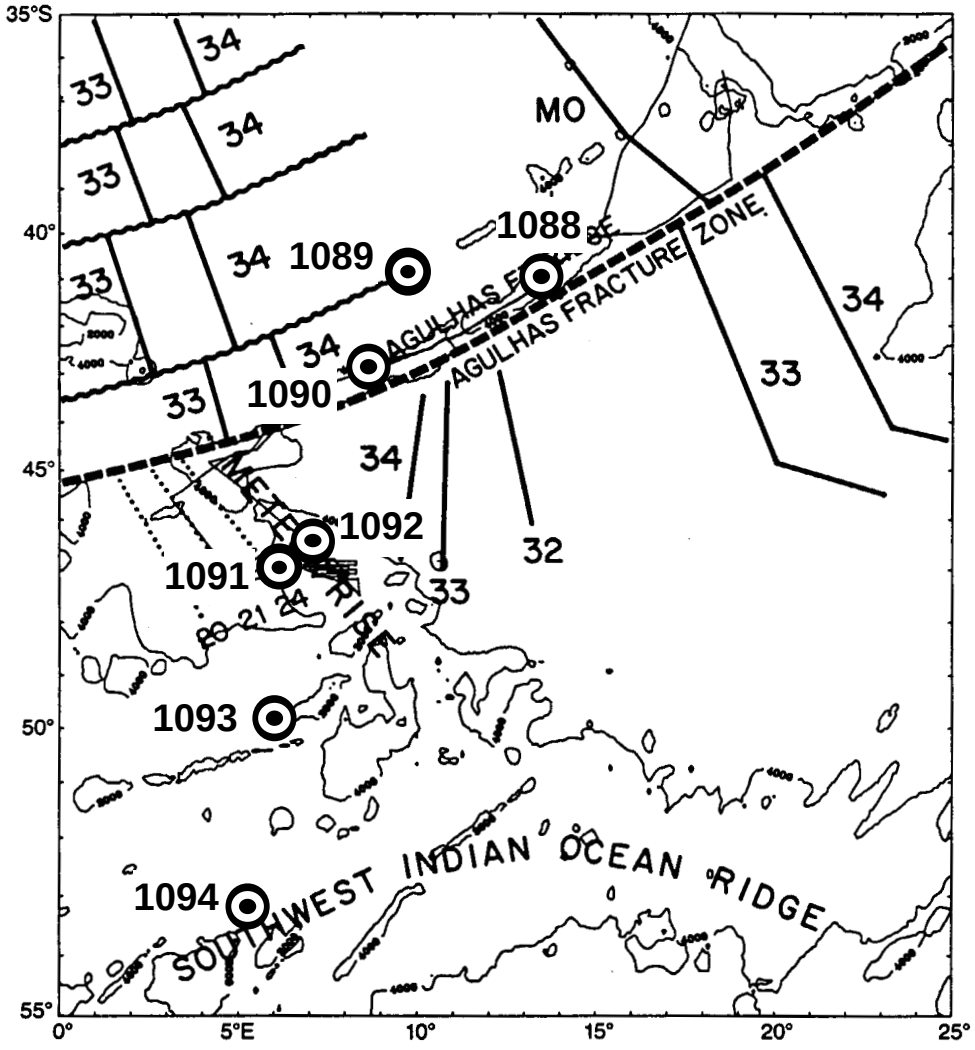

Figure F7. Tectonic reconstruction of the South Atlantic during the late Paleocene and middle Eocene with positions of sites drilled during DSDP Leg 36 (dots) and ODP Legs 114 (dots) and 177 (dots with circles) (after Ciesielski, Kristoffersen, et al., 1988).

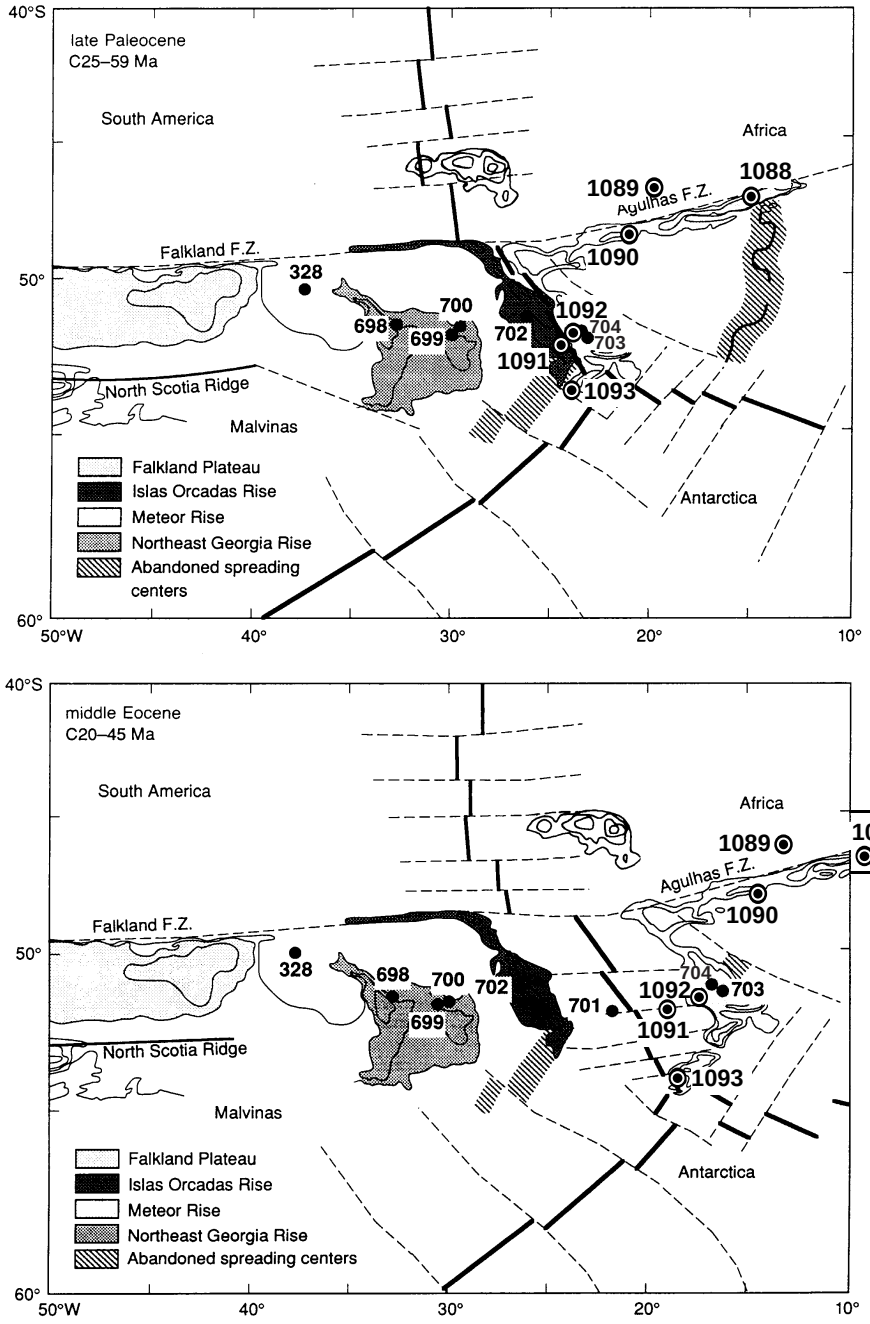

Figure F8. Temperature and salinity at water depths of Leg 177 sites taken from conductivity-temperature-depth profiles collected during site-survey *Thomas G. Thompson* Cruise TTN057. Temperature and salinity values are shown relative to components of North Atlantic Deep Water (NADW), which includes Labrador Sea Water (LSW), Gibbs Fracture Zone Water (GFZW), and Denmark Straits Overflow Water (DSOW). Also shown are mean values for Circumpolar Deep Water (CDW).

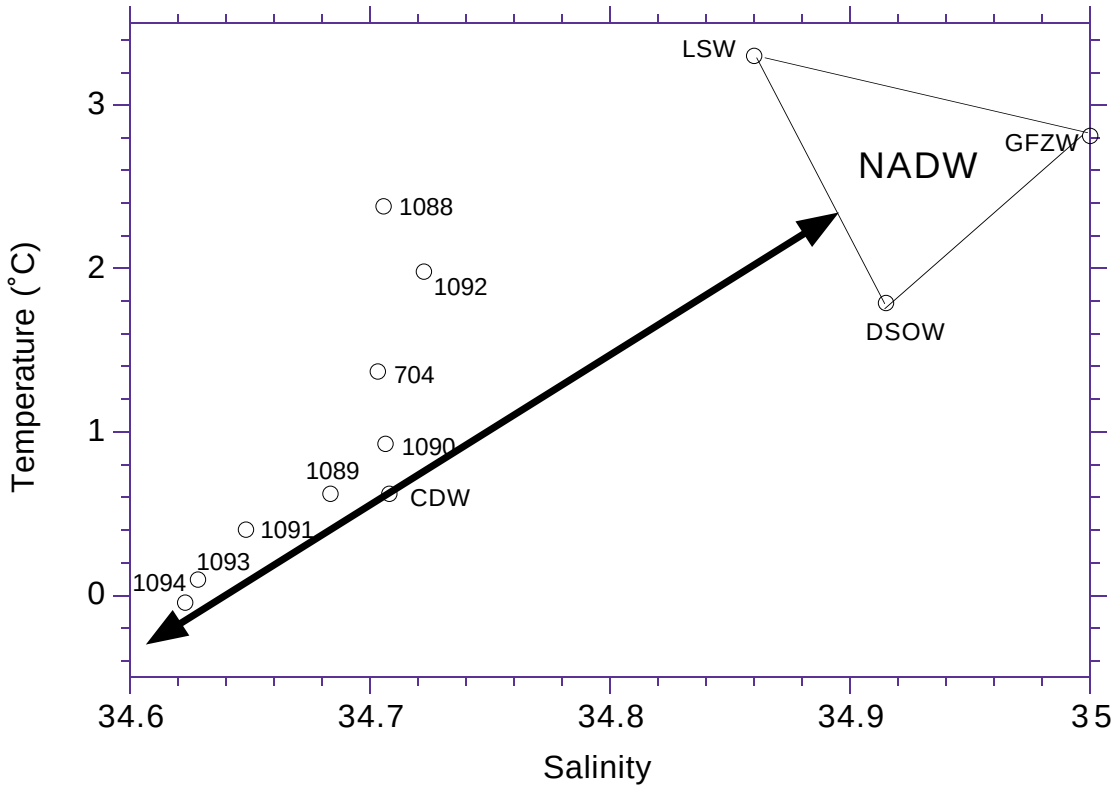

Figure F9. Positions of Leg 177 sites relative to the depositional regimes in the basins around South Africa (after Tucholke and Embley [1984] and Ciesielski, Kristoffersen, et al. [1988]). 1 = core of circumbasin erosional zone; 2 = basement exposed by current erosion; 3 = sediment wave field; 4 = zone of thin sediment along the mid-oceanic ridge axis and beneath the ACC; 5 = thick sediment drifts with weak acoustic laminae; 6 = generalized bathymetric contours as labeled (4500 m is a dashed line); 7 = limit of thick, moderately laminated drifts of diatom sediment extending north of the polar front; 8 = glide plane scars at the head of slumps and slides; 9 = approximate seaward limit of slumps and slides; 10 = seamounts; 12 = manganese nodules/pavement observed in seafloor photographs; 13 = current direction from seafloor photographs; 14 = direct current measurements; and 15 = flow of AABW inferred from bottom-water potential temperature.

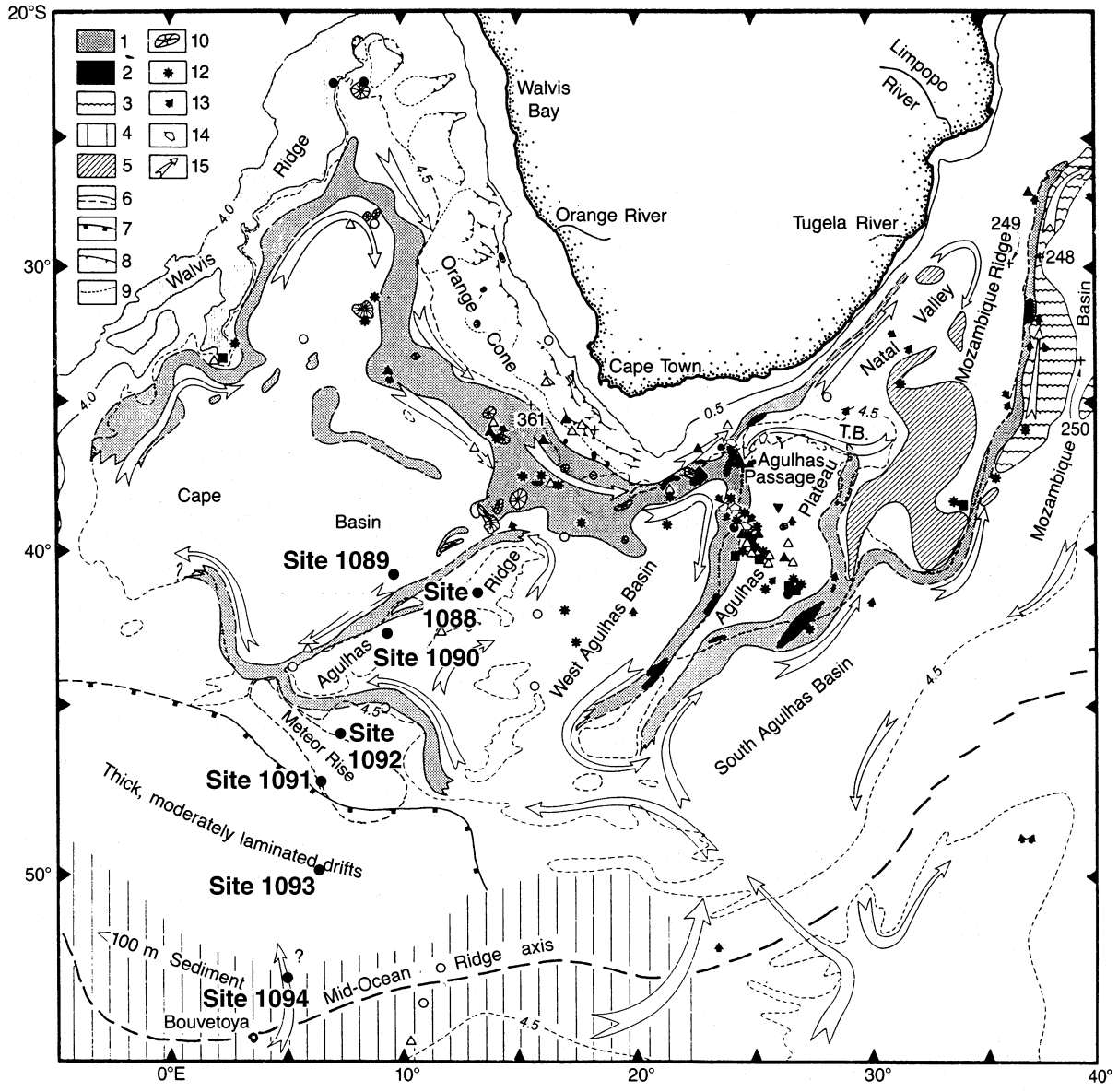

Figure F10. Age-depth plots for Leg 177 Sites 1088, 1090, and 1092 for the middle Eocene–Pleistocene.

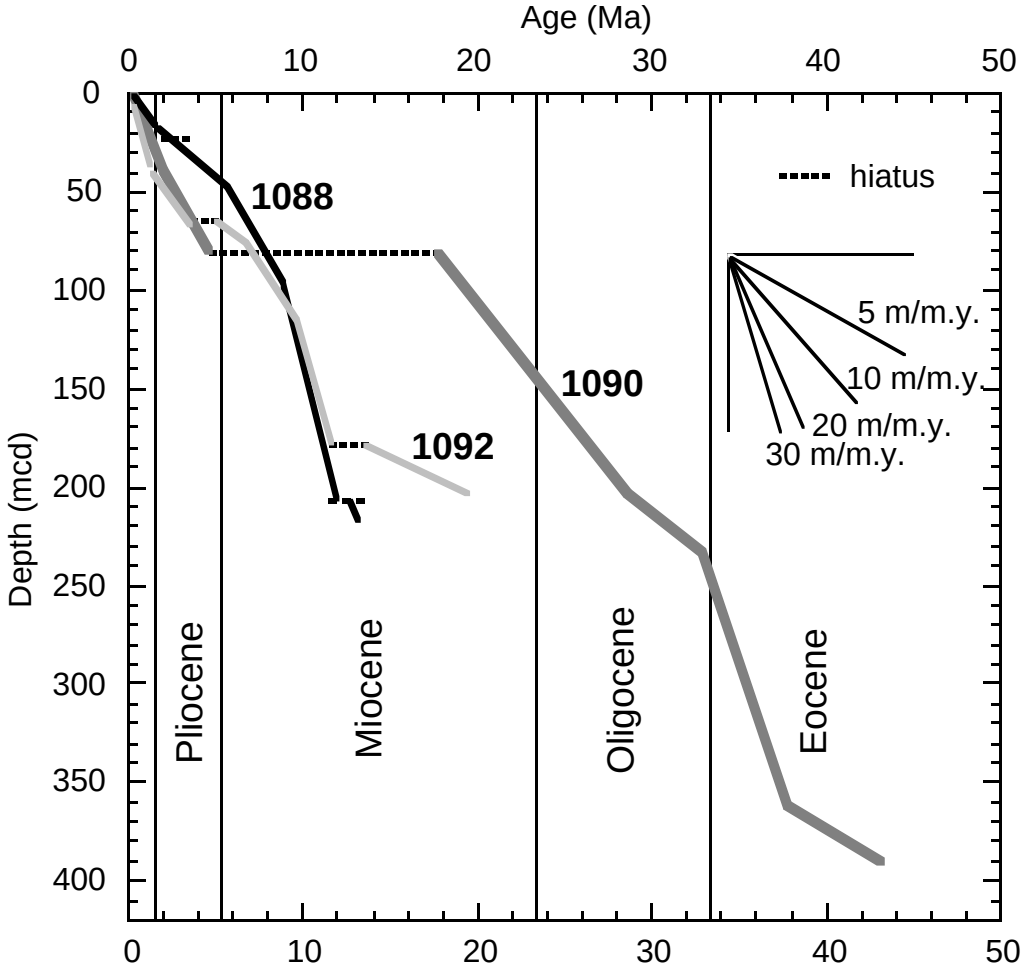

Figure F11. Correlation of percent red reflectance (650–750 nm) of Brunhes Chron expanded sections from Sites 1089 (41°S), 1091 (47°S), 1093 (50°S), and 1094 (53°S) along a north-south transect across the ACC. Dashed lines indicate marine isotopic stages inferred from peaks in blue reflectance that represent carbonate peaks. B/M = Brunhes/Matuyama boundary.

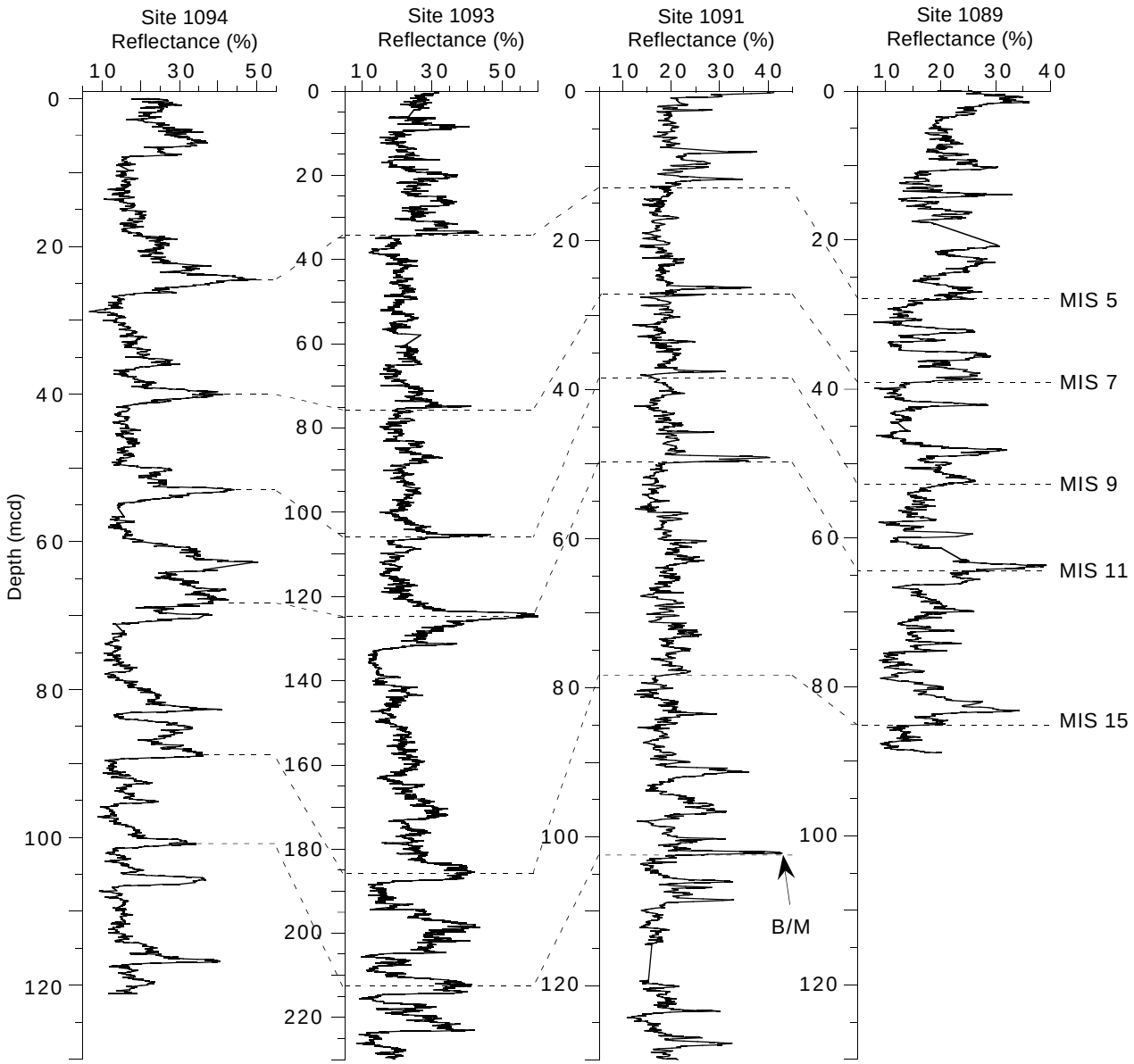

Figure F12. Age-depth plots for Leg 177 Sites 1089, 1091, 1093, and 1094 for the Pliocene–Pleistocene.

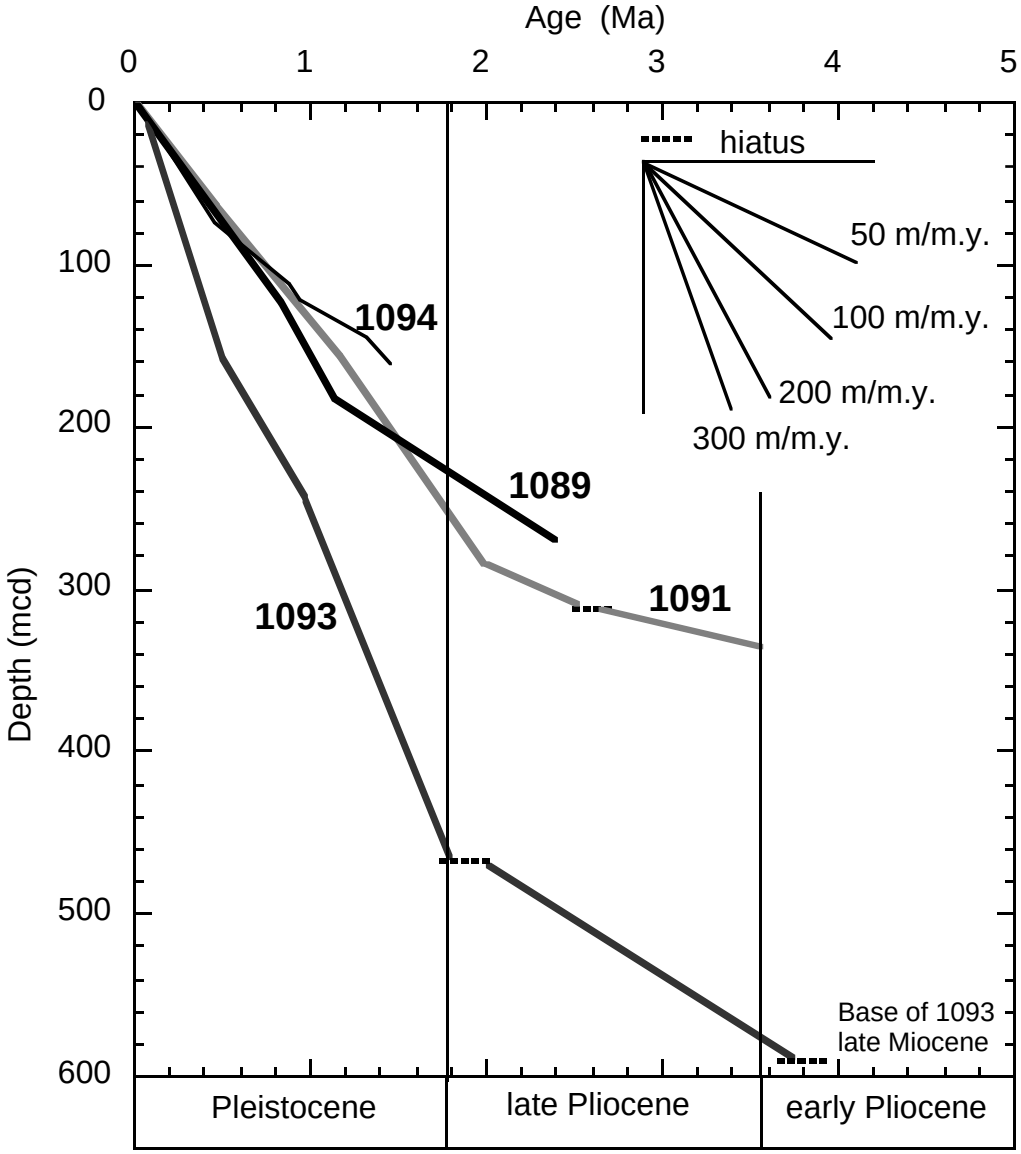

Figure F13. Percent blue and red reflectance at Site 1090. H = hiatus.

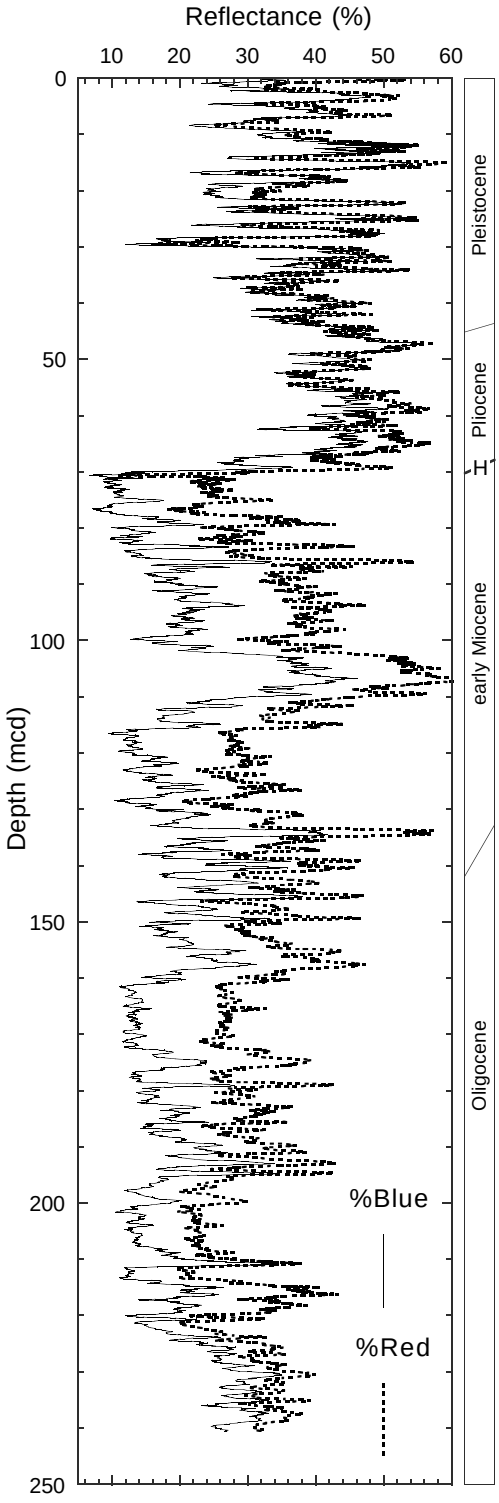

Figure F14. Interstitial water profiles of chloride (Cl), sulfate (SO_4), phosphate (PO_4), and manganese (Mn) from the high–sedimentation-rate diatom-ooze Sites 1091, 1093, and 1094. See text and individual site chapters for a more detailed explanation of the profiles.

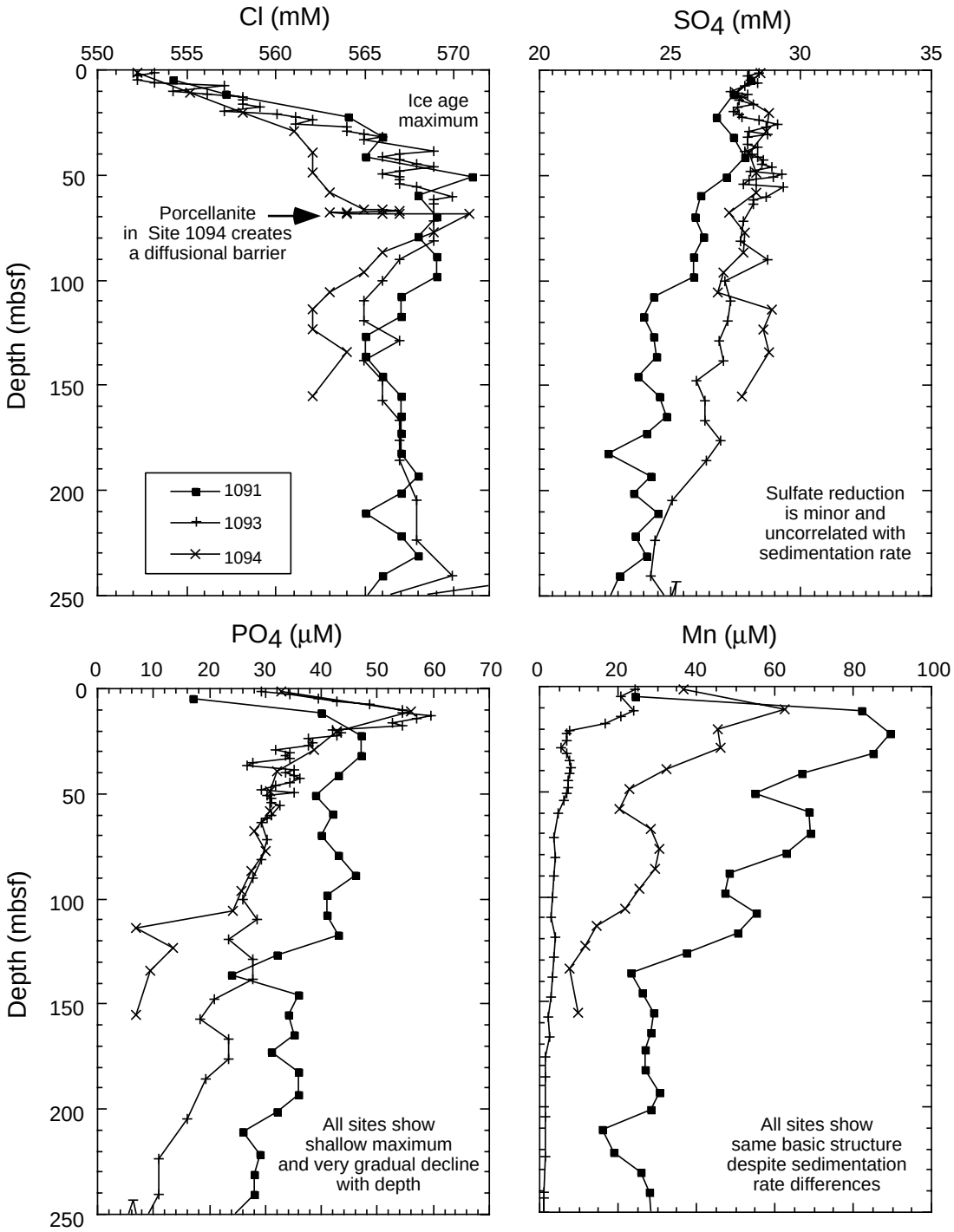

Figure F15. Summary of lithologies and paleomagnetic stratigraphies of expanded sections recovered at Sites 1089 (41°S), 1091 (47°S), 1093 (50°S), and 1094 (53°S) along a north-south transect across the ACC. The geomagnetic polarity time scale of Cande and Kent (1992) is shown on the right. See Figure **F2**, p. 36, for abbreviations; w.d. = water depth.

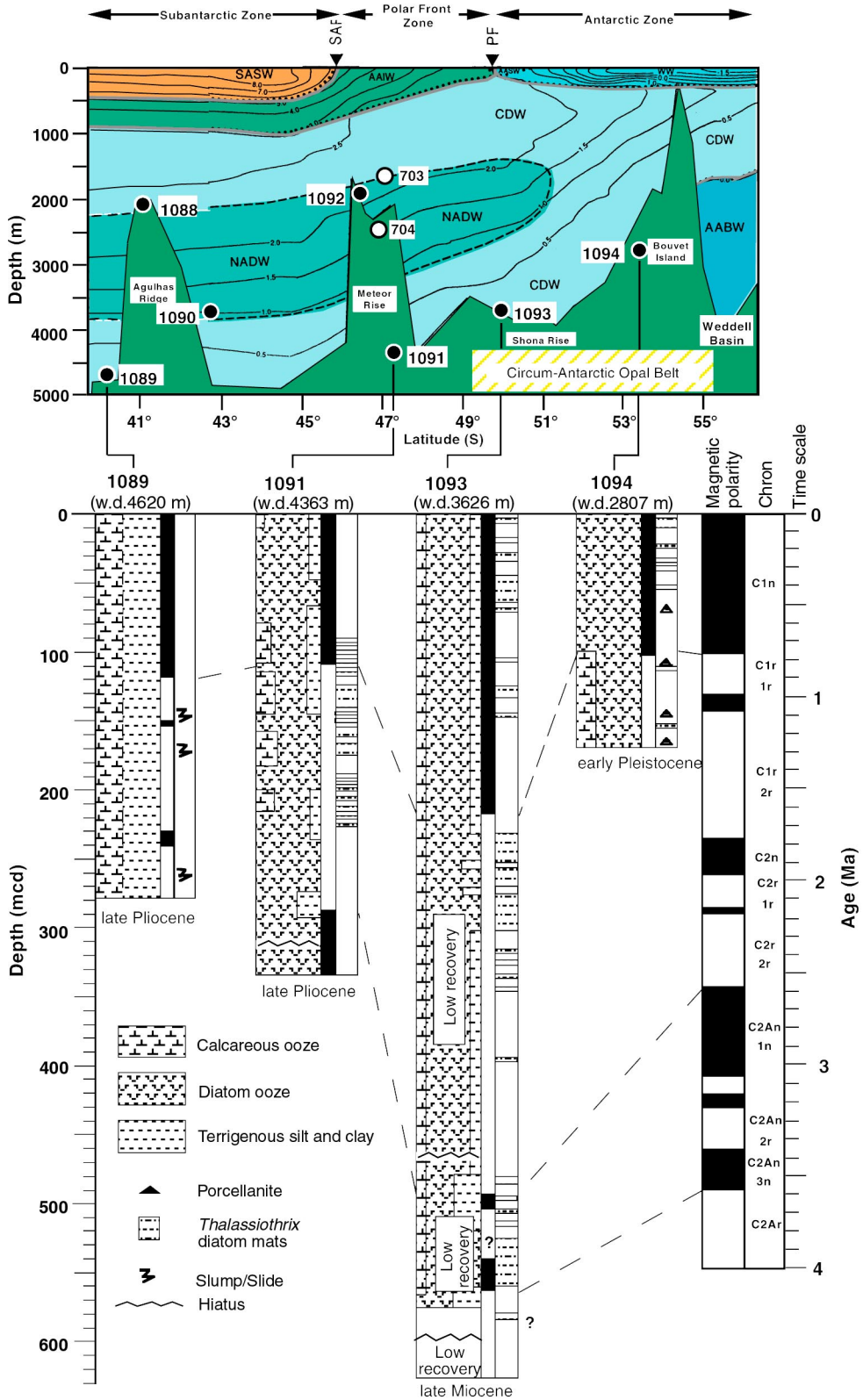

Figure F16. Example of a laminated diatom mat from interval 177-1093A-23H-4, 78–120 cm.

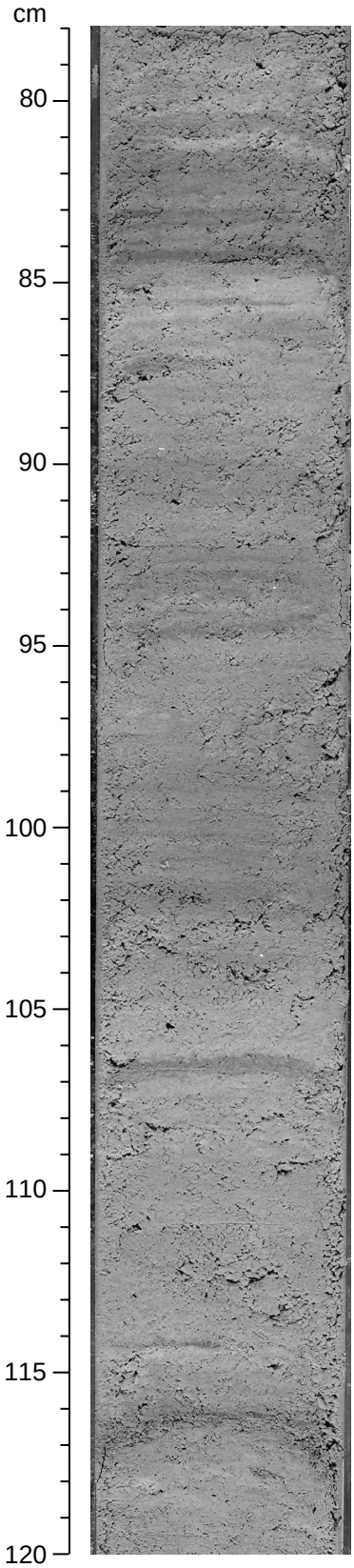

Figure F17. Downhole variations of percent blue reflectance (450–550 nm), volume-specific magnetic susceptibility, bulk density determined by gamma-ray attenuation (GRA; line = smoothed data) and moisture and density (MAD; open circles), and natural gamma radiation (lines = smoothed data from different holes) at Site 1094. Dashed lines indicate marine isotopic stages inferred from peaks in blue reflectance that represent carbonate peaks.

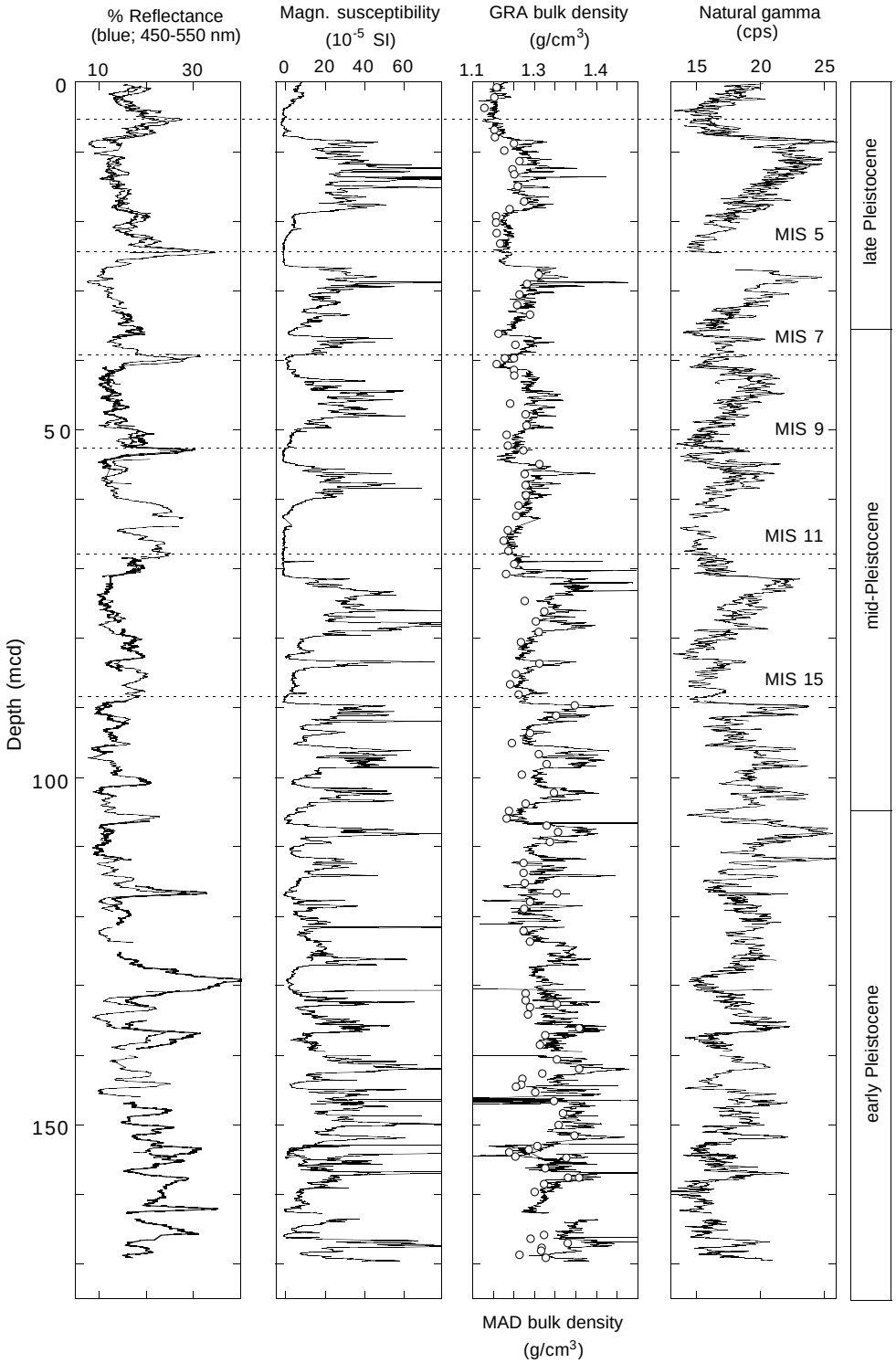

Figure F18. Summary of lithologies for Leg 177 Sites 1088 through 1094. See Figure F2, p. 36, for abbreviations; w.d. = water depth.

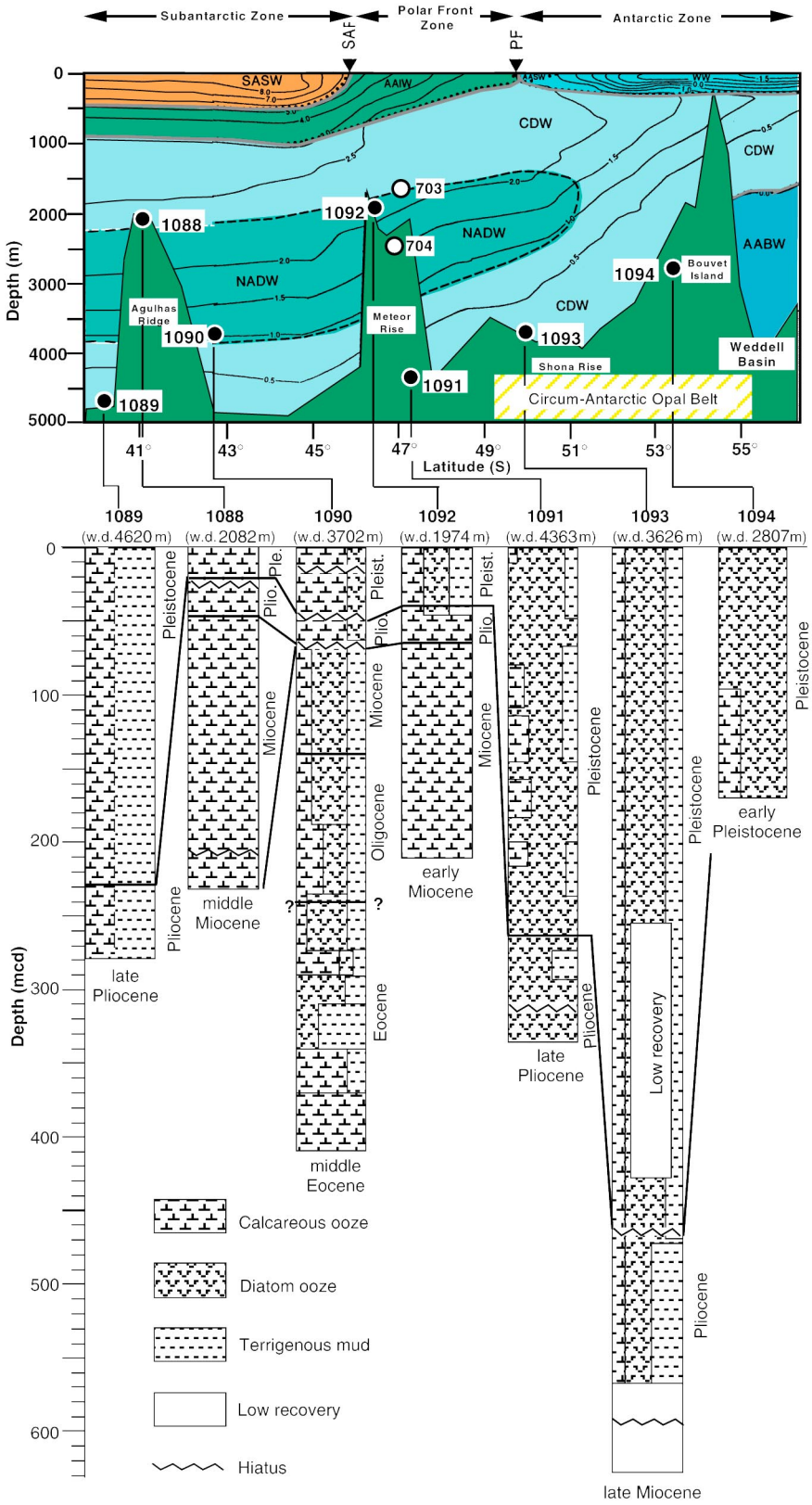

Figure F19. Variation in oxygen isotopic ratios of deep-sea benthic foraminifers from the Atlantic Ocean (left) relative to the global sea-level curve inferred from seismic stratigraphic analysis (middle) (after Barrett, 1994). Shown on the right are the recovered Leg 177 sequences that represent these time intervals.

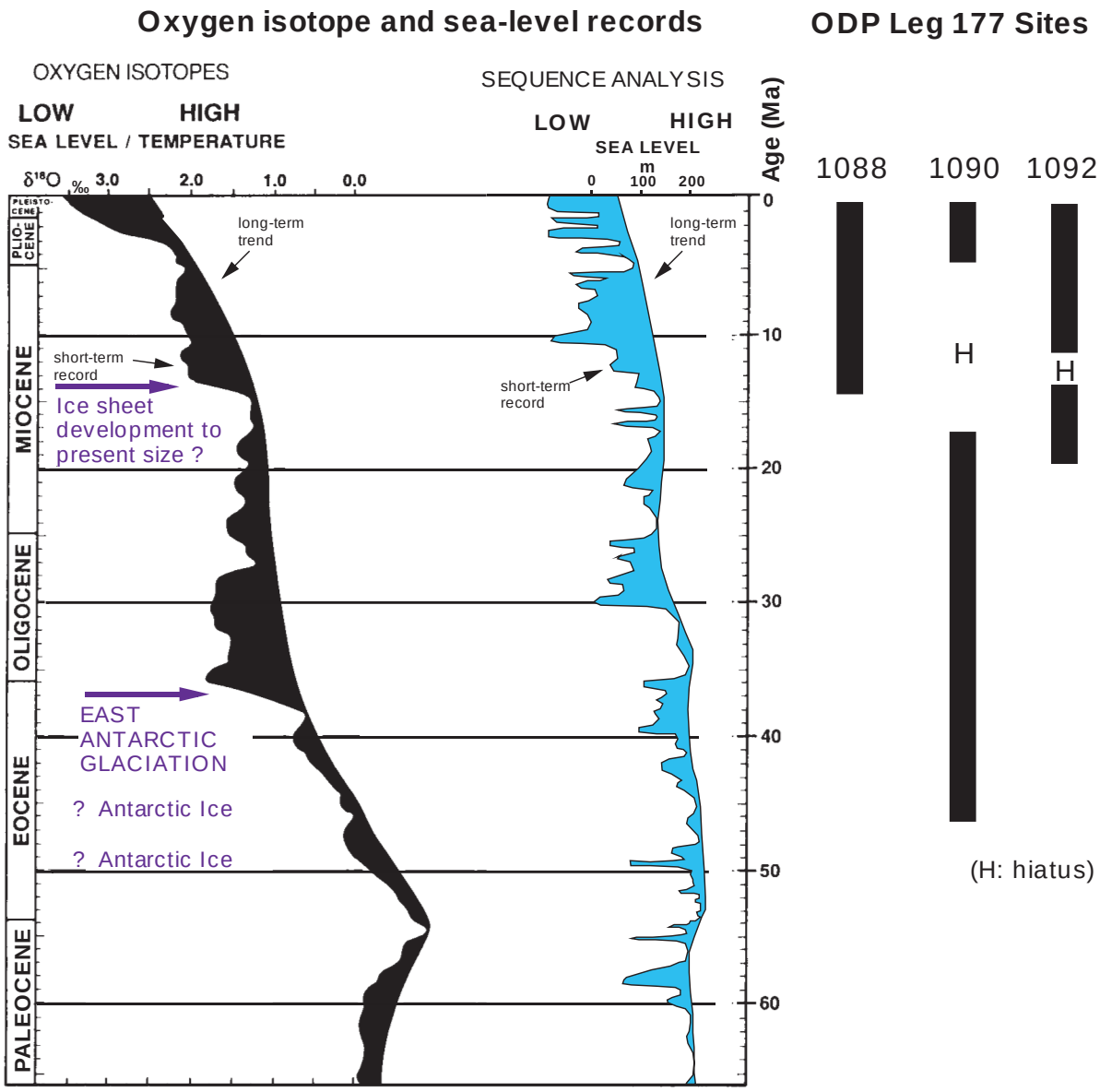

1‰ $\delta^{18}O$ = 110 m sea-level or 4°C water-temperature change
(modified from Barrett, 1994)

Table T1. Location, water depth, and coring summary of holes drilled during Leg 177.

Hole	Latitude	Longitude	Water depth (mbsl)	Number of cores	Interval cored (m)	Length recovered (m)	Recovery (%)	Drilled (m)	Total penetration (m)	Bottom of splice (mcd)	Time on hole (hr)	Time on site (days)
1088A	41°8.163′S	13°33.770′E	2082.2	1	9.5	9.9	104.6	0.0	9.50		12.00	0.5
1088B	41°8.163′S	13°33.770′E	2081.2	14	129.0	125.6	97.3	0.0	129.00		13.50	0.6
1088C	41°8.165′S	13°33.772′E	2082.9	14	114.9	93.9	81.7	118.5	233.40		23.25	1.0
Average:			2082.1									
Totals:				29	253.4	229.4	90.5	118.5	371.90	0.00	48.75	2.0
1089A	40°56.187′S	9°53.645′E	4619.3	23	216.3	149.6	69.2	0.0	216.30		45.00	1.9
1089B	40°56.182′S	9°53.640′E	4623.8	29	264.9	246.6	93.1	0.0	264.90		33.50	1.4
1089C	40°56.169′S	9°53.637′E	4621.2	22	192.4	160.3	83.3	2.0	194.40		27.50	1.1
1089D	40°56.187′S	9°53.632′E	4617.5	13	118.0	119.4	101.2	0.0	118.00		27.25	1.1
Average:			4620.5									
Totals:				87	791.6	675.9	85.4	2.0	793.60	94.00	133.25	5.6
1090A	42°54.821′S	8°53.984′E	3698.6	1	7.0	7.0	100.3	0.0	7.00		22.00	0.9
1090B	42°54.821′S	8°53.984′E	3699.4	43	397.5	373.2	93.9	0.0	397.50		47.75	2.0
1090C	42°54.812′S	8°53.990′E	3703.7	8	69.3	63.8	92.1	0.0	69.30		8.50	0.4
1090D	42°54.814′S	8°53.998′E	3702.1	24	225.9	213.6	94.6	0.0	225.90		25.50	1.1
1090E	42°54.818′S	8°53.994′E	3704.2	25	236.7	217.3	91.8	0.0	236.70		35.50	1.5
Average:			3701.6									
Totals:				101	936.4	874.9	93.4	0.0	936.40	212.00	139.25	5.8
1091A	47°5.681′S	5°55.120′E	4360.5	33	310.9	279.8	90.0	0.0	310.90		56.50	2.4
1091B	47°5.682′S	5°55.125′E	4356.6	29	273.8	203.5	74.3	0.0	273.80		32.25	1.3
1091C	47°5.689′S	5°55.166′E	4366.4	1	4.0	4.0	98.8	0.0	4.00		1.25	0.1
1091D	47°5.689′S	5°55.166′E	4366.8	22	203.1	165.2	81.3	0.0	203.10		24.50	1.0
1091E	47°5.695′S	5°55.152′E	4366.2	6	51.7	31.4	60.7	0.0	51.70		16.50	0.7
Average:			4363.3									
Totals:				91	843.5	683.8	81.1	0.0	843.50	234.00	131.00	5.5
1092A	46°24.708′S	7°4.792′E	1976.3	20	188.5	181.9	96.5	0.0	188.50		20.00	0.8
1092B	46°24.705′S	7°4.794′E	1972.9	18	168.9	144.5	85.6	0.0	168.90		12.25	0.5
1092C	46°24.697′S	7°4.796′E	1973.3	18	165.5	150.8	91.1	0.0	165.50		12.00	0.5
1092D	46°24.704′S	7°4.787′E	1972.9	4	28.5	28.3	99.3	36.4	64.90		10.25	0.4
Average:			1973.9									
Totals:				60	551.4	505.5	91.7	36.4	587.80	188.00	54.50	2.3
1093A	49°58.596′S	5°51.924′E	3623.9	34	309.4	263.7	85.2	0.0	309.40		34.60	1.4
1093B	49°58.592′S	5°51.933′E	3630.6	24	221.8	209.0	94.2	0.0	221.80		25.50	1.1
1093C	49°58.593′S	5°51.946′E	3631.7	18	169.5	119.5	70.5	0.0	169.50		23.50	1.0
1093D	49°58.591′S	5°51.934′E	3623.7	51	461.7	160.4	34.7	136.0	597.70		104.50	4.4
1093E	49°58.578′S	5°51.933′E	3623.7	4	19.0	11.5	60.5	23.5	42.50		7.75	0.3
1093F	49°58.578′S	5°51.933′E	3623.7	2	9.5	6.2	65.3	34.0	43.50		12.00	0.5
Average:			3626.2									
Totals:				133	1190.9	770.3	64.7	193.5	1384.4	252.0	207.85	8.7
1094A	53°10.812′S	5°7.824′E	2807.6	19	158.6	135.1	85.2	1.0	159.60		17.50	0.7
1094B	53°10.824′S	5°7.830′E	2806.7	4	38.0	23.6	62.1	0.0	38.00		5.25	0.2
1094C	53°10.828′S	5°7.808′E	2807.3	8	73.1	46.6	63.7	0.0	73.10		8.00	0.3
1094D	53°10.816′S	5°7.821′E	2807.7	17	152.0	100.8	66.3	19.1	171.10		30.50	1.3
Average:			2807.3									
Totals:				48	421.7	306.1	72.6	20.1	441.8	121.00	61.25	2.6
Leg 177 totals:				549	4988.9	4045.9	81.1	370.50	5359.4	1101.00	775.85	32.3

Table T2. Coring summary for Site 1088.

Core	Date (December 1997)	Time (UTC)	Interval (mbsf)	Length cored (m)	Length recovered (m)	Recovery (%)
177-1088A-						
1H	17	0945	0-9.5	9.5	9.94	104.6
Coring totals:				9.5	9.94	104.6
177-1088B-						
1H	17	1025	0.0-5.5	5.5	5.46	99.3
2H	17	1110	5.5-15.0	9.5	9.01	94.8
3H	17	1145	15.0-24.5	9.5	9.02	94.9
4H	17	1245	24.5-34.0	9.5	9.63	101.4
5H	17	1320	34.0-43.5	9.5	8.98	94.5
6H	17	1355	43.5-53.0	9.5	9.41	99.1
7H	17	1440	53.0-62.5	9.5	9.52	100.2
8H	17	1505	62.5-72.0	9.5	9.02	94.9
9H	17	1550	72.0-81.5	9.5	8.88	93.5
10H	17	1625	81.5-91.0	9.5	10.05	105.8
11H	17	1715	91.0-100.5	9.5	8.21	86.4
12H	17	1750	100.5-110.0	9.5	9.60	101.1
13H	17	1825	110.0-119.5	9.5	9.10	95.8
14H	17	2115	119.5-129.0	9.5	9.66	101.7
Coring totals:				129.0	125.55	97.3
177-1088C-						
	18	0335	0.0-5.8	5.8	5.81	100.2
		****** Drilled from 5.8 to 124.3 mbsf ******				
2H	18	0800	124.3-133.8	9.5	8.08	85.1
3H	18	0840	133.8-143.3	9.5	9.60	101.1
4H	18	0920	143.3-152.8	9.5	9.15	96.3
5H	18	1045	152.8-162.3	9.5	9.38	98.7
6X	18	1200	162.3-166.0	3.7	3.69	99.7
7X	18	1245	166.0-175.6	9.6	5.88	61.3
8X	18	1330	175.6-185.2	9.6	9.67	100.7
9X	18	1410	185.2-194.8	9.6	8.91	92.8
10X	18	1450	194.8-204.4	9.6	7.73	80.5
11X	18	1530	204.4-214.1	9.7	5.02	51.8
12X	18	1610	214.1-223.7	9.6	1.32	13.8
13X	18	1650	223.7-233.4	9.7	9.62	99.2
Coring totals:				114.9	93.86	81.7
Drilling total:				118.5		
Total:				233.4		

Notes: UTC = Universal Time Coordinated. An expanded coring summary table that includes lengths and depths of sections and sampling comments is available in ASCII format in the **TABLES** directory.

Table T3. Coring summary for Site 1089. (See table note. Continued on next page.)

Core	Date (December 1997)	Time (UTC)	Interval (mbsf)	Length cored (m)	Length recovered (m)	Recovery (%)
177-1089A-						
1H	20	0520	0.0-7.3	7.3	7.32	100.3
2H	20	0625	7.3-16.8	9.5	9.65	101.6
3H	20	0810	16.8-26.3	9.5	4.43	46.6
4H	20	0930	26.3-35.8	9.5	4.41	46.4
5H	20	1030	35.8-45.3	9.5	7.61	80.1
6H	20	1135	45.3-54.8	9.5	7.00	73.7
7H	20	1720	54.8-64.3	9.5	8.68	91.4
8H	20	1905	64.3-73.8	9.5	9.78	102.9
9H	20	2015	73.8-83.3	9.5	1.49	15.7
10H	20	2120	83.3-92.8	9.5	9.72	102.3
11H	20	2225	92.8-102.3	9.5	5.15	54.2
12H	20	2330	102.3-111.8	9.5	9.34	98.3
13H	21	0040	111.8-121.3	9.5	0.05	0.5
14H	21	0150	121.3-130.8	9.5	8.82	92.8
15H	21	0255	130.8-140.3	9.5	5.95	62.6
16H	21	0400	140.3-149.8	9.5	8.99	94.6
17H	21	0505	149.8-159.3	9.5	0.08	0.8
18H	21	0605	159.3-168.8	9.5	6.97	73.4
19H	21	0715	168.8-178.3	9.5	8.99	94.6
20H	21	0820	178.3-187.8	9.5	9.28	97.7
21H	21	0935	187.8-197.3	9.5	7.34	77.3
22H	21	1045	197.3-206.8	9.5	0.00	0.0
23H	21	1155	206.8-216.3	9.5	8.59	90.4
Coring totals:				216.3	149.64	69.2
177-1089B-						
1H	21	1810	0.0-4.8	4.8	4.80	100.0
2H	21	1910	4.8-14.3	9.5	8.92	93.9
3H	21	2005	14.3-23.8	9.5	8.90	93.7
4H	21	2055	23.8-33.3	9.5	8.67	91.3
5H	21	2155	33.3-42.8	9.5	8.65	91.1
6H	21	2250	42.8-52.3	9.5	8.43	88.7
7H	21	2345	52.3-61.8	9.5	8.49	89.4
8H	22	0045	61.8-71.3	9.5	8.27	87.1
9H	22	0145	71.3-80.8	9.5	8.99	94.6
10H	22	0245	80.8-90.3	9.5	7.50	78.9
11H	22	0345	90.3-99.8	9.5	8.84	93.1
12H	22	0440	99.8-109.3	9.5	8.68	91.4
13H	22	0540	109.3-118.8	9.5	8.68	91.4
14H	22	0640	118.8-128.3	9.5	8.39	88.3
15H	22	0735	128.3-137.8	9.5	8.43	88.7
16H	22	0830	137.8-147.3	9.5	8.65	91.1
17H	22	0935	147.3-156.8	9.5	8.03	84.5
18H	22	1030	156.8-166.3	9.5	8.64	90.9
19H	22	1130	166.3-175.8	9.5	9.08	95.6
20H	22	1220	175.8-185.3	9.5	9.45	99.5
21H	22	1315	185.3-194.8	9.5	8.96	94.3
22H	22	1410	194.8-204.3	9.5	9.55	100.5
23H	22	1500	204.3-213.8	9.5	9.43	99.3
24H	22	1555	213.8-223.3	9.5	9.68	101.9
25H	22	1650	223.3-232.8	9.5	9.53	100.3
26H	22	1745	232.8-242.3	9.5	9.26	97.5
27H	22	1835	242.3-251.8	9.5	8.57	90.2
28H	22	1930	251.8-257.9	6.1	6.09	99.8
29H	22	2035	257.9-264.9	7.0	7.06	100.9
Coring totals:				264.9	246.62	93.1
177-1089C-						
1H	23	0055	0.0-2.4	2.4	2.43	101.3
		****** Drilled from 2.4 to 4.4 mbsf ******				
2H	23	0200	4.4-13.9	9.5	5.05	53.2
3H	23	0300	13.9-23.4	9.5	3.57	37.6
4H	23	0400	23.4-32.9	9.5	8.43	88.7
5H	23	0510	32.9-42.4	9.5	8.06	84.8
6H	23	0615	42.4-51.9	9.5	9.11	95.9
7H	23	0720	51.9-61.4	9.5	9.01	94.8

Table T3 (continued).

Core	Date (December 1997)	Time (UTC)	Interval (mbsf)	Length cored (m)	Length recovered (m)	Recovery (%)
8H	23	0830	61.4-70.9	9.5	9.04	95.2
9H	23	0935	70.9-80.4	9.5	9.25	97.4
10H	23	1045	80.4-89.9	9.5	7.73	81.4
11H	23	1315	89.9-99.4	9.5	9.31	98.0
12H	23	1410	99.4-108.9	9.5	8.08	85.1
13H	23	1605	108.9-118.4	9.5	8.62	90.7
14H	23	1705	118.4-127.9	9.5	8.20	86.3
15H	23	1810	127.9-137.4	9.5	7.91	83.3
16H	23	1915	137.4-146.9	9.5	9.45	99.5
17H	23	2020	146.9-156.4	9.5	9.48	99.8
18H	23	2120	156.4-165.9	9.5	9.20	96.8
19H	23	2220	165.9-175.4	9.5	3.71	39.1
20H	23	2325	175.4-184.9	9.5	8.66	91.2
21H	24	0040	184.9-194.4	9.5	5.99	63.1
Coring totals:				192.4	160.29	83.3
Drilled total:				2.0		
Total:				194.4		
177-1089D-						
1H	24	0425	0.0-6.7	6.7	6.70	100.0
2H	24	0535	6.7-13.5	6.8	8.64	127.1
3H	24	0635	13.5-23.0	9.5	9.06	95.4
4H	24	0750	23.0-32.5	9.5	9.66	101.7
5H	24	0915	32.5-42.0	9.5	9.62	101.3
6H	24	1025	42.0-51.5	9.5	9.47	99.7
7H	24	1140	51.5-61.0	9.5	9.66	101.7
8H	24	1245	61.0-70.5	9.5	9.77	102.8
9H	24	1355	70.5-80.0	9.5	9.30	97.9
10H	24	1500	80.0-89.5	9.5	9.77	102.8
11H	24	1605	89.5-99.0	9.5	8.60	90.5
12H	24	1710	99.0-108.5	9.5	9.49	99.9
13H	24	1850	108.5-118.0	9.5	9.62	101.3
Coring totals:				118.0	119.36	101.2

Notes: UTC = Universal Time Coordinated. An expanded coring summary table that includes lengths and depths of sections and sampling comments is available in ASCII format in the **TABLES** directory.

Table T4. Coring summary for Site 1090. (See table note. Continued on next page.)

Core	Date (December 1997)	Time (UTC)	Interval (mbsf)	Length cored (m)	Length recovered (m)	Recovery (%)
177-1090A-						
1H	26	1545	0.0-7.0	7.0	7.02	100.3
Coring totals:				7.0	7.02	100.3
177-1090B-						
1H	26	1645	0.0-4.2	4.2	4.25	101.2
2H	26	1755	4.2-13.7	9.5	9.70	102.1
3H	26	1850	13.7-23.2	9.5	8.63	90.8
4H	26	1945	23.2-32.7	9.5	9.36	98.5
5H	26	2050	32.7-42.2	9.5	8.75	92.1
6H	26	2150	42.2-51.7	9.5	9.69	102.0
7H	26	2300	51.7-61.2	9.5	7.64	80.4
8H	26	2359	61.2-70.7	9.5	8.48	89.3
9H	27	0150	70.7-80.2	9.5	9.34	98.3
10H	27	0300	80.2-89.7	9.5	8.26	86.9
11H	27	0400	89.7-99.2	9.5	9.51	100.1
12H	27	0515	99.2-108.7	9.5	9.74	102.5
13H	27	0605	108.7-118.2	9.5	8.47	89.2
14H	27	0715	118.2-127.7	9.5	9.36	98.5
15H	27	0815	127.7-137.2	9.5	9.13	96.1
16H	27	0915	137.2-146.7	9.5	9.65	101.6
17H	27	1020	146.7-156.2	9.5	7.76	81.7
18H	27	1125	156.2-165.7	9.5	9.27	97.6
19H	27	1220	165.7-175.2	9.5	7.54	79.4
20H	27	1310	175.2-184.7	9.5	9.32	98.1
21X	27	1515	184.7-194.4	9.7	9.49	97.8
22X	27	1605	194.4-204.1	9.7	9.39	96.8
23X	27	1655	204.1-213.8	9.7	9.76	100.6
24X	27	1745	213.8-223.5	9.7	9.55	98.5
25X	27	1835	223.5-233.2	9.7	9.59	98.9
26X	27	1925	233.2-242.9	9.7	9.58	98.8
27X	27	2015	242.9-252.6	9.7	8.68	89.5
28X	27	2105	252.6-262.3	9.7	9.64	99.4
29X	27	2150	262.3-272.0	9.7	9.62	99.2
30X	27	2240	272.0-281.7	9.7	9.74	100.4
31X	27	2325	281.7-291.4	9.7	9.85	101.5
32X	27	0045	291.4-294.9	3.5	3.03	86.6
33X	28	0155	294.9-301.1	6.2	2.91	46.9
34X	28	0300	301.1-310.8	9.7	9.68	99.8
35X	28	0400	310.8-320.4	9.6	9.14	95.2
36X	28	0500	320.4-330.0	9.6	9.80	102.1
37X	28	0710	330.0-339.6	9.6	7.21	75.1
38X	28	0835	339.6-349.2	9.6	9.62	100.2
39X	28	0945	349.2-358.8	9.6	9.68	100.8
40X	28	1040	358.8-368.4	9.6	9.85	102.6
41X	28	1140	368.4-378.1	9.7	4.23	43.6
42X	28	1230	378.1-387.8	9.7	9.45	97.4
43X	28	1325	387.8-397.5	9.7	9.89	102.0
Coring totals:				397.5	373.23	93.9
177-1090C-						
1H	28	1640	0.0-2.8	2.8	2.85	101.8
2H	28	1745	2.8-12.3	9.5	7.31	76.9
3H	28	1835	12.3-21.8	9.5	8.81	92.7
4H	28	1920	21.8-31.3	9.5	8.53	89.8
5H	28	2010	31.3-40.8	9.5	8.94	94.1
6H	28	2100	40.8-50.3	9.5	9.66	101.7
7H	28	2150	50.3-59.8	9.5	8.63	90.8
8H	28	2250	59.8-69.3	9.5	9.05	95.3
Coring totals:				69.3	63.78	92.0
177-1090D-						
1H	29	0035	0.0-7.4	7.4	7.42	100.3
2H	29	0135	7.4-16.9	9.5	8.11	85.4
3H	29	0230	16.9-26.4	9.5	8.09	85.2
4H	29	0325	26.4-35.9	9.5	8.44	88.8
5H	29	0435	35.9-45.4	9.5	9.10	95.8
6H	29	0530	45.4-54.9	9.5	8.88	93.5

Table T4 (continued).

Core	Date (December 1997)	Time (UTC)	Interval (mbsf)	Length cored (m)	Length recovered (m)	Recovery (%)
7H	29	0625	54.9-64.4	9.5	8.05	84.7
8H	29	0725	64.4-73.9	9.5	9.62	101.3
9H	29	0820	73.9-83.4	9.5	9.10	95.8
10H	29	0920	83.4-92.9	9.5	9.81	103.3
11H	29	1020	92.9-102.4	9.5	8.99	94.6
12H	29	1125	102.4-111.9	9.5	9.30	97.9
13H	29	1220	111.9-121.4	9.5	8.74	92.0
14H	29	1315	121.4-130.9	9.5	9.36	98.5
15H	29	1410	130.9-140.4	9.5	9.21	96.9
16H	29	1510	140.4-149.9	9.5	9.16	96.4
17H	29	1605	149.9-159.4	9.5	9.48	99.8
18H	29	1700	159.4-168.9	9.5	9.11	95.9
19H	29	1805	168.9-178.4	9.5	7.27	76.5
20H	29	1910	178.4-187.9	9.5	9.12	96.0
21H	29	2005	187.9-197.4	9.5	9.45	99.5
22H	29	2100	197.4-206.9	9.5	9.86	103.8
23H	29	2155	206.9-216.4	9.5	8.29	87.3
24H	29	2315	216.4-225.9	9.5	9.68	101.9
Coring totals:				225.9	213.64	94.6
170-1090E-						
1H	30	0240	0.0-8.7	8.7	8.70	100.0
2H	30	0345	8.7-18.2	9.5	7.10	74.7
3H	30	0450	18.2-27.7	9.5	6.41	67.5
4H	30	0545	27.7-37.2	9.5	7.70	81.1
5H	30	0640	37.2-46.7	9.5	7.70	81.1
6H	30	0745	46.7-56.2	9.5	7.89	83.1
7H	30	0845	56.2-65.7	9.5	9.04	95.2
8H	30	0945	65.7-75.2	9.5	9.66	101.7
9H	30	1050	75.2-84.7	9.5	9.38	98.7
10H	30	1150	84.7-94.2	9.5	8.73	91.9
11H	30	1245	94.2-103.7	9.5	9.30	97.9
12H	30	1345	103.7-113.2	9.5	8.67	91.3
13H	30	1440	113.2-122.7	9.5	8.50	89.5
14H	30	1535	122.7-132.2	9.5	9.09	95.7
15H	30	1630	132.2-141.7	9.5	9.43	99.3
16H	30	1725	141.7-151.2	9.5	9.39	98.8
17H	30	1830	151.2-160.7	9.5	9.68	101.9
18H	30	1925	160.7-170.2	9.5	9.44	99.4
19H	30	2020	170.2-179.7	9.5	9.62	101.3
20H	30	2115	179.7-189.2	9.5	9.16	96.4
21H	30	2215	189.2-198.7	9.5	9.68	101.9
22H	30	2315	198.7-208.2	9.5	9.40	98.9
23H	31	0030	208.2-217.7	9.5	5.81	61.2
24H	31	0135	217.7-227.2	9.5	8.19	86.2
25H	31	0235	227.2-236.7	9.5	9.59	100.9
Coring totals:				236.7	217.26	91.8

Notes: UTC = Universal Time Coordinated. An expanded coring summary table that includes lengths and depths of sections and sampling comments is available in ASCII format in the **TABLES** directory.

Table T5. Coring summary for Site 1091. (See table note. Continued on next page.)

Core	Date (January 1998)	Time (UTC)	Depth (mbsf)	Length cored (m)	Length recovered (m)	Recovery (%)
177-1091A-						
1H	2	0510	0.0-6.9	6.9	6.89	99.9
2H	2	0635	6.9-16.4	9.5	7.58	79.8
3H	2	0900	16.4-25.9	9.5	9.05	95.3
4H	2	1005	25.9-35.4	9.5	8.80	92.6
5H	2	1115	35.4-44.9	9.5	8.75	92.1
6H	2	1220	44.9-54.4	9.5	9.17	96.5
7H	2	1320	54.4-63.9	9.5	9.36	98.5
8H	2	1425	63.9-73.4	9.5	6.77	71.3
9H	2	1525	73.4-82.9	9.5	8.13	85.6
10H	2	1630	82.9-92.4	9.5	9.33	98.2
11H	2	1730	92.4-101.9	9.5	9.35	98.4
12H	2	1835	101.9-111.4	9.5	7.45	78.4
13H	2	1935	111.4-120.9	9.5	9.78	102.9
14H	2	2040	120.9-130.4	9.5	9.69	102.0
15H	2	2155	130.4-139.9	9.5	8.07	84.9
16H	3	0025	139.9-149.4	9.5	8.49	89.4
17H	3	0140	149.4-158.9	9.5	8.42	88.6
18H	3	0250	158.9-168.4	9.5	8.04	84.6
19H	3	0405	168.4-177.9	9.5	7.35	77.4
20H	3	0515	177.9-187.4	9.5	6.90	72.6
21H	3	0645	187.4-196.9	9.5	7.66	80.6
22H	3	0805	196.9-206.4	9.5	7.39	77.8
23H	3	1120	206.4-215.9	9.5	7.33	77.2
24H	3	1235	215.9-225.4	9.5	9.64	101.5
25H	3	1345	225.4-234.9	9.5	9.84	103.6
26H	3	1450	234.9-244.4	9.5	9.18	96.6
27H	3	1600	244.4-253.9	9.5	9.88	104.0
28H	3	1725	253.9-263.4	9.5	9.37	98.6
29H	3	1840	263.4-272.9	9.5	9.80	103.2
30H	3	2140	272.9-282.4	9.5	8.58	90.3
31H	3	2305	282.4-291.9	9.5	7.41	78.0
32H	3	0010	291.9-301.4	9.5	7.32	77.1
33H	3	0115	301.4-310.9	9.5	9.00	94.7
Coring totals:				310.9	279.77	90.0
177-1091B-						
1H	4	0525	0.0-7.8	7.8	7.79	99.9
2H	4	0625	7.8-17.3	9.5	6.74	70.9
3H	4	0730	17.3-26.8	9.5	6.57	69.2
4H	4	0840	26.8-36.3	9.5	7.75	81.6
5H	4	0945	36.3-45.8	9.5	7.22	76.0
6H	4	1050	45.8-55.3	9.5	8.29	87.3
7H	4	1155	55.3-64.8	9.5	9.19	96.7
8H	4	1250	64.8-74.3	9.5	7.51	79.1
9H	4	1350	74.3-83.8	9.5	8.63	90.8
10H	4	1445	83.8-93.3	9.5	7.95	83.7
11H	4	1545	93.3-102.8	9.5	6.25	65.8
12H	4	1645	102.8-112.3	9.5	8.72	91.8
13H	4	1755	112.3-121.8	9.5	9.84	103.6
14H	4	1855	121.8-131.3	9.5	5.32	56.0
15H	4	1950	131.3-140.8	9.5	8.61	90.6
16H	4	2045	140.8-150.3	9.5	7.36	77.5
17H	4	2140	150.3-159.8	9.5	6.60	69.5
18H	4	2235	159.8-169.3	9.5	8.32	87.6
19H	4	2335	169.3-178.8	9.5	8.12	85.5
20H	5	0030	178.8-188.3	9.5	6.57	69.2
21H	5	0130	188.3-197.8	9.5	7.98	84.0
22H	5	0235	197.8-207.3	9.5	7.78	81.9
23H	5	0340	207.3-216.8	9.5	6.49	68.3
24H	5	0445	216.8-226.3	9.5	2.39	25.2
25H	5	0545	226.3-235.8	9.5	7.10	74.7
26H	5	0645	235.8-245.3	9.5	7.33	77.2
27H	5	0750	245.3-254.8	9.5	5.63	59.3
28H	5	0855	254.8-264.3	9.5	0.85	8.9
29H	5	1000	264.3-273.8	9.5	4.62	48.6
Coring totals:				273.8	203.52	74.3

Table T5 (continued).

Core	Date (January 1998)	Time (UTC)	Depth (mbsf)	Length cored (m)	Length recovered (m)	Recovery (%)
177-1091C-						
1H	5	1315	0.0-4.0	4.0	3.95	98.8
Coring totals:				4.0	3.95	98.8
177-1091D-						
1H	5	1410	0.0-3.6	3.6	3.61	100.3
2H	5	1515	3.6-13.1	9.5	3.07	32.3
3H	5	1615	13.1-22.6	9.5	3.97	41.8
4H	5	1725	22.6-32.1	9.5	4.90	51.6
5H	5	1845	32.1-41.6	9.5	4.12	43.4
6H	5	1940	41.6-51.1	9.5	8.25	86.8
7H	5	2035	51.1-60.6	9.5	7.94	83.6
8H	5	2135	60.6-70.1	9.5	7.28	76.6
9H	5	2225	70.1-79.6	9.5	9.69	102.0
10H	5	2330	79.6-89.1	9.5	7.73	81.4
11H	6	0030	89.1-98.6	9.5	7.80	82.1
12H	6	0130	98.6-108.1	9.5	8.66	91.2
13H	6	0230	108.1-117.6	9.5	8.59	90.4
14H	6	0335	117.6-127.1	9.5	9.06	95.4
15H	6	0435	127.1-136.6	9.5	9.10	95.8
16H	6	0540	136.6-146.1	9.5	9.05	95.3
17H	6	0640	146.1-155.6	9.5	9.21	96.9
18H	6	0745	155.6-165.1	9.5	8.42	88.6
19H	6	0845	165.1-174.6	9.5	8.19	86.2
20H	6	0950	174.6-184.1	9.5	8.36	88.0
21H	6	1045	184.1-193.6	9.5	9.30	97.9
22H	6	1210	193.6-203.1	9.5	8.88	93.5
Coring totals:				203.1	165.18	81.3
177-1091E-						
1H	6	1500	0.0-4.2	4.2	4.24	101.0
2H	6	1605	4.2-13.7	9.5	5.42	57.1
3H	6	1700	13.7-23.2	9.5	5.81	61.2
4H	6	1800	23.2-32.7	9.5	3.87	40.7
5H	6	1900	32.7-42.2	9.5	7.13	75.1
6H	6	2000	42.2-51.7	9.5	5.02	52.8
Coring totals:				51.7	31.49	60.9

Notes: UTC = Universal Time Coordinated. An expanded coring summary table that includes lengths and depths of sections and sampling comments is available in ASCII format in the **TABLES** directory.

Table T6. Coring summary for Site 1092. (See table note. Continued on next page.)

Core	Date (January 1998)	Time (UTC)	Interval (mbsf)	Length cored (m)	Length recovered (m)	Recovery (%)
177-1092A-						
1H	7	1715	0.0-8.0	8.0	8.05	100.6
2H	7	1805	8.0-17.5	9.5	8.16	85.9
3H	7	1840	17.5-27.0	9.5	8.79	92.5
4H	7	1915	27.0-36.5	9.5	9.79	103.1
5H	7	1950	36.5-46.0	9.5	9.37	98.6
6H	7	2020	46.0-55.5	9.5	8.93	94.0
7H	7	2045	55.5-65.0	9.5	9.37	98.6
8H	7	2115	65.0-74.5	9.5	8.77	92.3
9H	7	2145	74.5-84.0	9.5	9.67	101.8
10H	7	2215	84.0-93.5	9.5	9.68	101.9
11H	7	2245	93.5-103.0	9.5	9.37	98.6
12H	7	2310	103.0-112.5	9.5	10.13	106.6
13H	7	2340	112.5-122.0	9.5	9.10	95.8
14H	8	0050	122.0-131.5	9.5	9.16	96.4
15H	8	0125	131.5-141.0	9.5	9.58	100.8
16H	8	0200	141.0-150.5	9.5	8.96	94.3
17H	8	0245	150.5-160.0	9.5	8.06	84.8
18H	8	0325	160.0-169.5	9.5	8.57	90.2
19H	8	0355	169.5-179.0	9.5	9.18	96.6
20H	8	0515	179.0-188.5	9.5	9.40	98.9
Coring totals:				188.5	182.09	96.6
177-1092B-						
1H	8	0930	0.0-7.4	7.4	7.42	100.3
2H	8	1015	7.4-16.9	9.5	9.30	97.9
3H	8	1050	16.9-26.4	9.5	7.61	80.1
4H	8	1125	26.4-35.9	9.5	9.47	99.7
5H	8	1200	35.9-45.4	9.5	9.10	95.8
6H	8	1230	45.4-54.9	9.5	7.01	73.8
7H	8	1255	54.9-64.4	9.5	0.76	8.0
8H	8	1325	64.4-73.9	9.5	9.81	103.3
9H	8	1355	73.9-83.4	9.5	8.68	91.4
10H	8	1425	83.4-92.9	9.5	8.74	92.0
11H	8	1450	92.9-102.4	9.5	9.59	100.9
12H	8	1520	102.4-111.9	9.5	9.03	95.1
13H	8	1550	111.9-121.4	9.5	4.30	45.3
14H	8	1625	121.4-130.9	9.5	10.05	105.8
15H	8	1700	130.9-140.4	9.5	7.52	79.2
16H	8	1730	140.4-149.9	9.5	8.74	92.0
17H	8	1800	149.9-159.4	9.5	8.11	85.4
18H	8	1850	159.4-168.9	9.5	9.30	97.9
Coring totals:				168.9	144.54	85.6
177-1092C-						
1H	8	2130	0.0-4.0	4.0	4.04	101.0
2H	8	2200	4.0-13.5	9.5	7.82	82.3
3H	8	2230	13.5-23.0	9.5	9.62	101.3
4H	8	2255	23.0-32.5	9.5	9.12	96.0
5H	8	2325	32.5-42.0	9.5	8.43	88.7
6H	8	2355	42.0-51.5	9.5	0.10	1.1
7H	9	0025	51.5-61.0	9.5	6.12	64.4
8H	9	0100	61.0-70.5	9.5	8.21	86.4
9H	9	0135	70.5-80.0	9.5	9.59	100.9
10H	9	0205	80.0-89.5	9.5	9.79	103.1
11H	9	0240	89.5-99.0	9.5	8.83	92.9
12H	9	0315	99.0-108.5	9.5	9.56	100.6
13H	9	0345	108.5-118.0	9.5	9.80	103.2
14H	9	0420	118.0-127.5	9.5	9.97	104.9
15H	9	0455	127.5-137.0	9.5	10.00	105.3
16H	9	0535	137.0-146.5	9.5	9.94	104.6
17H	9	0605	146.5-156.0	9.5	9.83	103.5
18H	9	0645	156.0-165.5	9.5	10.02	105.5
Coring totals:				165.5	150.79	91.1

Table T6 (continued).

Core	Date (January 1998)	Time (UTC)	Interval (mbsf)	Length cored (m)	Length recovered (m)	Recovery (%)
177-1092D-						
		****** Drilled from 0.0 to 36.4 mbsf ******				
1H	9	0945	36.4-45.9	9.5	9.67	101.8
2H	9	1020	45.9-55.4	9.5	8.98	94.5
3H	9	1050	55.4-64.9	9.5	9.63	101.4
Coring totals:				28.5	28.28	99.2
Drilled total:				36.4		
Total:				64.9		

Notes: UTC = Universal Time Coordinated. An expanded coring summary table that includes lengths and depths of sections and sampling comments is available in ASCII format in the **TABLES** directory.

Table T7. Coring summary for Site 1093. (See table note. Continued on next two pages.)

Core	Date (January 1998)	Time (UTC)	Interval (mbsf)	Length cored (m)	Length recovered (m)	Recovery (%)
177-1093A-						
1H	11	0020	0.0-8.5	8.5	8.54	100.5
2H	11	0125	8.5-18.0	9.5	9.64	101.5
3H	11	0220	18.0-27.5	9.5	9.74	102.5
4H	11	0330	27.5-37.0	9.5	10.04	105.7
5H	11	0425	37.0-46.5	9.5	9.91	104.3
6H	11	0525	46.5-56.0	9.5	9.61	101.2
7H	11	0620	56.0-65.5	9.5	9.70	102.1
8H	11	0715	65.5-75.0	9.5	9.69	102.0
9H	11	0810	75.0-84.5	9.5	9.82	103.4
10H	11	0905	84.5-94.0	9.5	9.48	99.8
11H	11	0955	94.0-103.5	9.5	9.81	103.3
12H	11	1055	103.5-113.0	9.5	9.66	101.7
13H	11	1155	113.0-122.5	9.5	9.48	99.8
14H	11	1250	122.5-132.0	9.5	9.29	97.8
15H	11	1350	132.0-141.5	9.5	9.91	104.3
16H	11	1445	141.5-151.0	9.5	9.52	100.2
17H	11	1535	151.0-160.5	9.5	9.93	104.5
18H	11	1625	160.5-170.0	9.5	9.92	104.4
19H	11	1720	170.0-179.5	9.5	9.90	104.2
20H	11	1815	179.5-189.0	9.5	9.83	103.5
21H	11	1915	189.0-198.5	9.5	9.53	100.3
22H	11	2000	198.5-208.0	9.5	9.06	95.4
23H	11	2045	208.0-217.5	9.5	9.73	102.4
24H	11	2145	217.5-227.0	9.5	9.66	101.7
25H	11	2230	227.0-234.5	7.5	8.21	109.5
26H	11	2330	234.5-241.5	7.0	9.24	132.0
27X	12	0045	241.5-251.0	9.5	0.00	0.0
28X	12	0320	251.0-260.7	9.7	6.90	71.1
29X	12	0415	260.7-270.4	9.7	3.98	41.0
30H	12	0630	270.4-275.4	5.0	3.91	78.2
31X	12	0745	275.4-280.5	5.1	0.02	0.4
32X	12	0845	280.5-290.1	9.6	0.01	0.1
33X	12	0950	290.1-299.8	9.7	0.00	0.0
34X	12	1055	299.8-309.4	9.6	0.02	0.2
Coring totals:				309.4	263.69	85.2
177-1093B-						
1H	12	1535	0.0-7.1	7.1	7.15	100.7
2H	12	1640	7.1-16.6	9.5	9.16	96.4
3H	12	1730	16.6-26.1	9.5	5.34	56.2
4H	12	1820	26.1-35.6	9.5	9.79	103.1
5H	12	1915	35.6-45.1	9.5	9.69	102.0
6H	12	2005	45.1-54.6	9.5	8.03	84.5
7H	12	2100	54.6-64.1	9.5	9.34	98.3
8H	12	2150	64.1-73.6	9.5	9.54	100.4
9H	12	2245	73.6-83.1	9.5	9.69	102.0
10H	12	2335	83.1-92.6	9.5	8.86	93.3
11H	13	0035	92.6-102.1	9.5	9.74	102.5
12H	13	0140	102.1-111.6	9.5	8.63	90.8
13H	13	0230	111.6-121.1	9.5	9.88	104.0
14H	13	0330	121.1-130.6	9.5	9.18	96.6
15H	13	0425	130.6-140.1	9.5	8.53	89.8
16H	13	0520	140.1-149.6	9.5	9.28	97.7
17H	13	0610	149.6-159.1	9.5	9.07	95.5
18H	13	0705	159.1-168.6	9.5	8.36	88.0
19H	13	0800	168.6-178.1	9.5	9.63	101.4
20H	13	0900	178.1-187.6	9.5	8.86	93.3
21H	13	0950	187.6-197.1	9.5	7.79	82.0
22H	13	1045	197.1-206.6	9.5	8.39	88.3
23H	13	1145	206.6-216.1	9.5	9.25	97.4
24H	13	1250	216.1-221.8	5.7	5.80	101.8
Coring totals:				221.8	208.98	94.2
177-1093C-						
1H	13	1710	0.0-8.0	8.0	8.00	100.0
2H	13	1800	8.0-17.5	9.5	5.86	61.7

Table T7 (continued).

Core	Date (January 1998)	Time (UTC)	Interval (mbsf)	Length cored (m)	Length recovered (m)	Recovery (%)
3H	13	1855	17.5-27.0	9.5	7.69	80.9
4H	13	1945	27.0-36.5	9.5	9.65	101.6
5H	13	2035	36.5-46.0	9.5	8.05	84.7
6H	13	2135	46.0-55.5	9.5	6.22	65.5
7H	13	2250	55.5-65.0	9.5	9.19	96.7
8H	13	2345	65.0-74.5	9.5	9.10	95.8
9H	14	0230	74.5-84.0	9.5	8.55	90.0
10H	14	0330	84.0-93.5	9.5	7.18	75.6
11H	14	0425	93.5-103.0	9.5	7.61	80.1
12H	14	0525	103.0-112.5	9.5	8.39	88.3
13H	14	0615	112.5-122.0	9.5	1.92	20.2
14H	14	0710	122.0-131.5	9.5	6.17	64.9
15H	14	0805	131.5-141.0	9.5	5.41	56.9
16H	14	0910	141.0-150.5	9.5	3.19	33.6
17H	14	1005	150.5-160.0	9.5	5.04	53.1
18H	14	1105	160.0-169.5	9.5	2.24	23.6
Coring totals:				169.5	119.46	70.5
177-1093D-						
	****** Drilled from 0.0 to 136.0 mbsf ******					
1H	15	1020	136.0-145.5	9.5	6.92	72.8
2H	15	1115	145.5-155.0	9.5	2.23	23.5
3H	15	1210	155.0-164.5	9.5	5.00	52.6
4H	15	1305	164.5-174.0	9.5	8.92	93.9
5H	15	1405	174.0-183.5	9.5	8.83	92.9
6H	15	1500	183.5-193.0	9.5	5.77	60.7
7H	15	1550	193.0-202.5	9.5	2.36	24.8
8H	15	1645	202.5-212.0	9.5	5.97	62.8
9H	15	1730	212.0-221.5	9.5	0.00	0.0
10H	15	1830	221.5-231.0	9.5	5.34	56.2
11H	15	1925	231.0-240.5	9.5	6.77	71.3
12H	15	2015	240.5-250.0	9.5	5.07	53.4
13H	15	2110	250.0-259.5	9.5	6.25	65.8
14H	15	2305	259.5-269.0	9.5	0.58	6.1
15H	16	0020	269.0-278.5	9.5	1.44	15.2
16H	16	0130	278.5-288.0	9.5	0.05	0.5
17H	16	0240	288.0-297.5	9.5	0.53	5.6
18H	16	0345	297.5-307.0	9.5	0.02	0.2
19X	16	0515	307.0-313.0	6.0	0.00	0.0
20X	16	0735	313.0-319.0	6.0	0.02	0.3
21X	16	0830	319.0-328.6	9.6	0.01	0.1
22H	16	0955	328.6-329.6	1.0	1.20	120.0
23X	16	1110	329.6-338.3	8.7	0.00	0.0
24X	16	1310	338.3-348.0	9.7	0.03	0.3
25X	16	1425	348.0-357.7	9.7	0.02	0.2
26X	16	1545	357.7-367.4	9.7	0.00	0.0
27X	16	1700	367.4-377.0	9.6	6.02	62.7
28X	16	1830	377.0-386.2	9.2	1.88	20.4
29X	16	1950	386.2-395.9	9.7	0.00	0.0
30X	16	2105	395.9-405.5	9.6	2.15	22.4
31X	16	2220	405.5-415.1	9.6	0.00	0.0
32X	16	2340	415.1-424.7	9.6	0.24	2.5
33X	17	0030	424.7-434.3	9.6	9.73	101.4
34X	17	0125	434.3-443.9	9.6	7.10	74.0
35X	17	0215	443.9-453.3	9.4	9.25	98.4
36X	17	0310	453.3-462.9	9.6	9.71	101.1
37X	17	0400	462.9-472.5	9.6	9.89	103.0
38X	17	0455	472.5-482.0	9.5	7.78	81.9
39X	17	0720	482.0-491.6	9.6	7.17	74.7
40X	17	0815	491.6-501.3	9.7	4.09	42.2
41X	17	0910	501.3-510.9	9.6	1.44	15.0
42X	17	1020	510.9-520.6	9.7	0.00	0.0
43X	17	1145	520.6-530.2	9.6	0.00	0.0
44X	17	1310	530.2-539.9	9.7	1.16	12.0
45X	17	1420	539.9-549.5	9.6	5.48	57.1
46X	17	1545	549.5-559.1	9.6	3.06	31.9
47X	17	1750	559.1-568.8	9.7	0.44	4.5
48X	17	2030	568.8-578.4	9.6	0.19	2.0

Table T7 (continued).

Core	Date (January 1998)	Time (UTC)	Interval (mbsf)	Length cored (m)	Length recovered (m)	Recovery (%)
49X	18	0120	578.4-588.0	9.6	0.12	1.3
50X	18	0445	588.0-597.7	9.7	0.50	5.2
Coring totals:				461.7	160.73	34.8
Drilled total:				136.0		
Total:				597.7		
177-1093E-						
			****** Drilled from 0.0 to 4.0 mbsf ******			
1H	19	0340	4.0-13.5	9.5	6.55	68.9
			****** Drilled from 13.5 to 33.0 mbsf ******			
2H	19	0515	33.0-42.5	9.5	4.99	52.5
Coring totals:				19.0	11.54	60.7
Drilled total:				23.5		
Total:				42.5		
177-1093F-						
			****** Drilled from 0.0 to 34.0 mbsf ******			
1H	19	0800	34.0-43.5	9.5	6.24	65.7
Coring totals:				9.5	6.24	65.7
Drilled total:				34.0		
Total:				43.5		

Notes: UTC = Universal Time Coordinated. An expanded coring summary table that includes lengths and depths of sections and sampling comments is available in ASCII format in the **TABLES** directory.

Table T8. Coring summary for Site 1094.

Core	Date (January 1998)	Time (UTC)	Interval (mbsf)	Length cored (m)	Length recovered (m)	Recovery (%)
177-1094A-						
1H	21	0430	0.0-4.6	4.6	4.59	99.8
2H	21	0520	4.6-14.1	9.5	9.20	96.8
3H	21	0600	14.1-23.6	9.5	8.26	86.9
4H	21	0740	23.6-33.1	9.5	8.26	86.9
5H	21	0825	33.1-42.6	9.5	8.15	85.8
6H	21	0920	42.6-52.1	9.5	7.90	83.2
7H	21	1005	52.1-61.6	9.5	8.79	92.5
8H	21	1100	61.6-71.1	9.5	9.04	95.2
9H	21	1145	71.1-80.6	9.5	8.07	84.9
10H	21	1235	80.6-90.1	9.5	9.24	97.3
11H	21	1320	90.1-99.6	9.5	7.93	83.5
12H	21	1410	99.6-109.1	9.5	8.75	92.1
13H	21	1455	109.1-118.6	9.5	7.82	82.3
14H	21	1545	118.6-128.1	9.5	5.07	53.4
15H	21	1625	128.1-137.6	9.5	9.27	97.6
16H	21	1715	137.6-147.1	9.5	7.25	76.3
17H	21	1810	147.1-150.1	3.0	0.00	0.0
18H	21	1910	150.1-158.6	8.5	7.49	88.1
	****** Drilled from 158.6 to 159.6 mbsf ******					
Coring totals:				158.6	135.08	85.2
Drilled total:				1.0		
Total:				159.6		
177-1094B-						
1H	22	0035	0.0-9.5	9.5	9.29	97.8
2H	22	0130	9.5-19.0	9.5	9.42	99.2
3H	22	0225	19.0-28.5	9.5	0.19	2.0
4H	22	0330	28.5-38.0	9.5	4.68	49.3
Coring totals:				38.0	23.58	62.0
177-1094C-						
1H	22	0500	0.0-8.9	8.9	8.94	100.4
2H	22	0550	8.9-18.4	9.5	9.95	104.7
3H	22	0630	18.4-27.9	9.5	9.64	101.5
4H	22	0710	27.9-37.4	9.5	0.00	0.0
5H	22	0800	37.4-46.9	9.5	8.35	87.9
6H	22	0850	46.9-56.4	9.5	8.48	89.3
7H	22	0940	56.4-65.9	9.5	0.00	0.0
8H	22	1025	65.9-73.1	7.2	1.28	17.8
Coring totals:				73.1	46.64	63.8
177-1094D-						
	****** Drilled from 0.0 to 19.1 mbsf ******					
1H	22	1335	19.1-28.6	9.5	0.0	0.0
2H	22	1415	28.6-38.1	9.5	5.28	55.6
3H	22	1455	38.1-47.6	9.5	9.03	95.1
4H	22	1535	47.6-57.1	9.5	8.49	89.4
5H	22	1615	57.1-66.6	9.5	0.05	0.5
6H	22	1650	66.6-76.1	9.5	9.53	100.3
7H	22	1735	76.1-85.6	9.5	6.22	65.5
8H	22	1810	85.6-95.1	9.5	7.63	80.3
9H	22	1855	95.1-104.6	9.5	5.83	61.4
10H	22	1935	104.6-114.1	9.5	6.47	68.1
11H	22	2015	114.1-123.6	9.5	5.87	61.8
12H	22	2055	123.6-133.1	9.5	8.08	85.1
13H	22	2135	133.1-142.6	9.5	4.30	45.3
14H	23	0045	142.6-152.1	9.5	8.77	92.3
15H	23	0130	152.1-161.6	9.5	8.95	94.2
16H	23	0210	161.6-171.1	9.5	6.26	65.9
Coring totals:				152.0	100.76	66.3
Drilled total:				19.1		
Total:				171.1		

Notes: UTC = Universal Time Coordinated. An expanded coring summary table that includes lengths and depths of sections and sampling comments is available in ASCII format in the **TABLES** directory.